PhD degree in Molecular Medicine

European School of Molecular Medicine (SEMM),

University of Milan and University of Naples "Federico II"

Faculty of Medicine

Settore disciplinare: MED/04

Identification of molecular mechanisms responsible for degradation of the tumor suppressor protein NUMB in cancer

Letizia Amadori

IFOM-IEO Campus, Milan

Matricola n. R08905

Supervisor: Prof. Pier Paolo Di Fiore

IFOM-IEO Campus, Milan

Added Supervisor: Prof. Salvatore Pece

IFOM-IEO Campus, Milan

Anno accademico 2012-2013

TABLE OF CONTENTS

FIGURES AND TABLES INDEX

ABBREVIATIONS LIST

SOP: sensory organ precursor

PTB: Phospho Tyrosine Binding

PRR: Proline-rich region

SH3: Src homology 3

EH: Eps15 homology

PTBL: Phospho Tyrosine Binding long

PTBS: Phospho Tyrosine Binding short

PRRL: Proline-rich region long

PRRS: Proline-rich region short

ACD: asymmetric cell division

CNS: central nervous system

PAR: polarity complex

aPKC: atypical protein kinase C

Eps15: Epidermal growth factor receptor substrate 15

Eps15L1: Epidermal growth factor receptor pathway substrate 15-like 1

EMT: epithelial–mesenchymal transition

MDCK: Madin Darby Canine Kidney

NICD: NOTCH intracellular domain

CSL: mammalian CBF1 and *Drosophila* Su(H) and LAG-1

Shh: Sonic Hedgehog

Dhh: Desert Hedgehog

Ihh: Indian Hedgehog

SC: stem cell

GCP: granule cell progenitor

MDM2: Mouse double minute 2

TCTP: Translationally controlled tumor protein

HRF: histamine releasing factor

CSC: cancer stem cell

NSCLC: non-small cell lung carcinoma

UPS: Ubiquitin Proteasome System

RGC: radial glial cell

HECT: Homologous to E6-AP C-Terminus

RING: Really Interesting New Gene

RLD: RCC1-like domain

WWD: tryptophan-tryptophan domain

BRCA1: breast cancer type 1

BARD1: BRCA1-associated RING domain protein 1

RNF4: RING finger protein 4

BIRC7: Baculoviral IAP repeat-containing protein 7

cIAP: cellular inhibitor of apoptosis 1

RBX: RING-Box protein

CRL: Cullin-RING ligase

SCF : Skp1-Cullin1-F-box

NF-κB: nuclear factor κB

Bcl-2: B-cell lymphoma 2

IL: interleukin

VEGF : vascular endothelial growth factor

IκBα: inhibitor κB-α

MM: multiple myeloma

NHL: non-Hodgkin limphoma

SKP: S-phase kinase-associated protein

Cks: Cyclin-dependent kinases regulatory subunit

Protacs: protein-targeting chimeric molecule 1

NAE: NEDD8 activating enzyme E1

CAND1: Cullin-associated NEDD8-dissociated protein 1

FBXW: F-box/WD repeat-containing protein

FBX: F-box protein

IB: immunoblotting

IP: immunoprecipitation

IF: immunofluorescence

IHC: immunohistochemistry

GST: Glutatione S-transferase

FFPE: formalin-fixed paraffin-embedded

MW: molecular weight

s.e.: short exposure

L.e.: long exposure

RNAi: RNA-interference

CTRL: control

HRP: horseradish-peroxidase

TMB: tetramethylbenzidine

ELISA: enzyme-linked immunosorbent assay

EtOh: ethanol

OD: optical density

s.dev: standard deviation

CTF: Cell Titer Fluor

rNUMB: recombinant NUMB

siRNA: small interfering RNA

shRNA: short hairpin RNA

CV: Coefficient of variation

MAD: Median Absolute Deviation

WB: western blot

GFP: Green Fluorescence Protein

TRIP: thyroid hormone receptor interactor

DAPI: 4',6-diamidino-2-phenylindole

q-RT-PCR: quantitative Real Time-PCR

pLL3.7: pLentilox 3.7

KD: knock-down

LOF: loss of function

LRR: leucin rich repeat

WD: tryptophan-aspartic acid

1 ABSTRACT

NUMB was initially described as a cell fate determinant involved in neurogenesis. More recently, NUMB has been implicated in different types of human cancers, in which it has a tumor suppressor role. In particular, data from our laboratory revealed that loss of NUMB protein occurred in approximately 50% of breast cancers and 30% of non-small cell lung cancers, and leads to increased oncogenic NOTCH activity and decreased p53 tumor suppressor function.

Mechanistically, loss of NUMB in human breast cancers is due to its deregulated ubiquitination and ensuing proteasomal degradation, as witnessed by the restoration of physiological NUMB levels in NUMB-deficient primary breast tumor cells upon proteasome inhibition with MG-132. Therefore, the molecular mechanism underlying NUMB degradation in cancer most likely involves deregulation of components of the cellular machinery normally regulating the ubiquitination/phosphorylation status of the NUMB protein, such as E3-ubiquitin ligases/kinases.

In this thesis, we devised a high-throughput phenotypic screening to identify the molecular determinants responsible for NUMB loss among E3 ligase family. The screening assay measures restoration of NUMB expression upon siRNA-mediated silencing of candidate enzymes, in a NUMB-deficient model-system. We identified the breast cancer epithelial cell line MDA-MB-361, as a suitable cell model system for the screening assay as it recapitulates the phenotype of NUMB-deficient primary tumor cells. Indeed, NUMB protein levels in these cells are restored to physiological levels by MG-132 treatment. For the high-throughput phenotypic assay, we developed and optimized for a miniaturized format, a NUMB capture ELISA assay.

Using the high-throughput screening platform, we assessed the involvement of over 600 E3 ligases in NUMB downregulation, and identified 21 candidate E3 ligases. We then went through the validation of these 21 candidate hits, which is the topic of this thesis. Upon validation of the top six candidates of E3 ligases list, we confirmed that the E3 ligase, RBX1 (RING-Box 1), mediates the downregulation of NUMB in both MDA-MB-361 cells and human primary NUMB-deficient breast and lung tumor cells. Indeed, we demonstrated that silencing *RBX1* in these cells restores NUMB protein levels, while no effect was observed in NUMB-proficient cell lines or primary tumor cells. Moreover, we also established a physical interaction between NUMB and RBX1 in MDA-MB-361 cells indicating that RBX1 directly mediates NUMB degradation.

RBX1 belongs to the tetrameric E3 ligase complex, Skp1/Cullin1/F-box (SCF), in which the specificity for substrates is mediated by the F-box protein. Intriguingly, among the 21 candidates from the high-throughput screening, we identified the F-box protein, FBXW8 (F-box and WD repeat domain containing 8), which has been described to form a complex with RBX1. We, therefore, assessed the role of FBXW8 in NUMB donwregulation in high-resolution studies in MDA-MB-361 cells and confirmed its involvement. We are currently validating FBXW8 also in primary tumors cells from human breast and lung cancers.

In conclusion, our data indicate that an SCF E3 ligase complex involving RBX1 and FBXW8, likely mediates NUMB hyperdegradation in human cancers. This result has potential translational ramifications as RBX1 and FBXW8 could represent novel molecular targets for therapeutic intervention in NUMB-deficient cancers.

2 INTRODUCTION

This thesis is concerned with the molecular mechanisms responsible for excessive NUMB degradation in human tumors. Here, in the introduction, I will first provide an overview of the history of NUMB, from its discovery in *Drosophila*, to its classification over evolution in different model systems and its molecular structure (section 2.1.1). Then, I will depict a portrait of the different functions of NUMB in the cell, from: i) a physiological point-of-view, starting from the control of asymmetric cell division to the control of signaling pathways (section 2.1.2); ii) a pathological point-of-view, going through the deregulation of NUMB physiological functions in cancer (section 2.1.3). Finally, the last part of the introduction will provide a brief description of the molecular players of the Ubiquitin Proteasome System (UPS) (section 2.2) and the rationale according to which these players might represent potential therapeutic target(s) in NUMB-deficient cancers (section 2.3).

2.1 NUMB: AN HISTORICAL AND MOLECULAR PERSPECTIVE

2.1.1 Classification and structure

NUMB (alias S171; C14orf41; c14_5527) was originally identified as a critical cell fate determinant in *Drosophila* (d-NUMB), in which mutant embryos displayed an alteration of sensory organ precursor (SOP) lineage choices [1]. In particular, it has been shown that loss of d-NUMB function causes neuronal differentiation defects, while its ectopic expression causes an increase in neuron differentiation to the disadvantage of other differentiated cell types [1-4].

The relevance of NUMB in vertebrates was demonstrated by studies in mice, which led to the identification of two mammalian homologues, mouse NUMB and mouse NUMB-Like (m-NUMB and m-NUMB-Like, respectively) [5,6,7]. The N-terminal portion m-NUMB-Like (amino acids 42 to 331) shows strong sequence similarity to both m-NUMB and d-NUMB [6], with 76% and 63.7% identity, respectively (Figure 1). Overall, the similarity between m-NUMB-like and m-NUMB is present throughout the protein, while the homology between m-NUMB-Like and d-NUMB is primarily confined to the N-terminal portion of the protein [6].

m-NUMB shares with d-NUMB cell functions when expressed in *Drosophila* [6,7]. Similarly, the identification of a chicken NUMB homologue able to antagonize NOTCH-mediated inhibition of differentiation of neuroepithelial cells, suggests that the function of vertebrate NUMB is similar to that of d-NUMB [8].

Structurally, NUMB resembles an adaptor or scaffold protein and is involved in bringing together multiple proteins into a functional pathway or unit. It is composed of an amino-terminal phosphotyrosine binding (PTB) domain [9], a C-terminal proline-rich region (PRR)

containing several putative Src homology 3 (SH3) domain-binding sites [5], and an Eps15 homology (EH) domain binding motif [10].

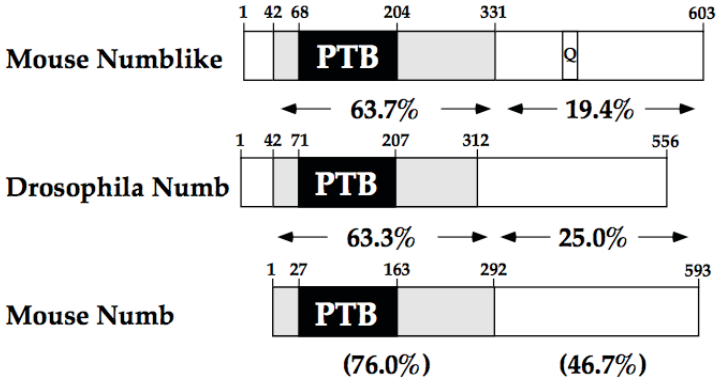

Figure 1. Schematic diagram of mouse NUMBlike, *Drosophila* NUMB and mouse NUMB proteins. Amino acid identity between adjacent proteins is represented by percentages written between diagrams; homology between mouse NUMBlike and mouse NUMB is represented by percentages in parentheses. PTB is a presumptive phosphotyrosine binding domain and Q represents poly-glutamine repeats. Figure taken from [6].

The existence of human NUMB (h-NUMB) was documented a decade after the debut of d-NUMB, in a study conducted by Verdi *et al*. The authors identified four NUMB isoforms from a human neuronal precursor cDNA library [11]. The differences between the alternative spliced variants lie within two regions of NUMB: the PTB domain and the PRR. Two of the four isoforms, h-NUMB 1 and h-NUMB 2, contain the so-called PTB long (PTBL) domain, which differs from the PTB short (PTBS) domain, present in h-NUMB 3 and h-NUMB 4, due to the inclusion of an 11 amino acid insert [11]. The isoforms h-NUMB 1 and h-NUMB 3 contain the PRR long (PRRL) domain, while h-NUMB 2 and h-NUMB 4 harbor the PRR short (PRRS) domain, which lacks a 48 amino acid insert present in the long version [11] (Figure 2).

Studies carried out in immortalized mouse neural crest cell lines and in primary cultures of rat neural crest stem cells (SCs) with overexpressed h-NUMB isoforms, demonstrated

that PRRS- and PRRL-containing h-NUMB isoforms promote either neuronal differentiation (PRRS) or proliferation (PRRL), covering distinct functions during mammalian neurogenesis [11]. The four isoforms have been identified also in mouse by Dho *et al.*, in which the authors show that the insert in the PTB domain may be an important determinant in the localization of NUMB to the plasma membrane.

Thus, the different functions of mammalian NUMB, which will be better described in section 2.1.2, could be in part explained by the diverse isoforms and the heterogeneity of interacting proteins [5,11-13].

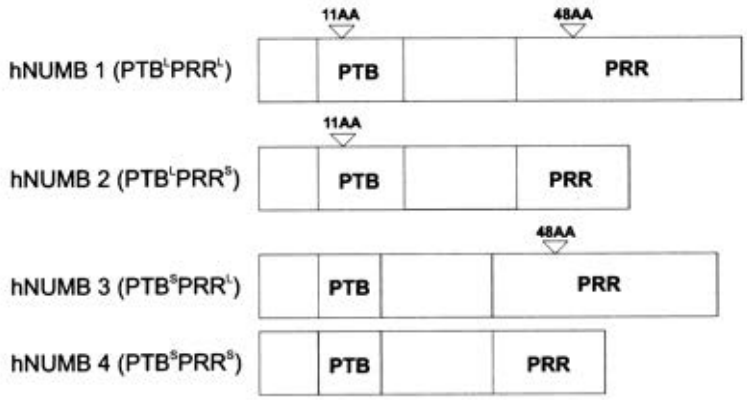

Figure 2. Schematic diagram of the four h-NUMB isoforms.

Human NUMB (h-NUMB) isoforms differ in two domains: the phosphotyrosine binding (PTB) domain and the proline-rich region (PRR). The PTB domain can be either short (PTBS) or (PTBL) depending on the presence of an 11 amino acid (11AA) insert. Similarly, the PRR is either short (PRRS) or long (PRRL) depending on the inclusion of a 48 amino acid (48AA) insert. Figure adapted from [11].

2.1.2 The multiple NUMB functions: a physiological point-of-view

2.1.2.1 Asymmetric cell division

NUMB owes its name to the fact that its loss of function in *Drosophila* mutants causes a dramatic loss of sensory neurons, causing flies to become "numb". NUMB was described as the first known determinant of cell fate specification in the fly, more than twenty years ago [1]; it was also the first time that the possible involvement of an intrinsic cellular player in asymmetric cell division (ACD) was rationalized. Indeed, NUMB acquires an asymmetric distribution during cytokinesis and is concentrated at one of the two spindle poles during mitosis, while it is uniformly distributed around the plasma membrane of the SOP during interphase. So, two different fates characterize the daughter cell that inherits NUMB, the pIIb cell, and the cell that does not, the pIIa cell [2] (Figure 3).

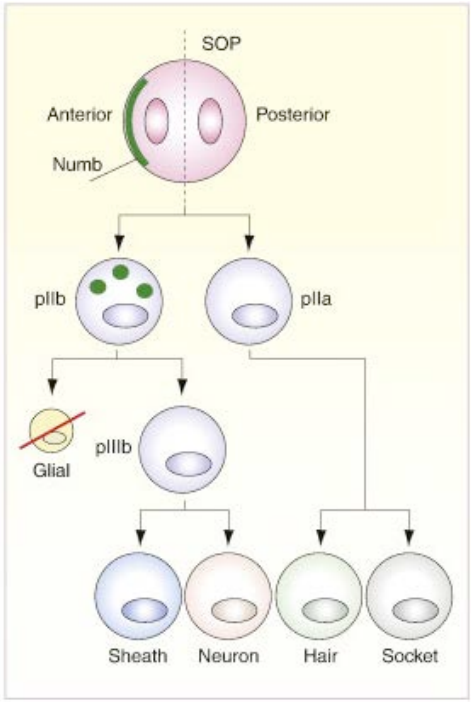

Figure 3. NUMB and asymmetric cell division in *Drosophila* SOP.

The figure depicts asymmetric cell divisions (ACDs) in *Drosophila* SOP. The plane of division with orientations is indicated. NUMB is shown in green, as a crescent in the dividing SOP. For simplicity, only the first ACD is depicted in detail. However, all other divisions of the pIIb are asymmetric and involve asymmetric partitioning of NUMB. Figure adapted from [14].

At the molecular level, it has been shown that NUMB acts by functionally inhibiting the NOTCH pathway [15]: the evidence that led to this conclusion came from experiments performed in the SOP system, where it was clear that gain-of-function *NOTCH* mutations phenocopied *Numb* loss-of-function [15]. Finally, NUMB and NOTCH were shown to interact physically [15].

Similarly to the SOP system, NUMB also acts as a cell fate determinant in neurons of the central nervous system (CNS) in *Drosophila* [3,4] and in mammals [7]. The strongest demonstration of this came when the role of NUMB in the development of the CNS in mammals was analyzed for the first time in knock-out mice, and it was shown that loss-of-NUMB led to severe CNS alterations [16], putting NUMB and NOTCH linked to ACD in a true SC compartment.

NUMB localization and subsequent segregation in the *Drosophila* system requires the presence of components of the evolutionarily conserved polarity (PAR) complex: Bazooka (PAR3 in mammals)-Par6-aPKC (atypical protein kinase C) [2,17]. In mammals, there is evidence suggesting that NUMB is similarly asymmetrically partitioned at mitosis during ACD through a process controlled by the PAR3–PAR6–aPKC complex; mammalian NUMB binds to PAR3 and aPKC [18,19] and is phosphorylated (and relocalized) by aPKC [18,20].

NUMB asymmetric cellular distribution may promote distinct fates in stem/progenitor cells by interacting with components of signaling pathways triggered by specific micro-environmental cues. The identity and function of the micro-environmental key factors that crosstalk with NUMB to trigger the cell fate choice are not fully understood as yet. Nevertheless, a number of pathways that control stem/progenitor cell development have been described to interact with NUMB. For instance, NOTCH or Hedgehog (Hh) activation and loss-of-function of p53 promote SC maintenance and expansion [21,22].

2.1.2.2 Endocytosis

For many years, the molecular mechanisms through which NUMB functions remained unclear. Initial hypotheses and interpretations of data describing NUMB counteraction of NOTCH focused predominantly on the NOTCH signaling pathway [15]. Then, it became increasingly clear that NUMB is present in almost all cells, and that, in the great majority of these, cell division and the subsequent NUMB segregation at mitosis, is symmetric. But, in some settings, the asymmetric partitioning of NUMB, and consequently different cell fate specification, leads to biochemical asymmetry, suggesting that NUMB is involved in a basic function in cellular regulation.

The first indication of how NUMB could function, derived from the study of protein-protein interactions in the endocytic network [10,23-25]. h-NUMB was found to interact with the EH domain of two endocytic proteins, epidermal growth factor receptor substrate 15 (Eps15) and epidermal growth factor receptor pathway substrate 15-like 1 (alias Eps15R, Eps15L1) [26-28], suggesting a putative involvement of NUMB in processes connected with the transport and sorting of molecules within the cell [10,29]. Subsequently, NUMB itself was described as an endocytic protein [30], based on its subcellular localization in endocytic organelles, its co-trafficking with internalizing receptors, its interaction with the major clathrin adaptor AP2 and the ability of dominant negative NUMB mutants to inhibit both constitutive and ligand-induced endocytosis [30]. In the following years, a number of studies pointed to two major levels of involvement of NUMB in internalization [31-34] and recycling [35,36], consolidating the role of NUMB in endocytosis. However, it should be pointed out that the molecular mechanisms through which NUMB affects recycling are only now starting to be addressed.

2.1.2.3 Cell adhesion, cell migration and epithelial-mesenchymal transition

The role of NUMB in endosomal trafficking of transmembrane receptor proteins, made clear an additional function in the regulation of cell adhesion. Indeed, NUMB has been reported to physically interact via its PTB and C-terminal domains [37] with the cadherin/catenin complex, which is the association of E-cadherins, alpha-catenins and beta-catenins with the actin cytoskeleton. This cadherin/catenin complex is involved in the regulation of plasma membrane dynamics, cell migration and cell shape [38]. Continuous internalization of cadherins and recycling to and from the cell surface via the endocytic machinery, is required for the maintenance of adherence junctions [18,37]. Moreover, a number of proteins involved in cell-cell adhesion have been identified as binding partners for NUMB, such as cadherins and integrins [39]. Indeed, NUMB has been described to bind integrin-βs [18], thus leading to integrin endocytosis and directional cell migration toward integrin substrates.

The fact that NUMB is responsible for establishing cell adhesion suggests that it could also be involved in cell migration. Indeed, NUMB is also important in directional integrin trafficking in migrating cells, in which NUMB localizes to clathrin-containing structures at the leading edge and around focal adhesions [18]. Depletion of NUMB results in reduced integrin endocytosis and reduced integrin-stimulated cell migration [18].

NUMB also regulates epithelial polarity and cell-cell adhesion in epithelial–mesenchymal transition (EMT). EMT is a critical event in embryogenesis and plays a fundamental role in cancer progression and metastasis [40]. In epithelial cells, under a normal physiological condition to stabilize adherens and tight junctions, NUMB binds to E-cadherin or the PAR protein complex via PAR3 [19]. Knockdown of *NUMB* by shRNA in Madin Darby Canine Kidney (MDCK) cells leads to a lateral mislocalization of PAR3 and aPKC, a decrease in cell-cell adhesion, apical translocation of E-cadherin and beta-

catenin, an increase in cell migration and proliferation and active F-actin polymerization. These data suggest that NUMB has a role in the regulation of polarity, cell-cell adhesion and migration during EMT [19].

2.1.2.4 Role of NUMB in the control of signaling pathways

NOTCH pathway

NUMB was originally identified as an inhibitor of NOTCH signaling in *Drosophila* [1,41]. Activation of NOTCH involves cleavage with Delta-like and Jagged ligands (Figure 4), which promotes the translocation of the NOTCH intracellular domain (NICD) from the membrane to the nucleus, where it converts CSL proteins (acronym derived from mammalian CBF1 and *Drosophila* Su(H) as well as LAG-1) from transcriptional repressors into transcriptional activators, thereby turning on the expression of target genes [42-45].

One theory of how NUMB regulates NOTCH is that NUMB acts as an adapter between NOTCH and its E3-ubiquitin ligase, Itch [46], thus causing the polyubiquitination and degradation of cytoplasmic NICD, but not of a membrane-bound form of NOTCH [47]. Indeed, NUMB was shown to interact with Itch in same region in which NOTCH binds Itch, and the co-expression of NUMB and Itch further enhances the ubiquitination of NICD compared with expression of Itch alone [47].

In addition, to facilitating NOTCH ubiquitination, NUMB may also control the intracellular trafficking of NOTCH, thereby suppressing its function. McGill *et al.* in 2009 demonstrated that NUMB overexpression in mammalian cells leads to NOTCH trafficking, while NUMB deletion leads to NOTCH recycling. These data indicate that NUMB regulates NOTCH post-endocytic sorting events leading to NOTCH degradation in mammals [35].

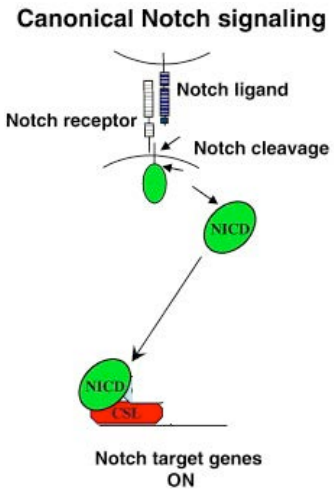

Figure 4. Canonical NOTCH pathway.

The NOTCH pathway has been simplified to include only the principal components. The NOTCH-ligands interaction leads to the release of the NOTCH intracellular domain (NICD). This fragment of NOTCH enters the cell nucleus where it interacts with CSL (CBF-1 in mammals, Suppressor of hairless in *Drosophila*) to modulate transcription. Figure adapted from [48].

Hedgehog pathway

Hh was initially discovered by Christiane Nusslein-Volhard and Eric Wieschaus nearly 30 years ago as a ''segment-polarity'' gene that controls *Drosophila* embryonic cuticle pattern [49]. Hh is a secreted molecule that undergoes autocatalytic cleavage to give an active N-terminal fragment [50], which is modified by addition of a cholesterol moiety at its C-terminus [51]. While there is only a single *Drosophila* Hh gene, three vertebrate homologues have been identified, Sonic (Shh), Desert (Dhh), and Indian hedgehog (Ihh) [52-54]. The most widely studied of the vertebrate Hh genes is Shh, which is expressed throughout the developing CNS, lung, limb, gut, hair-follicle and teeth [55-57].

The Hh pathway is a master regulator of tissue development [22] and much of what is known of the function of this pathway has derived from studies conducted in *Drosophila,* even if many of the key mechanisms of the pathway could be found throughout evolution, even in humans; indeed, the Hh pathway has been implicated in numerous other cellular processes, beside tissue development: from cell proliferation

and differentiation, to migration, to DNA repair [58]. It also plays a key role in tissue repair/regeneration and in SC self-renewal [59]. Not surprisingly, the subversion of the Hh pathway has been implicated in a variety of developmental abnormalities, and in different types of cancers [22,59].

Physiologically, Hh has been demonstrated to interact directly with the transmembrane protein Patched both in *Drosophila* and in vertebrates [53,54]. In vertebrates, this interaction enhanced another transmembrane protein, Smoothened, which activates Gli transcription factors (Gli1, Gli2, Gli3) [60,61]. Gli1 is a Hh-transcriptional target and is a strong constitutive transcriptional activator that enhances its own expression, thus reinforcing the signaling strength [22].

Studies conducted in mouse cerebellar granule cell progenitors (GCPs), demonstrated that the Hh expression keeps GCPs proliferating and undifferentiated, while its termination leads GCPs to differentiate [62]. Interestingly, this transition was associated to NUMB expression in developing GCPs and to the NUMB association with Gli1 and the recruitment of the E3-ubiquitin ligase Itch, thus causing Gli1 proteasome-dependent degradation [62]. This leads to the suppression of Hh signaling and consequent GCPs differentiation, thus arresting growth and promoting cell differentiation. This novel regulatory loop, responsible for subversion of Hh signaling during neural-progenitor differentiation, is NUMB-dependent and may be a relevant event in brain tumorigenesis, giving a more clear indication of NUMB influence on neurogenesis.

p53 pathway

p53 was discovered in 1979 as a 53 kDa protein that formed a complex with the SV40 tumor-virus oncoprotein, the large T-antigen [63,64]. p53 protein was shown to bind to specific DNA sequences [65], acting as a transcription factor and promoting the transcription of selected genes that contain these sequences [66]. Depending on the gene type activated, p53 leads to the activation of different downstream pathways (Figure 5), such as apoptosis [67], DNA repair, growth arrest [68] and cell cycle arrest [69]. p53 protein levels and its activity could be induced by a number of different stress signals such as DNA damage or UV irradiation [70,71], leading to the prevention of genome instability and protection from tumorigenesis [72,73]. Indeed, it became evident that p53 acts as a tumor suppressor in cancer because 50% of all human cancers were shown to contain mutations in both alleles of the p53 gene and p53 was expressed at high levels in many tumor types, where its function is disrupted [74-76].

Another cause of p53 inactivation is oncogene activation and one of the most oncogenic protein regulators of p53 is the E3 ubiquitin ligase Mouse double minute 2 (MDM2, also called HDM2 in humans). MDM2 is responsible for p53 ubiquitination [77,78] and subsequent proteasomal degradation. MDM2 expression is controlled by a regulatory feed-back loop in which it is a transcriptional target of p53 that cause increased MDM2 levels, which in turn lowers p53 levels [79].

A tumor suppressor gene already described for binding and inhibiting MDM2 is ARF, which competes with MDM2 and leads to p53 raising levels and activity [80].

A similar function was attributed to NUMB, which controls the function of p53 by associating and inactivating MDM2, thereby preventing the ubiquitination and degradation of p53 in a normal mammary epithelial cell line, MCF10A [81].

Of note, the downregulatory function of NUMB over MDM2 occurs in the context of a

NUMB/p53/MDM2 tri-complex [81]. This results in increased p53 levels, activity and p53-dependent phenotypes (Figure 5). Indeed, the functional ablation of NUMB in MCF10A cells results in reduced p53 levels and activity, accompanied by DNA-damage, deregulated apoptosis, and cell cycle checkpoint activation response [81].

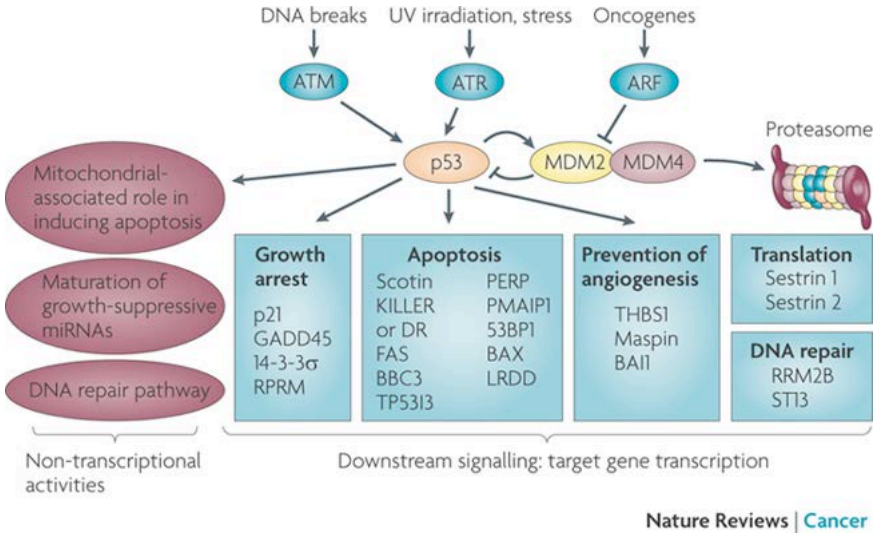

Figure 5. The p53 pathway.

The p53-activated transcriptional and non-transcriptional signaling pathways induced following diverse cellular stresses (DNA breaks, UV irradiation, oncogenes), are depicted in figure. p53 regulates the transcription activation of MDM2, leading to the formation of an auto-regulatory feed-back loop. Figure adapted from [82].

TCTP pathway

Translationally controlled tumor protein (TCTP) was initially identified as a factor implicated in cell growth [83,84]. This protein was named TCTP because its mRNA is controlled at the translational level [85-87].

TCTP is ubiquitously expressed, suggesting an important role in normal physiological functions. Indeed, it has been demonstrated that TCTP is an essential protein in mice since knockout mice deficient in this protein die at embryonic stage day E9.5-E10.5 [88].

In cancer, TCTP plays important roles in a number of cell events, such as cell proliferation, gene regulation, heat shock response, and stress response [89-92].

Since TCTP is overexpressed in many types of cancer cells and silencing of the gene decreases the viability of the cells [93], it was postulated that TCTP acts as an oncogene. Tuynder *et al*. developed a system to select cells with a reverted phenotype using H-1 parvovirus, which preferentially kills tumor cells [94,95]. In reverted cells, TCTP was found to be downregulated. In addition, silencing of TCTP with siRNA leaded to a reverted tumor phenotype, supporting this idea [94-96]. These results suggest that TCTP is directly involved in malignant transformation.

One line of evidence indicates that TCTP-dependent transformation could depend on TCTP regulation of p53 and *vice versa*. It is known that TCTP competes with NUMB for MDM2 binding. As already described above, NUMB enters in a tricomplex with p53 and MDM2, thereby preventing the MDM2-mediated p53 ubiquitination [81]; in this scenario, TCTP competes with NUMB for MDM2 binding, promoting p53 ubiquitination and consequently degradation [97]. In addition, TCTP increases the MDM2-mediated ubiquitination of p53 [97].

2.1.3 The multiple consequences of aberrant regulation of NUMB: NUMB and cancer

2.1.3.1 NUMB as a tumor suppressor in human cancers

Not surprisingly, considering its role in many critical cellular processes, subversion of NUMB has been linked also to important human pathologies, including neurodegeneration [98-100] and particularly, cancer. Experimental evidence demonstrated that NUMB has a tumor suppressor role in *Drosophila* [2,15,19], where it was identified as negative regulator of NOTCH oncogenic signaling through its direct interaction with NOTCH via PTB domain [2,15]. In NUMB mutant larval neuroblasts, disruption of asymmetric self-renewing divisions results in the overproliferation of neuroblasts and ultimately in tumor formation [101]. Remarkably, these tumors can be serially propagated

for years in the abdomen of new adult healthy animals, showing that transformed cells have acquired an immortal phenotype (SC-like phenotype) [101]. This is relevant to cancer because it establishes that NUMB can act as a tumor suppressor in a model system. In mouse, NUMB was also identified as a tumor suppressor in an *in vivo* RNA screen in a model of mouse lymphomagenesis [102].

In human breast cancer, NUMB expression is lost in about 50% of tumors [103] and NUMB-deficient tumors have poor prognosis with respect to NUMB-proficient tumors [81]. Moreover, NUMB-deficient tumors display a less-differentiated phenotype [81,103,104] and expression of CSCs markers; this latter result is interesting, in light of the recent finding that poorly differentiated breast tumors harbor a higher CSC-content than well-differentiated tumors [105].

When NUMB is lost in breast tumors, this single event leads to the subversion of two distinct functional pathways: i) the hyper-activation of the NOTCH-driven oncogenic pathway and ii) the downregulation of the p53-induced tumor suppressor pathway [81,103], thus inducing a proliferative phenotype. The direct relevance of these findings to human breast cancer is seen in the fact that ectopic re-expression of NUMB in NUMB-deficient (but not NUMB-proficient) tumors, inhibits proliferation and reverts NOTCH signaling to basal levels [103]. Moreover, restoration of NUMB levels in NUMB-deficient human primary breast tumor cells rescues p53 expression and sensitizes cells to chemotherapeutic treatments [81]. Conversely, NUMB ablation in NUMB-proficient human breast primary tumor cells confers chemoresistance [81].

Reduced NUMB levels, also correlate with poor prognosis in salivary gland carcinomas, although no additional molecular or mechanistic details are currently known for these tumors [106]. In non-small cell lung carcinomas (NSCLCs), the expression of NUMB is lost in about 30% of tumors [107], again with concomitant activation of the NOTCH pathway, and addiction to high NOTCH levels.

There are also additional NUMB-independent mechanisms leading to NOTCH activation in these tumors (10%), such as gain-of-function mutations [107], and activation of NOTCH correlates with poor clinical outcomes in NSCLC patients without p53 mutations [107]. In both breast cancers and NSCLCs, loss of NUMB expression is due to its exaggerated ubiquitination and ensuing degradation; NUMB protein levels could be restored by the proteasome inhibitor MG-132 and the restoration event is coupled by hyper-ubiquitination in NUMB-deficient, but not NUMB-proficient, tumors [103,107]. Loss of NUMB occurs in the absence of genetic alterations of the *NUMB* locus and in the presence of normal levels of its mRNA [103,107]. It is likely, therefore, that the hyperdegradation of NUMB in cancer is caused by the deregulation of enzymes involved in the ubiquitination process and related to the Ubiquitin Proteasome System (UPS), such as E3-ubiquitin ligases and deubiquitinases, or possibly of regulators of this process, such as kinases or phosphatases. The identification of such enzymes responsible for loss-of-NUMB in cancer, therefore, offers new possibilities in the development of targeted therapeutic strategies capable of restoring physiological levels of NUMB in NUMB-deficient cancers.

2.1.3.2 Mechanisms of action of NUMB in cancer: the cellular level in the control of the SC compartment

The tumor suppressor role of NUMB in cancer could be related to its ability to control stem/progenitor cell fate. It has been known for many years that only a fraction of the cells in a human tumor can give rise to tumors when transplanted in immunocompromised mice [108,109]. These cells are defined as cancer stem cells (CSCs), and the hypothesis contemplates that CSCs are the only cells capable of self-renewal (and thus of tumor transplantation) (Figure 6). Thus, it is conceivable that NUMB is the target of transformation in the SC compartment.

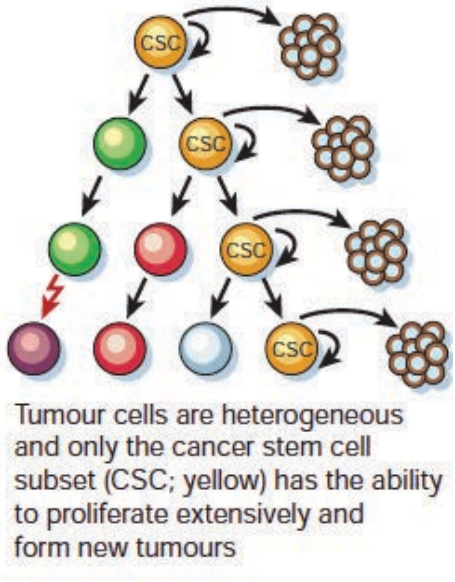

Figure 6. The CSC theory.

Despite most cancer cells have only limited proliferative potential, a subset of them can form new tumors on transplantation and proliferate extensively in clonogenic assays. The model shown predicts that a distinct subset of cells is enriched for the ability to form new tumors, whereas most cells are depleted of this ability. Figure adapted from [108].

2.1.3.3 Mechanisms of action of NUMB in cancer: the circuitry level

The tumor suppressor function of NUMB is easily explained at the biochemical and molecular level by the multiple functions of NUMB connected with growth promoting and growth suppressing circuitries (Figure 7). For example, in the absence of NUMB, both NOTCH and Hh signaling are augmented, with pro-proliferative and anti-differentiative effects, while the signaling of the tumor suppressor p53 is attenuated. Indeed, hyperactive NOTCH and Hh functions has been described in several tumors, such as liver, lung, and breast tumors [22,48].

In addition, subversion of NUMB is predicted to have a major impact on the entire homeostasis of endocytosis, itself proposed as a tumor suppressor mechanism [110-112].

Finally, the alteration of many polarity functions, connected with the PAR complex [113-115], could contribute to transformation events, such as the deregulation of PAR complex

activity as a key factor for initiation of transformation [19], initiated or sustained by loss-of-NUMB. From this point of view, the recent implication of NUMB in the control of EMT is particularly interesting: loss of NUMB causes a loss of adherent junctions [37], comprising a phenotype consistent with the disruption of cadherin function in mouse radial glial cells (RGCs) [37]. These cellular phenotypes are characteristic of EMT, which – in turn – is a strategy adopted by tumor cells to acquire invasive properties, and resistance to cell death, senescence, immunosurveillance, immunotherapy and chemotherapy [40,116,117], thus confirming the involvement of NUMB in tumor-related phenotypes.

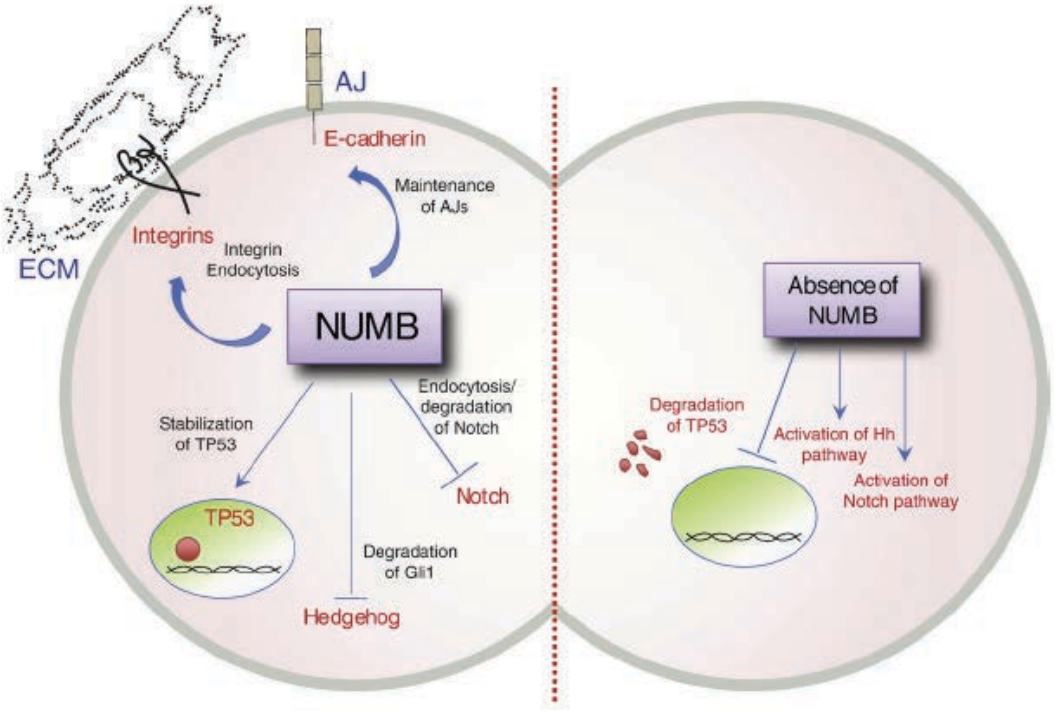

Figure 7. NUMB in cancer.

The figure depicts a "hypothetical division" of a mammalian SC, with NUMB segregating into one of the daughter cells. The pathways that would be present in the daughter that inherits NUMB (on the left), and in the daughter that does not inherit it (on the right), are shown. The impact on NUMB in cancer (viewed from the perspective of the SC hypothesis of tumorigenesis) would result from loss of NUMB in the cell that physiologically inherits it, and on the actual target of transformation. Figure taken from [14].

2.2 THE UBIQUITIN PROTEASOME SYSTEM (UPS)

2.2.1 Polyubiquitination is a multi-step phenomenon: E1, E2 and E3 enzymes are the players

Ubiquitin is a 76-residue polypeptide that acts as a small modifier molecule that labels proteins in a highly specific manner. Like phosphorylation, ubiquitination is a phenomenon relevant both in physiological, as well as pathological, cellular mechanisms [118]; the progression of cell cycle [119], the induction of inflammatory response [120] and DNA repair [121] are just a few of the many processes regulated by ubiquitination.

Substrates could be marked with a polymer of ubiquitin (polyubiquitin chain) or they could be marked with one or a few ubiquitins. In the first case they are destined for a multisubunit ATP-dependent protease known as the 26 proteasome [118,122,123], while the other ones are targeted for endocytosis, to be finally proteolyzed in the lysosomes [124] (Figure 8).

Polyubiquitination usually results in the formation of a bond between the C-terminus of ubiquitin (G76) and the amino group of a substrate lysine residue. Ubiquitin conjiugation could involve seven acceptor lysine residues, which could create ubiquitin chains different in terms of topology, length and functional outcomes [125]. Indeed, the linking between lysine 48 (K48) and G76 leads substrates to be selectively targeted to the proteasome [126-128], while the linking between lysine 63 (K63) and G76 to form the multichain of ubiquitins leads to non-proteolytical signaling [126-128], such as the enzymes activation or inactivation, the protein trafficking regulation or the assembly of protein signaling complexes [129-132].

Substrate targeting by UPS occurs via a two-step process: covalent attachment of multiple ubiquitin molecules to the protein substrate (polyubiquitination), followed by

substrate degradation by the 26S proteasome [133]. The attachment of ubiquitin to a substrate requires the consecutive action of three enzymes [118]: i) an activating enzyme (E1), which activates ubiquitin by the formation of a thioester bond; ii) a conjugating enzyme (E2), that transiently carries the activated ubiquitin molecule, and iii) a ligase (E3) that transfers the activated ubiquitin from the E2 to a lysine residue in the substrate protein [134]. A hierarchical organization of the enzymatic conjugating cascade can be described: there is one E1; a significant but limited number of E2s, each of which may interact with several E3 ligases, and a much larger number of E3 ligases, which can recognize more than one substrate, and cooperate with one or a few E2s [118,123].

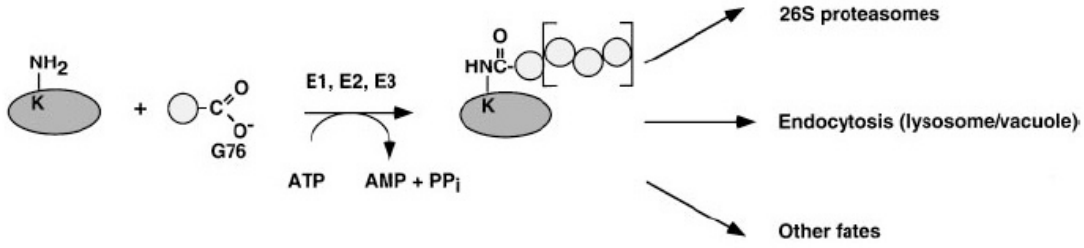

Figure 8. Overview of signaling by ubiquitin.

The substrate is represented by the dark gray oval, and the ubiquitin by the light gray circle (with carboxyl group of G76). The number of ubiquitins conjugated to the substrate may vary (brackets). Depending on the Lys-48/Lys-63 ubiquitin conjiugation, the substrate undergoes different fates, as indicated by arrows. Figure taken from [135].

2.2.1.1 Ubiquitin-activating enzyme (E1)

From the yeast *Saccharomyces cerevisiae* to humans, there is only one E1 enzyme responsible for the activation of ubiquitin for the entire array of downstream conjugating enzymes [136,137]. At the beginning of the reaction, a ubiquitin adenylate intermediate (formed from the binding of MgATP and then of ubiquitin), serves as the donor of ubiquitin to a cysteine in the E1 active site. Each fully loaded E1 molecule carries a thiol-linked ubiquitin, which is transferred to the next enzyme in the conjugating cascade, the E2, through a transthioesterification reaction, in which an E2 catalytic cysteine attacks the backside of the E1-ubiquitin complex [138].

Throughout this mechanism, the E1 enzyme is bound to two ubiquitin molecules, catalyzing also ubiquitin C-terminal acyl adenylation [139]. This secondary ubiquitin does not form the same thioester complex described previously and its function remains largely unknown even if it is believed that it may promote conformational changes of the E1 enzyme during the transthioesterification process [140].

Indeed, E1 has minimal affinity for ubiquitin prior to the binding of ATP [134,138], which suggests that an ATP-dependent conformation change may be necessary to increase the accessibility of a ubiquitin binding site [141], even if the E1 structure-function relationship remains poorly characterized.

2.2.1.2 Ubiquitin conjugating enzyme (E2)

After the activation of ubiquitin by E1, the activated ubiquitin is then transferred to an E2 cysteine, before binding the E3 for substrate attachment.

All E2s share a conserved core domain consisting of ~150 amino acids and they differ for N- or C-terminal extensions, which confer the specificity for the interactions with a specific E3 ligase. As consequence, even if they share common features among each

others, E2 enzymes are responsible for distinct biological functions [142].

Indeed, E2 enzymes are present in all eukaryotes, underlying the significant impact of Ub systems in biology, and genes encoding for E2 proteins are present throughout the genome [143,144].

The protein family has become larger during evolution: lower eukaryotes have fewer E2 enzymes than higher eukaryotes (16 E2 enzymes in *Saccharomyces cerevisae* vs 35 described in humans) [143]. A wide range of tissues and cell types have been found to contain ESTs, mRNAs, and proteins of E2 enzymes, thus indicating a general involvement of these enzymes in ubiquitin conjugation.

2.2.1.3 E3 ubiquitin ligase families: HECT vs. RING ligases

The E3-ubiquitin ligases catalyze the final step of the polyubiquitination cascade, thus conferring a high degree of specificity and selectivity towards their target substrates; for that reason, they are considered to be the most important components of the UPS. As a consequence, they are the most structurally complex and diverse enzymes in the pathway, each responsible for the surveillance of a specific set of target proteins [145]. Based on sequence motifs and the mechanism of ubiquitin conjugation, E3-ubiquitin ligases can be divided into three major classes: i) the HECT (Homologous to E6-AP C-Terminus) E3s; ii) the monomeric (or dimeric) RING (Really Interesting New Gene) E3s; iii) the multimeric RING finger E3 complexes (Figure 9).

i) The HECT E3 ligases

The peculiar feature, from a structural point of view, of this E3 subfamily is the presence in the C-terminal region of the HECT domain, that was originally characterized in the E6-associated protein (E6-AP) and is the region responsible for the association with the E2, and for the catalytic E3 activity, a characteristic which distinguish the HECT from the

other types of E3 ligases [146].

First of all, they act through three steps: i) binding to an E2; ii) forming a ubiquitin-thioester intermediate with the catalytic Cys residue located at the C-terminus of the HECT domain for the loading of ubiquitin; iii) promoting substrate ubiquitination by the transfer of ubiquitin to the target protein.

The HECT-type E3 family can be classified into three further subfamilies, differing for their protein-protein interaction domains, which are the part of the protein determing the substrate specificity: HECT E3s containing RCC1-like domains (RLDs), C2-WW-HECT E3 ligases possessing tryptophan-tryptophan (WW) domains, and Single-HECT E3 ligases lacking either RLDs or WW domains [147].

The intrinsic catalytic activity of the HECT family, makes these E3 ligases to be an easy target for drug development in anticancer therapy.

ii) The monomeric (or dimeric) RING E3 ligases

The RING finger E3 ligases bind the E2 through the RING finger motif containing a Zn2+ binding domain. While monomeric (or dimeric) RING finger proteins bind both the E2 and the substrate, the RING finger protein belonging to the multimeric RING finger complexes, binds the E2 but not directly the substrate, which is recognized by other members of the complex [148,149].

The classification between mono and dimeric RING E3 ligases is due to the diffferent RING-type domains found in many different structural contexts, which can give rise to homodimers and heterodimers instead of single-chain enzymes.

Homodimeric RING-type E3 ligases include cIAP, RNF4, BIRC7, IDOL, and the U-box proteins (a new class of E3 ligases containing a 70 amino acid U-box domain) CHIP and Prp19 [150-156]. Examples of well-characterized heterodimeric E3 ligases include BRCA1–BARD1 or MDM2–MDMX (HDMX/HDM4 in humans).

While for homodimeric RING E3 ligases, both RINGs have the intrinsic capacity to functionally interact with E2s, this appears not to be the case for some heterodimeric RINGs, such as BRCA1–BARD1 or BRCA1–RING1B, in which only one dimer is able to interact with E2s [157-159]. Usually the RING domain is responsible for dimerization, even if some RING-type E3 ligases have been shown to dimerize or form oligomers through domains that are structurally distinct and remote from the RING [125,160,161].

iii) The multimeric RING E3 ligases

There are RING-type E3 ligases that exist as multi-subunit assemblies. The most well-known example of such complexes are the Cullin-RING Ligases (CRLs) [148,162], which contain a small RING protein (in most cases RBX1/ROC1/Hrt1) and a Cullin-family scaffold protein (CUL-1,2, 3, 4a, 4b, 5, or 7), which interacts directly with the RING-domain enzyme (Figure 9) through its C-terminal domain [149].

At the N-terminus, the Cullin protein is linked to an adaptor protein through cullin-repeat motifs; this adaptor, in turn, binds another factor, that specifically recognizes the substrate to be target for ubiquitination [148,162].

The prototypical CRLs are exemplified by the Cul1-containing complexes, commonly referred to as the Skp1-Cullin1-F-box (SCF) ligases. SCF ligases are composed of the small RING protein RBX1, the scaffold protein, Cullin 1, the adaptor protein, Skp1, and an F-box substrate-specific factor, of which ~70 members have been identified [148,149,163]. The ligase activity of SCF is determined by the cullin-RBX complex, which is responsible for the transfer of ubiquitin from the E2 to protein substrates [164], while the specificity of the SCF is determined by the F-box protein that bridges the ligase complex to its substrates. The F-box domain in the F-box protein mediates its interaction with SCF, while the WD40 or LRR (Leucin Rich Region) domains mediate interactions with the

substrates [165]. A single F-box protein can recognize and target multiple substrates (e.g. Skp2 targets p27, p21, p57), and different F-box proteins can recognize and target the same substrate (e.g. cyclin E is targeted by both Skp2 and Fbxw7). Interestingly, a single F-box protein can target the degradation of several substrates with opposite biological functions (e.g. Skp2 targets p21/p27, as well as cyclin A/D1/E) [166]. Thus, different combinations of the SCF components determine distinct substrate specificities and will thus be associated with distinct biological functions.

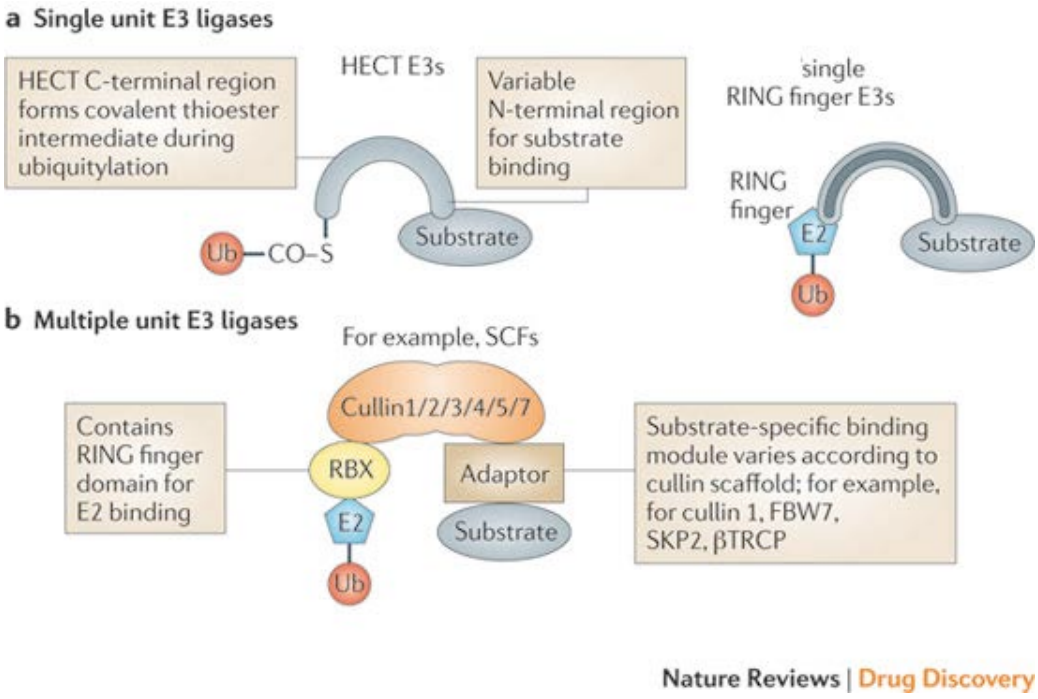

Figure 9. Classification of E3 ligases.

There are three major classes of ubiquitin ligases: HECT domain proteins, monomeric RING finger E3 ligases and multisubunit RING E3 complexes. a. HECT domain E3 ligases transfer ubiquitin (Ub) from an E2 to E3 via transthiolation and then ubiquitin is transferred directly from E3 to a substrate amino group. .b. The RING finger E3 ligases bind the E2 through the RING finger motif containing a Zn2+ binding domain. Monomeric RING finger proteins bind both the E2 and the substrate. In the multimeric RING finger complexes, the RING finger protein binds the E2 while other proteins in the complex bind the substrate. Figure adapted from [167].

2.3 TARGETING THE UPS SYSTEM IN CANCER TREATMENT

Ubiquitination by UPS system controls many proteins involved in cellular mechanisms such as apoptosis, cell cycle progression, and gene transcription, which are all relevant to tumorigenesis [168,169]. Indeed, many components of the UPS are associated with cancer and could be potential targets for therapeutic strategies against the disease [170,171]. In recent years, substantial progress has been made in understanding the molecular basis of ubiquitin action in cancer-relevant processes. (Figure 10). For example, the HECT-type E3 ligases were found to have an oncogenic potential after the identification of a number of their substrates with a tumor suppressor activity, as well as the presence of genetic aberrations and abnormal expression of some of the family members in human cancers. Moreover, the dysregulation of the HECT E3 adaptors could also influence cellular transformation, a typical cancer-related feature [147].

A lot of SCF E3 ligases, through specific degradation of their substrates, are responsible for the regulation of many biological processes; this is because these substrates are involved in regulation of basic cellular mechanisms, such as DNA replication, cell cycle progression, signal transduction and gene transcription [148,149,172]. Thus, it is not surprising that aberrant regulation of SCF E3 ubiquitin ligases leads to hyperproliferation, genomic instability, and cancer [172]. Among the components of SCF, some are oncogenes (e.g. Skp2) that promote degradation of tumor suppressors and are amplified and/or overexpressed in human cancers, whereas others are tumor suppressors (e.g. Fbxw7) that target oncoproteins for degradation and are mutated in human cancers.

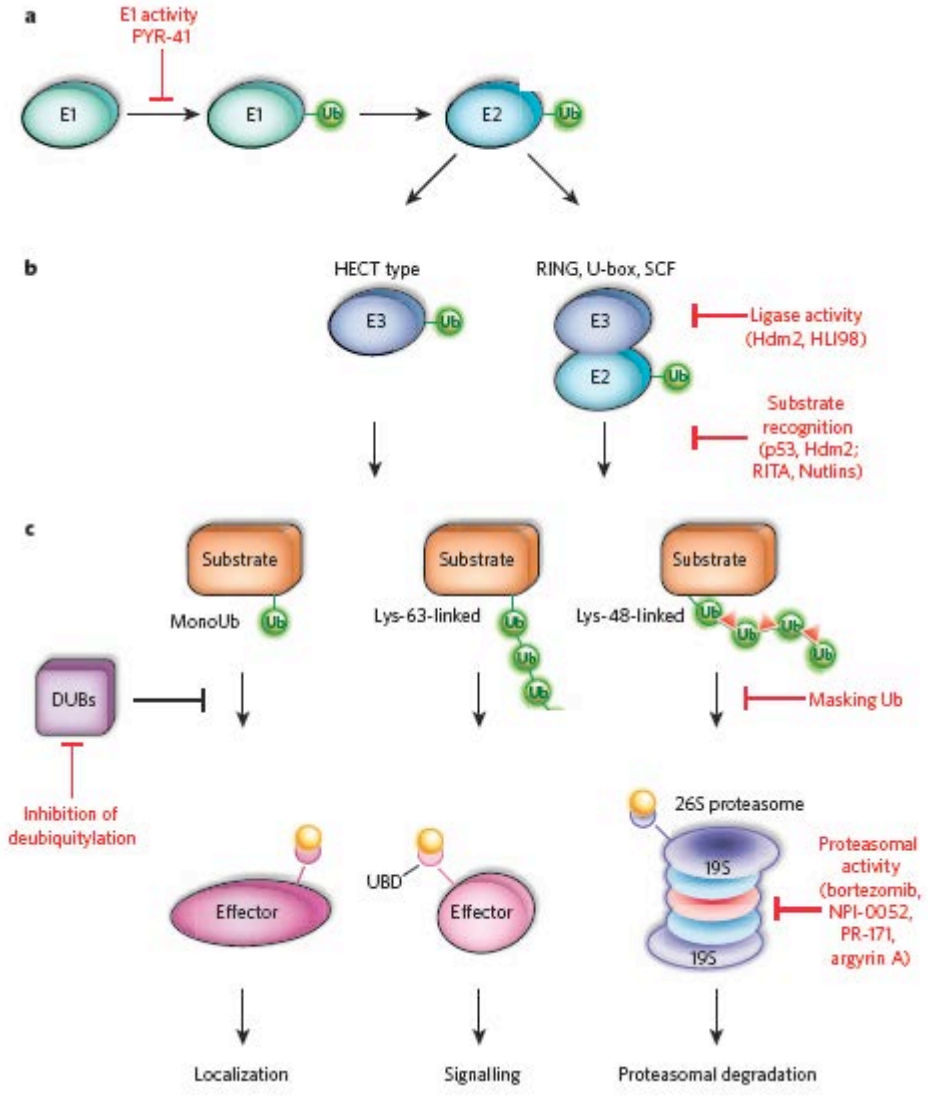

Figure 10. The ubiquitin proteasome system offers several possibilities for therapeutic intervention. Known points of intervention and appropriate drugs are shown in red. a, Global changes can be achieved by blocking early steps of the conjugation cascade, for example at the level of the E1 and E2 enzymes. b, The inhibition of distinct E3 enzyme activities allows for more specific interference. By targeting the E3 ligase-substrate binding, it is possible to detect a specific substrate (the use of RITA or the Nutlins is a clear example). The deubiquitinating enzymes (DUBs) are another example of this mode of action. c, Ubiquitin receptors then recognize the ubiquitinated substrate and mediate the cellular response, or DUBs can deubiquitinate the substrate. Another highly specific way of interfering with ubiquitination process would be to compete with the ubiquitin-binding domains (UBDs) of specific effector proteins. Proteins polyubiquitinated in Lys-48 are destined to proteasome degradation. Substances that block enzymatic activity of proteasome, such as Bortezomib, NPI-0052, PR-171 and argyrin A, are already available. Figure adapted from [170].

2.3.1 Targeting the proteasome in tumors: the case of Bortezomib and other drugs

Alterations in the proteasome are associated with several human diseases, such as cardiac dysfunction, neurodegenerative disorders, cachexia and rheumatoid diseases [173]. Initial screening of the National Cancer Institute's (NCI) tumor cell lines revealed that the boronic-acid derivative Bortezomib (Velcade®) is active against a broad range of tumor types [174].

From the molecular point of view, the mechanism of action of Bortezomib involves the inhibition of a transcription factor, the nuclear factor κB (NF-κB) [175]. NF-κB is activated in response to cell stress induced by cytotoxic agents, radiation, or DNA damage among others, thus controlling cell survival. NF-κB is normally bound in the cytosol to the inhibitor κB-α (IκBα) and translocates to the nucleus when IκBα is ubiquitinated and degraded, activating the transcription of target genes [176]. Bortezomib blocks the activation of NF-κB by preventing proteasomal degradation of IκBα, thus promoting apoptosis of cancer cells, but also sensitizing these cells to chemotherapy [177-179], radiation [180], or immunotherapy [181].

Bortezomib-mediated proteasome inhibition, in certain cell types, promotes cell death, not through the inhibition of NF-κB signaling, but by inducing endoplasmic reticulum (ER) stress, which in turn promotes cell death [182].

Indeed, many successful preclinical studies *in vivo* conducted in multiple myeloma (MM), adult T-cell leukemia, as well as in solid tumors such as lung, breast, prostate, pancreatic, head and neck, and colon cancer, and melanoma, have shown the benefits of Bortezomib in terms of antitumor activity [175,177,181,183-188].

In particular, in a xenograft model of MM, Bortezomib treatment leaded to inhibition of tumor growth, an increase in cells survival, and a decrease in tumor angiogenesis [185]; in murine xenograft models of prostate [189] and pancreatic cancer [187], after Bortezomib

treatment, an inhibition of almost 70% in tumor growth in both cases was observed; in murine xenograft models of head and neck [175], colon cancer [177], as well as melanoma [184], proapoptotic and/or antiangiogenic effects were determined. Finally, an evaluation of the effects of Bortezomib in murine xenograft models of both lung and breast cancer was also conducted [188], demonstrating that treatment with Bortezomib led to a reduction in tumor growth as well as a decrease in the number of metastases and of the surviving fraction of breast tumor cells [188].

A number of clinical studies evaluating the activity and safety of Bortezomib have been conducted in patients with MM or with other types of cancer, such as relapsed mantle-cell lymphoma, colon, ovary, lung, melanoma, head and neck, and prostate [190-193]. For MM and non-Hodgkin's lymphoma (NHL), phase III trials have been conducted using Bortezomib alone or in combination with other anti-myeloma agents [193]. In addition to hematologic malignancies, many clinical trials are underway employing Bortezomib in combination with other anticancer agents against solid tumors [194].

After these promising results with Bortezomib, new proteasome inhibitors have been developed, such as PR-171 (Carfilzomib), for which a clinical trial is already ongoing, NPI-0052 (Marizomib), CEP-18770 (Cephalon) [195-197] and arginin A [198]. Importantly, it has already been demonstrated, in *in vitro* studies on cancer cells, that it could be possible to combine low doses of proteasome inhibitors, such as NPI-0052 and Bortezomib, to obtain synergistic effects [199]. The outstanding challenge in the clinic is to define appropriate combinations, as well as doses of the different proteasome inhibitors described above, which offer therapeutic advantages over Bortezomib. Moreover, development of proteasome inhibitors, with distinct substrate selectivity, improved bio-availability and lower toxicity, may open the door to widespread usage in solid tumors.

Overall, considering the remarkable therapeutic results of Bortezomib as a single agent or in combination with other anticancer agents [200], the use of proteasome inhibitors promises to be one of the most important therapeutic strategies in clinical oncology.

2.3.2 Targeting the ubiquitin ligase system

Several E3 ligases have been linked to the development of cancer, largely because of their ability to trigger the degradation of oncogenes or tumor suppressors [171,172]. Well-studied E3 enzymes with oncogenic capacity are the RING-type E3 enzyme MDM2, a crucial negative regulator of the tumor suppressor protein p53 [77,78], and the multi-subunit SCF ligases that regulate cell cycle progression [201], such as Skp2, a substrate-specific subunit of the SCF ligase complex, whose inactivation in tumors expressing low levels of the cell cycle inhibitor p27 is likely to be beneficial. It was initially believed that targeting the active site of E3 enzymes or their interaction with substrates would create selective drugs with fewer side effects respect to proteasome inhibitors.

Thus, following the hypothesis that E3 ligases are potential therapeutic targets, in the past decade, the biotech and pharmaceutical industries have sought to develop inhibitors and agonists of ubiquitin ligases [202-205]. The most well-known examples are the Nutlins, which inhibit p53/MDM2 binding or small compounds called RITA (2,5-bis(5-hydroxy- methyl-2-thienyl)furan), which have been shown to bind the amino terminus of p53 and to promote growth arrest [206].

Indeed, given the lack of specificity of proteasome inhibitors, it may be useful taking advantage of the enzymatic nature, abundance and specific substrate recognition properties of E3 ligases, which could become a more specific and effective therapeutic targets with the possibility to limit side effects.

From a cancer point of view, the substrate specificity of an E3 ligase determine the ability of the ligase to behave as either an oncogene or tumor suppressor, because of its

control of the ubiquitination status of substrates with tumor suppressor and oncoprotein function. For that reason, the inappropriate degradation of these substrates due to aberrant expression, dysfunction or deregulated regulation of E3 ligases could be tightly linked to malignant transformation and chemoresistance, making E3 ligases attractive targets for cancer therapy.

3 AIMS AND RATIONALE OF THE STUDY

NUMB has been identified as a tumor suppressor in different types of cancers, such as breast, lung and salivary gland carcinomas [103,106,107]. In breast and lung cancer, loss of NUMB expression was shown to be due to its excessive ubiquitination and ensuing proteasomal degradation, as confirmed by the ability of the proteasome inhibitor MG-132 to restore physiological NUMB levels in NUMB-deficient tumor cells [103,107]. Thus, it is likely that deregulation of components of the UPS could underlie loss of NUMB in cancer.

Ubiquitination is a post-translational modification that was originally described as a tagging mechanism for misfolded and disused proteins, which targets them for proteasome-mediated degradation. Now, ubiquitination is implicated in almost all cellular processes involved in cell growth and survival. It is therefore not surprising that alterations in ubiquitin and UPS have been detected (i.e.: mutations/overactivation of E3 ligases and so on) in many human pathologies, including cancer, in which it has a role in the genesis of different types of tumors [130,172]. This is, for instance, the case of some HECT-type E3 ligases with oncogenic potential, such as Huwe1, WWP1 or Smurf1, whose genetic aberrations and altered expression underpin the dysfunction of a number of tumor suppressor molecules comprised among their protein substrates in different types of human cancers, influencing also cellular transformation [207-210].

Moreover, some components of the SCF complex, such as Skp2, have oncogene properties and lead to the degradation of tumor suppressors and are amplified and/or overexpressed in human cancers, whereas some others behave as tumor-suppressors

(e.g. Fbxw7) and, once mutated in human cancers, loose their ability to direct degradation of oncoproteins [172].

Based on the accumulated knowledge of the involvement of its deregulation in cancer, the UPS has emerged as an attractive target for cancer therapy. In example, Bortezomib (originally codenamed PS-341 and marketed as Velcade® or Cytomib®) represents the first therapeutic proteasome inhibitor to be tested in humans and it is currently approved for the treatment of relapsed multiple myeloma and mantle cell lymphoma [193]. Bortezomib has also been tested as a single agent in preclinical studies and clinical trials for adult T-cell leukemia, lung, breast, ovary, prostate, pancreatic, gastric, head and neck, colon cancer, melanoma and multiple myeloma [176,190,193].

A new generation of proteasome inhibitors has been developed, such as MLN9708, CEP-18770, PR-047 and NPI-0052 [211], in order to resolve some of the key pharmacological issues associated with Bortezomib, such as poor efficacy in solid tumors and therapy-associated peripheral neuropathy. Extensive clinical evaluation of these second-generation inhibitors is now required.

Among the UPS players, the E3 ligases are considered to be the most important components of the ubiquitin machinery in terms of targetability, as they are responsible for substrate specificity. Well known examples of E3 ligases that have been described as putative therapeutical targets for cancer treatment are MDM2, Fbxw7 or components of the multimeric SCF-β–TrCP complex [202,203,205].

In line with this rationale, the aim of this PhD thesis was the identification of specific E3 ligases involved in the regulation of NUMB degradation in NUMB-deficient tumors. The long-term aim is the development of targeted therapeutic strategies capable of restoring physiological levels of NUMB in NUMB-deficient cancers.

To reach this goal, we proposed a high-throughput RNA-interference (RNAi)-based

screening of all enzymes belonging to human E3 ligase families. To set-up the high-throughput RNAi screening, it was first necessary to identify a suitable cellular model system, which recapitulates the alteration underlying loss of NUMB in NUMB-deficient cancer. As the role of NUMB as a tumor suppressor has been best described in breast tumors, we focused on cell models of NUMB-deficient breast cancers. A suitable cell model system for the RNAi screening would be a breast cancer cell line that expresses low basal levels of NUMB, compared to normal breast epithelial cells, which can be restored to physiological levels upon proteasome inhibition. To identify such a cell line, we screened NUMB levels following MG-132 treatment in a panel of breast cancer cell lines (see section 4.2 of Results). The second step in setting up the high-throughput screening was to optimize an ELISA-based assay to efficiently detect NUMB protein levels in a 384-well format (see sections 4.3 of Results).

Having set up the high-throughput RNAi screening platform, we automatized the assay to perform different rounds of screening, which ultimately yielded a list of candidate E3 ligases potential regulators of NUMB stability (section 4.4 of Results). We then performed a functional validation of selected candidates by investigating the effects of their silencing on NUMB levels in amenable NUMB-deficient cell lines as well as in primary tumor cells derived from breast and lung cancers (see section 4.5 of Results). Then, with the aim to elucidate the molecular mechanisms responsible for NUMB degradation in cancer, we investigated the possible interaction of NUMB with its putative negative regulators (see section 4.5.7 of Results).

Finally, to assess the therapeutic value of targeting the UPS in NUMB-deficient breast cancers, we developed a pre-clinical model based on the xenograft of NUMB-deficient and NUMB-proficient breast tumor cell lines (see section 4.6 of Results), respectively MDA-MB-361 and MDA-MB-231 and evaluated the consequences of the treatment with the proteasome inhibitor MG-132 on the growth of these cells in xenografted mice.

4 RESULTS

4.1 GENERATION OF A SPECIFIC ANTIBODY AGAINST HUMAN NUMB

All the analyses performed in this thesis work were performed using a monoclonal anti-NUMB antibody (moAb21) generated in house, which recognizes all the four different NUMB isoforms [81]. This antibody has been generated against a peptide corresponding to a sequence unique to the NUMB protein (amino acid residues 537-551) and not present in NUMB-Like (NUMB-L), a protein that shares colinear topology and extensive sequence homology with NUMB [6,10]. In this context, it should be borne in mind that, while loss of NUMB is a well-established alteration in breast cancer [81,103], this does not appear to be the case for the NUMB-L protein [103]. Therefore, the moAb21 monoclonal antibody represents a tool of paramount importance to avoid the confounding effects due to the presence of the NUMB-L protein in the analysis of the ELISA results from the siRNA phenotypic screening based on the determination of NUMB levels upon ablation of E3 ligases in a model of NUMB-deficient breast tumors (see paragraph 4.3 below) .

A new batch of the anti-NUMB moAb21 was freshly produced starting from the corresponding hybridoma (final concentration: 1.99 µg/µl) and tested for its anti-NUMB immunoreactivity in different assays, including immunoblotting (IB), immunoprecipitation (IP) and immunofluorescence (IF) (Figure 11). As expected [81], in the IB analysis of total cell lysates from MCF10A cells, the moAb21 recognized two doublets corresponding to the four described human NUMB isoforms generated by alternative splicing of the *NUMB* mRNA (Figure 11A). The different isoforms result from the presence of two sequence inserts within the PTB domain and the central region of the protein (isoforms 1-4; MW: 72, 66, 71, 65 kDa, respectively) [5,11]. Of note, the two bands disappeared in NUMB-silenced human epithelial MCF10A cells, demonstrating

that the antibody specifically recognizes all the NUMB isoforms (Figure 11A). We also confirmed that the moAb21 antibody recognizes mouse NUMB by performing IB analysis on total lysates of cells coming from murine mammary epithelial cells (Figure 11B). Also in this case, all the four isoforms described for mouse NUMB [12] are recognized by the moAb21 antibody.

We also used the moAb21 to perform IP experiments using total cell lysates from MCF10A cells. IB analysis of immunoprecipitates obtained with increasing amounts of moAb21 showed that the NUMB protein was efficiently enriched in the IP samples compared to the control input, with almost complete immunodepletion of the protein from the total cell lysates achieved already at low antibody concentrations (Figure 11C). Based on these results, we concluded that the moAb21 antibody is able to efficiently recognize the NUMB protein in its native conformation, arguing for its suitability in the ELISA assay (see section 4.3 below). In IF experiments, immunostaining of MCF10A cells with the moAb21 antibody typically showed a plasma membrane/cytoplasmic signal, which is consistent with the expected subcellular localization of NUMB [30] (Figure 11D, red signal). This signal was significantly reduced in NUMB-silenced MCF10A cells indicating the specificity of the moAb21 antibody also in IF assay (Figure 11D, red).

We finally tested the suitability of the moAb21 antibody for immunohistochemistry (IHC) analysis of formalin-fixed paraffin-embedded (FFPE) samples. To this aim, we prepared FFPE samples of NUMB-silenced MCF10A cells to be compared to scrambled siRNA-MCF10A cells, as a control. IHC staining of these paired samples with the moAb21 antibody yielded a signal in control MCF10A cells that disappeared in NUMB-silenced cells, indicating that the antibody specifically and efficiently recognizes NUMB in IHC experiments (Figure 12). Altogether, these results confirmed that we successfully generated a new batch of the NUMB-specific moAb21 antibody that is suitable for use in a wide range of techniques including IB, IP, IF and IHC.

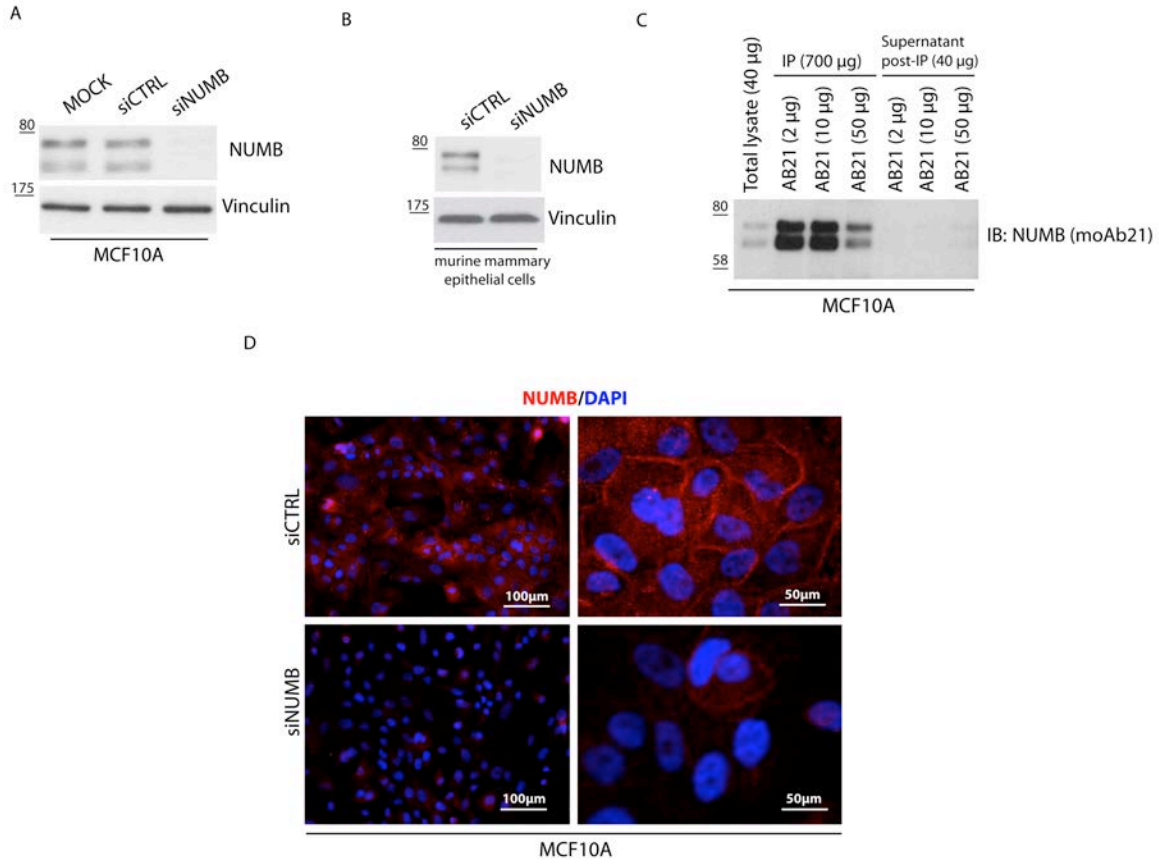

Figure 11. Characterization of the moAb21 monoclonal antibody.

A) Immunoblotting (IB) analysis of control vs. NUMB-interfered human MCF10A cells. Total cell lysates (40 µg) from control (MOCK- and scrambled siRNA, siCTRL) or NUMB-silenced (siNUMB) MCF10A cells were immunoblotted with the moAb21 antibody. Vinculin was detected as a loading control. MW markers are shown on the left of the blots. B) Immunoblotting (IB) analysis of murine mammary epithelial cells. Total cell lysates (40 µg) from scrambled siRNA (siCTRL) or NUMB-silenced (siNUMB) murine mammary epithelial cells were immunoblotted with the moAb21 monoclonal antibody. Vinculin was detected as a loading control. MW markers are shown on the left of the blots. C) NUMB immunoprecipitation (IP) from MCF10A cells. Increasing concentrations of the moAb21 antibody (2, 10, 50 µg) were used to immunoprecipitate NUMB from MCF10A total cell lysates (700 µg). The blot shows enrichment of NUMB in immunoprecipitates (700 µg) compared to the total cell lysate input (40 µg) and the efficiency of NUMB immunodepletion in post-IP supernatants (40 µg). MW markers are shown on the left of the blot. D) Analysis of moAb21 immunoreactivity by immunofluorescence (IF). Scrambled (siCTRL) or NUMB-silenced (siNUMB) MCF10A cells were fixed and stained with moAb21, followed by anti-mouse Cy3-conjugated secondary antibody (red). Nuclei were counterstained with DAPI (blue). Representative overlaid images at two different magnifications are shown. Scale bars: left panels, 100 µm; right panels, 50 µm. Blots and images are representative of 3 repeats.

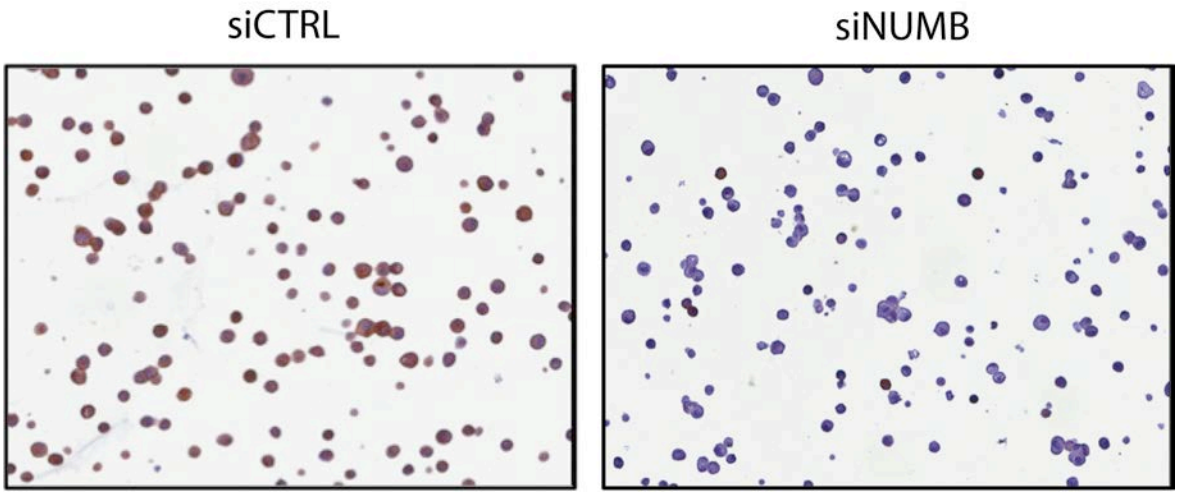

Figure 12. The moAb21 anti-NUMB antibody specifically recognizes the NUMB protein in FFPE samples by IHC analysis.

IHC analysis of FFPE samples of scrambled (siCTRL) and NUMB-silenced (siNUMB) MCF10A cells. Representative images are shown. Magnification 40X.

4.2 IDENTIFICATION OF A CELLULAR MODEL SYSTEM OF NUMB-DEFICIENT BREAST TUMORS SUITABLE FOR HIGH-THROUGHPUT SCREENING.

The overall idea of this thesis work is to identify upstream mechanisms responsible for exaggerated NUMB ubiquitination and ensuing degradation in breast cancer. To this aim we devised a phenotypic RNAi screening using a commercially available siRNA library for E3 ligases (Dharmacon RNAi Technologies), to identify candidate enzyme(s) whose functional ablation is able to restore NUMB levels in a model of NUMB-deficient breast tumors. The first step towards this aim was therefore the identification of a cell-based model system mimicking the alteration of NUMB in breast cancer and suitable for the high-throughput analysis of a large number of candidate hits upon siRNA. Primary tumor epithelial cells isolated from NUMB-deficient breast tumors would represent the ideal cell model for this analysis in that they faithfully recapitulate the molecular alteration of naturally occurring human breast cancers. However, a major hurdle in the use of primary cell cultures in high-throughput studies is the limited amount of cells that can be obtained from human breast biopsy specimens. Therefore, we opted to use an established breast cancer cell line that recapitulates the phenotype of NUMB-deficient primary tumor cells, i.e., the presence of basally low levels of NUMB protein that can be promptly rescued to normal by hindering ubiquitination and consequent UPS-mediate degradation of the protein.

4.2.1 Screening of breast cell lines for NUMB expression.

We first needed to identify a suitable cellular model system to identify a cell line that expresses low basal levels of the NUMB protein, despite the presence of normal levels of *NUMB* mRNA transcripts. We therefore screened a panel of commercially available, non-tumorigenic and tumorigenic breast cell lines for their intrinsic NUMB status, both at the protein and transcript level, by IB and quantitative RT-PCR (q-RT PCR) analysis, respectively. In this screening, we observed that NUMB was expressed to varying degrees in the breast tumor cell lines compared with the non-tumorigenic mammary epithelial cell line MCF10A, which is a well-established model for normal mammary epithelial cells (Figure 13). In particular, MCF10A is a spontaneously immortalized, but non-transformed human mammary epithelial cell line derived from the breast tissue of a patient with fibrocystic changes. MCF10A cells are commonly recognized as a normal breast epithelial cell line because of lack of tumorigenicity in nude mice and lack of anchorage-independent growth. However, some genetic abnormalities have been characterized, in particular the deletion of the locus containing p16-p14ARF and amplification of MYC. MCF10A cells also express wild-type p53 [212]. Among the breast tumor cell lines analyzed, we identified by IB several cell lines with overall low basal levels of NUMB protein compared to MCF10A cells, such as MDA-MB-361, MCF7, BT474 and MDA-MB-415, although differences were also noted in the behavior of the different isoforms across the different cell lines (Figure 13A). All cell lines displayed *NUMB* mRNA levels comparable to those of MCF10A cells, confirming that the low level of NUMB observed in some of these cell lines is due to post-transcriptional events (Figure 13B).

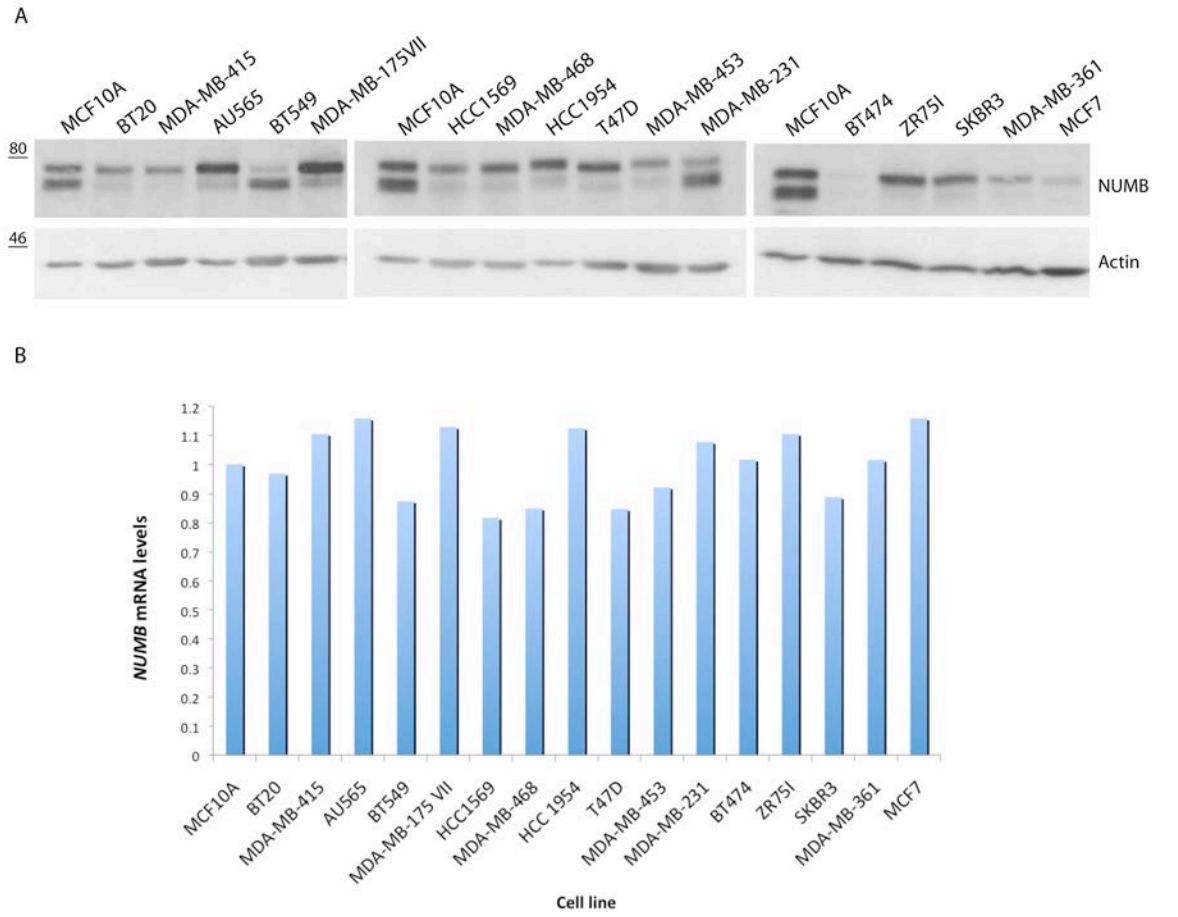

Figure 13. Analysis of NUMB expression levels in a panel of breast cancer cell lines.

A) Total cell lysates (20 µg) from the indicated cell lines were immunoblotted with the moAb21 antibody. The expression level of NUMB in the NUMB-proficient quasi-normal breast cell line MCF10A was used as a reference standard for NUMB expression in the normal mammary gland. Actin was detected as a loading control. MW markers are reported to the left of the blots. B) *NUMB* mRNA expression levels in the indicated breast cancer cell lines were assessed by q-RT PCR analysis. Results were normalized to *NUMB* mRNA levels detected in MCF10A cells.

4.2.2 Analysis of NUMB expression in breast cell lines upon proteasome inhibition with MG-132.

Loss of NUMB expression in primary epithelial cells derived from NUMB-deficient tumors can be promptly rescued by treatment of these cells with the proteasome inhibitor MG-132 [103]. Based on this notion, we set out to investigate whether a similar restoration of NUMB expression could be achieved in the NUMB-deficient breast cell lines identified in our preliminary screening.

To this purpose, we analyzed pre-/post-treatment changes in NUMB expression levels in the panel of selected breast cancer cell lines treated with the proteasome inhibitor MG-132, or with solvent, as a control.

Based on results of this analysis, we decided to select the MDA-MB-361 and BT474 cell lines as models that best recapitulate the alteration of NUMB in NUMB-deficient breast cancer by featuring basally low levels of almost all NUMB isoforms followed by restoration of the protein to physiological levels upon treatment with MG-132 (Figure 14).

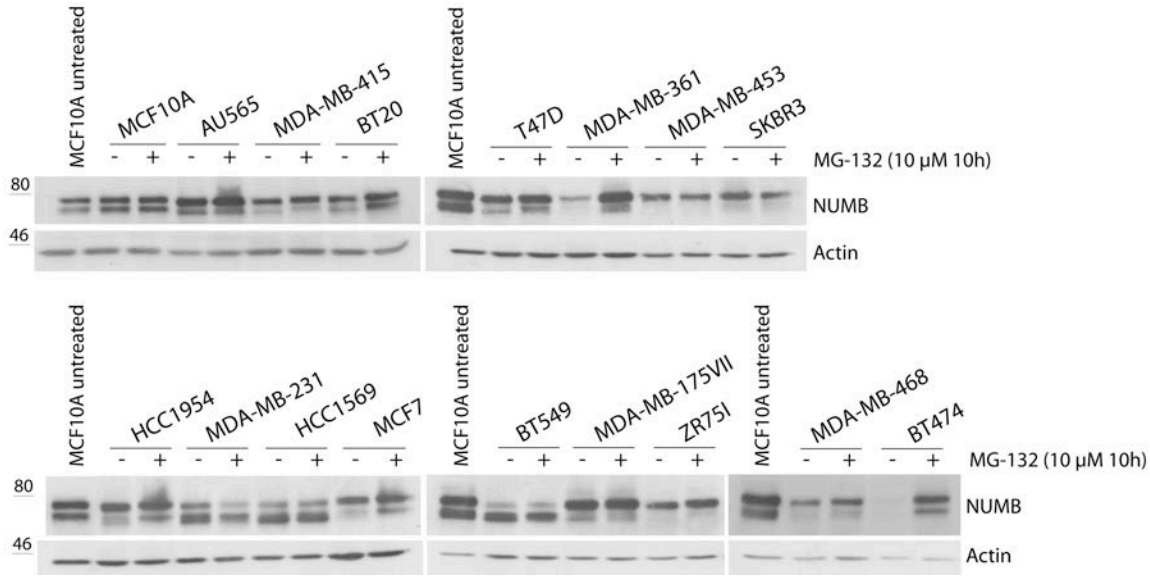

Figure 14. Analysis of NUMB expression in breast cancer cell lines pre-/post- MG-132 treatment.
The indicated breast cell lines were treated with the proteasome inhibitor MG-132 (10 μM for 10 h), or with EtOH (10 μM for 10 hours) as a control, and lysed. Protein lysate (20 μg) was loaded on the gel and NUMB protein levels were determined by IB. The expression level of NUMB in the MCF10A cell line was used as a reference standard for physiological NUMB status in normal mammary epithelial cells. Protein loading was controlled using an anti-actin antibody. MW markers are shown on the left of the blots.

4.2.2.1 Optimization of MG-132 treatment conditions in BT474 and MDA-MB 361 NUMB-*deficient breast tumor cell lines.*

To optimize treatment conditions, we tested different concentrations of MG-132 and treatment times (Figure 15). In BT474 cells, we observed efficient NUMB restoration only after a 6–hour treatment with 20 μM MG-132. In contrast, in MDA-MB-361 cells NUMB restoration was most evidence after a 24-hour treatment with 5 μM MG-132. To control for the efficiency of proteasome inhibition under the different experimental conditions, we analyzed the expression of p53 and beta-catenin, which are known to undergo proteasomal degradation [77,78,213]. We observed an effect of MG-132 on p53 and beta-catenin levels under all conditions confirming the efficacy of the inhibitor. On note, MDA-MB-361 cells do not express p53 due to a mutation in the p53 promoter [214].

Moreover, we analyzed the expression of clathrin and AP2 as internal controls of proteins that, under the experimental conditions used, are insensitive to MG-132 treatment.

From the analysis of the kinetics response of MDA-MB-361 and BT474 cells to different MG-132 concentrations it is possible to conclude that, while MDA-MB-361 cells seem to display a slower rate of degradation of the NUMB protein, evidenced by the fact that full rescue of NUMB expression is achieved with a treatment period of 24 h, this cell line appears to respond to substantially lower concentrations of MG-132, which minimizes the potential toxic and/or off-target effects due to bulk proteasome inhibition. Based on these observations, we concluded that MDA-MB-361 cells better suit the experimental conditions required for the ELISA-based siRNA phenotypic screening, while BT474 might be considered as a tool for subsequent validation of candidate hits stemming out of the screening.

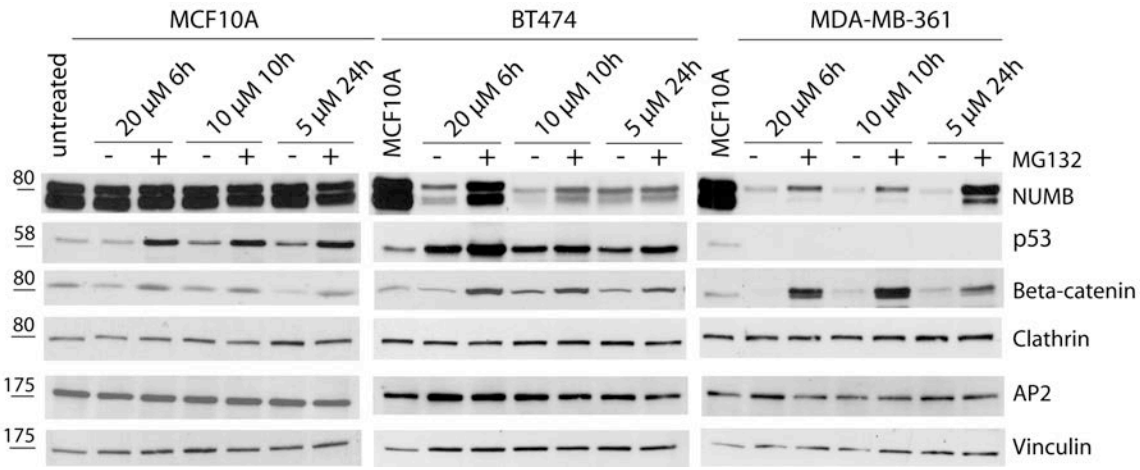

Figure 15. Restoration of NUMB protein levels in BT474 and MDA-MB-361 cells upon proteasome inhibition.

The effect of MG-132 treatment, at the indicated concentrations and time-points, on the levels of NUMB, p53, clathrin and AP2 in the NUMB-deficient breast cancer cell lines, BT474 and MDA-MB-361, and in the NUMB-proficient normal breast cell line, MCF10A, was determined by IB using the indicated antibodies. Protein loading was controlled using an anti-vinculin antibody. MW markers are shown on the left of the blots. Results are representative of 3 independent experiments.

To further confirm the mechanistic link between basally low NUMB expression and aberrant proteasomal degradation in MDA-MB-361 cells, we exposed these cells to increasing concentrations (5 to 500 nM for 24 h) of another proteasome inhibitor, the compound MG-341 (Bortezomib, Velcade®), observing a remarkable restoration of NUMB levels already with low concentrations of this drug (Figure 16). Of note, Bortezomib treatment of the quasi-normal mammary epithelial cell line MCF10A yielded no effects on the basal NUMB expression levels (Figure 16).

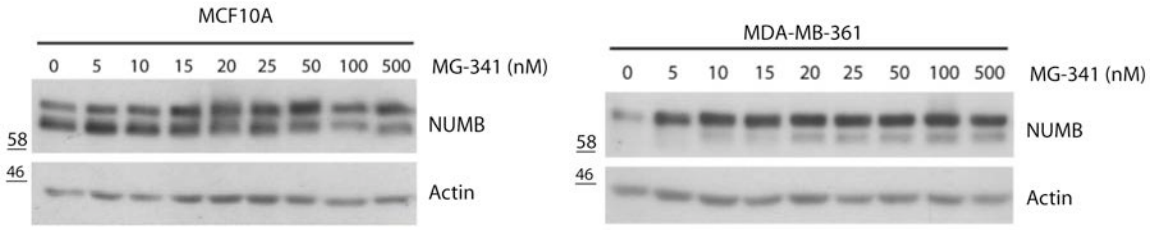

Figure 16. Analysis of the effects of the treatment of the MCF10A and MDA-MB-361 cells with the proteasome inhibitor Bortezomib.

The NUMB-proficient quasi-normal breast cell line MCF10A (left panel) and the NUMB-deficient breast cancer cell line MDA-MB-361 (right panel) were exposed to the indicated concentrations of MG-341 (Bortezomib, Velcade®) for 24 h. NUMB levels were assessed with the moAb21 antibody. Protein loading was controlled using an anti-actin antibody. MW markers are shown on the left of the blots. Results are representative of 3 independent experiments.

4.3 DEVELOPMENT OF AN ELISA-BASED HIGH-THROUGHPUT PLATFORM.

4.3.1 Optimization of a capture ELISA assay to detect NUMB protein.

To perform the RNAi screening in high-throughput mode we opted to use a 384-well plate format. In this format, we are able to use a maximum of 20,000 cells/well. Hence, it was necessary to identify a suitable method for quantifying NUMB protein in such a limited number of cells. For this purpose, we employed a commercially available ELISA capture assay for the quantification of total NUMB levels (DuoSet IC Human/Mouse/Rat Total NUMB, R&D Systems). In this assay, the NUMB protein is captured from total cell lysates using a mouse anti-human NUMB polyclonal antibody coated onto the ELISA plate. Captured NUMB is then detected using a biotinylated sheep anti-human NUMB polyclonal antibody specific for total NUMB, streptavidin-conjugated to horseradish peroxidase (streptavidin-HRP), and a chromogenic HRP substrate, tetramethylbenzidine (TMB) (Figure 17A).

Considering the high degree of homology between NUMB and NUMB-L, we firstly verified, by IB analysis, the specificity of both the capture and detection anti-NUMB polyclonal antibodies using purified NUMB and NUMBL recombinant proteins. We noted that the commercial mouse polyclonal capture antibody recognized both NUMB and NUMBL (Figure 17B), while the detection antibody specifically recognized NUMB, with no cross-reaction with NUMBL. Considering that the concomitant reaction of the capture antibody against either NUMB or NUMB-L would unavoidably affect interpretation of results based on the phenotypic restoration of NUMB expression upon siRNA of candidate E3 ligases, we decided to replace in the ELISA platform the commercial polyclonal capture antibody with the moAb21 anti-NUMB antibody

produced in-house, which selectively recognizes the NUMB protein (Figure 11, Section 4.1 of Results).

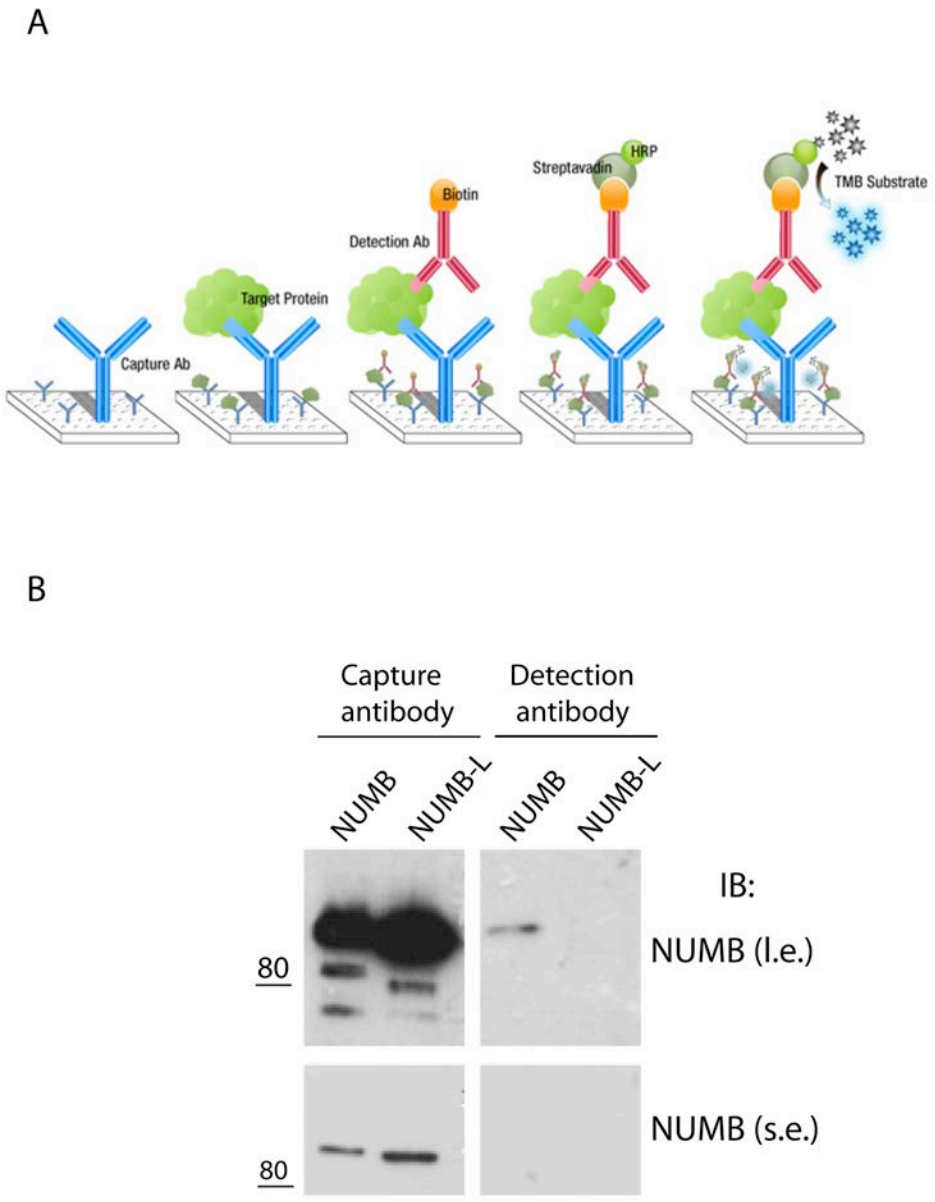

Figure 17. Optimization of a capture ELISA to measure total NUMB levels in cell lysates. A) Schematic representation of the capture ELISA. NUMB protein is captured from total cell lysates using a mouse polyclonal anti-NUMB antibody coated onto the ELISA plate. Captured NUMB is detected using a biotinylated polyclonal antibody specific for total NUMB, Streptavidin-HRP, and a chromogenic HRP substrate, tetramethylbenzidine (TMB).

(B) The specificity of both capture and detection polyclonal anti-NUMB antibodies was assessed by immunoblotting using purified NUMB and NUMB-L recombinant proteins (5 ng). s.e., short exposure; l.e., long exposure. MW markers are reported to the left of the blot.

To optimize the use of our moAb21 antibody in the ELISA protocol, we first compared the standard curves obtained in a binding assay challenging the commercially available capture mouse polyclonal antibody and the moAb21 antibody against a range of concentrations of a recombinant NUMB protein produced in *E. Coli* and provided by the manufacturer (Figure 18). The moAb21 monoclonal antibody produced a standard binding curve comparable to that obtained with the capture antibody provided by the manufacturer, arguing for the suitability of this reagent to the customization of the ELISA protocol.

The first question we decided to address in the establishment of the ELISA-based platform was how the sensitivity of the ELISA compared to IB analysis in detecting variations of NUMB expression upon MG-132 treatment of NUMB-deficient and -proficient cells.

To this aim, we tested by ELISA the same preparation of cell lysates, from cells grown in 10-cm plates, analyzed by IB analysis shown in Figure 15.

To perform a direct quantitative comparison of ELISA and IB results, we performed densitometric analysis of IB results. From this comparison, it was evident that, while ELISA and IB are reasonably comparable in the detection of small variations of the NUMB protein (compare, for instance, IB densitometry and ELISA results of MG-132 treatment of BT474 with 10 μM for 10h and 5 μM for 24h), ELISA appears to be far less sensitive than IB in scoring large increase in NUMB expression (for instance, BT474 treated with 20 μM MG-132 for 6h or MDA-MB-361 exposed to 5 μM MG-132 for 24h). This is likely due to the limited dynamic range of the ELISA that does not appear to efficiently score NUMB protein increases greater than 1.5/2-fold (Figure 19A,B).

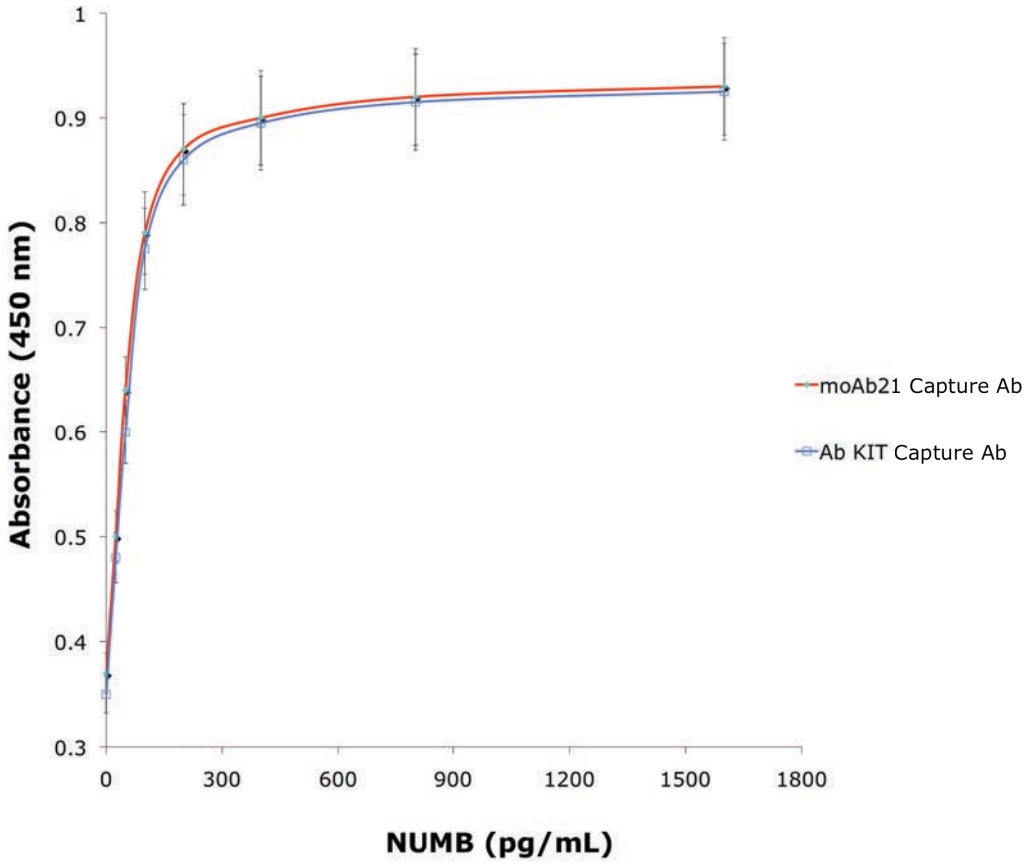

Figure 18. Test of the efficacy of the moAb21 anti-NUMB monoclonal antibody *vs*. the commercial anti-NUMB poyclonal antibody.

Comparison of the moAb21 anti-NUMB mouse monoclonal antibody (red line) and anti-NUMB mouse poyclonal antibody (blu line) provided by the kit. The indicate concentrations of a recombinant purified human NUMB protein (0-1600 pg/ml) were used to test efficacy of the two antibodies. Equivalent concentrations (4 µg/ml) of moAb21 or of the commercial mouse polyclonal antibody were used for the coating of the ELISA plates; after 3 washes, a blocking buffer was added for 1 h. After another round of washes, recombinant protein NUMB was added at the indicated concentrations and incubated for 2 h and then, after 3 washes, the biotinylated detection antibody (100 ng/ml) was added and incubated for 2 h. Finally, streptavidin coniugated to horseradish-peroxidase (streptavidin-HRP) and the TMB substrate provided by the kit were added to the plate. Each data point represents the mean ± s.dev (n = 3) of a representative experiment of 3 repeats.

A

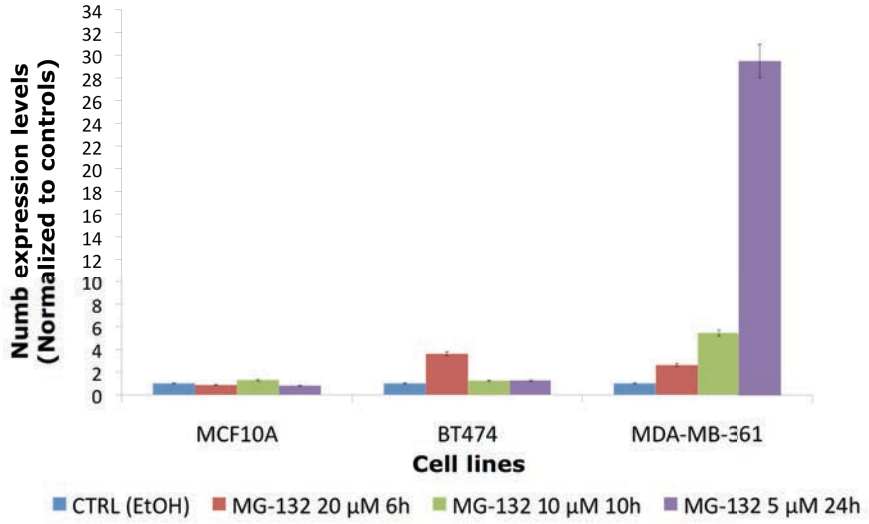

B

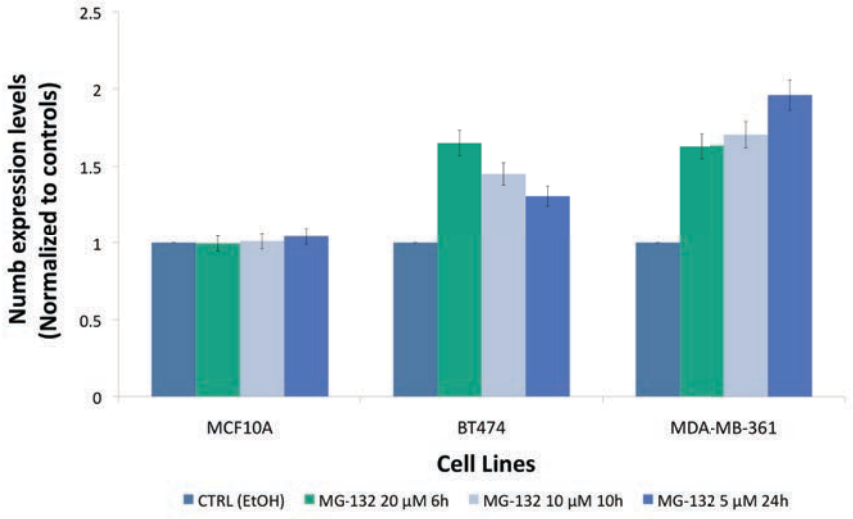

Figure 19. Comparison of the sensitivity of ELISA *vs*. IB in the detection of NUMB protein levels.

A) Quantitative densitometry of the IB results depicted in Figure 5 showing the response of MCF10A, BT474 and MDA-MB-361 cells to MG-132 treatment. For the densitometric assessment of NUMB levels, for the different cell lines, values relative to each individual treatment were normalized to the control (EtOH=1) and then normalized to the corresponding vinculin level. B) ELISA determination of NUMB variations performed in a 384-well plate format using the same cellular extracts used for the IB analysis depicted in Figure 5, and quantified by densitometry as in A). ELISA was performed using the anti-NUMB moAb21 as a capture antibody (4 µg/ml) incubated overnight; after 3 washes, a blocking buffer was added for 1 h. After another round of washes, protein lysates (1 µg) from cells grown in 10-cm plates were added and incubated for 2 h and then, after 3 washes, the biotinylated detection antibody (100 ng/ml) was added and incubated for 2 h. Finally, streptavidin-coniugated to horseradish peroxidase (streptavidin-HRP) and the TMB substrate were added to the plate. Optical density (OD) of each well was determined immediately using a microplate reader set to 450 nm. Protein lysates from each data point were plated in triplicate in 384-well plates. Each data point represents the mean ± S.D of three independent experiments run in triplicate. For each cell line, each treated sample was normalized to control sample (EtOH=1).

The next step towards the optimization of the ELISA platform, for the purpose of the high-throughput screening, was the miniaturization of the ELISA protocol to a 384-well format and the introduction of a method to measure the number and viability of cells directly in wells.

To this aim, we performed the ELISA protocol using MCF10A cells (1 x 10^3/well) and MDA-MB-361 or BT474 cells (6 x 10^3/well) plated into a 384-well plate. To measure the viability and number of cells, we exploited the Cell Titer Fluor Cell Viability (CTF) Assay from Promega. This assay measures a conserved and constitutive cellular protease activity and utilizes a fluorogenic, cell-permeant, peptide substrate (glycylphenylalanyl-aminofluorocoumarin, GF-AFC), which enters intact cells where it is cleaved by the live-cell protease activity to generate a fluorescent signal proportional to the number of living cells. This fluorescent signal can be monitored using a wavelenght (excitation, 380nm; emission, 505nm) compatible with the absorbance of the ELISA protocol (450nm).

The CTF substrate was added immediately before the ELISA substrate. The analysis of the absorbance values relative to basal NUMB levels in the different cell lines, calculated in the presence or absence of the CTF substrate, demonstrated that the introduction of the CTF-based measurement of cell number/viability does not perturb the sensitivity of the ELISA (Figure 20).

Therefore, the successful introduction of the CTF-based viability assay and the reduction of the ELISA to a 384-well plate format represents a further step towards the development of a fully automatized and miniaturized ELISA platform.

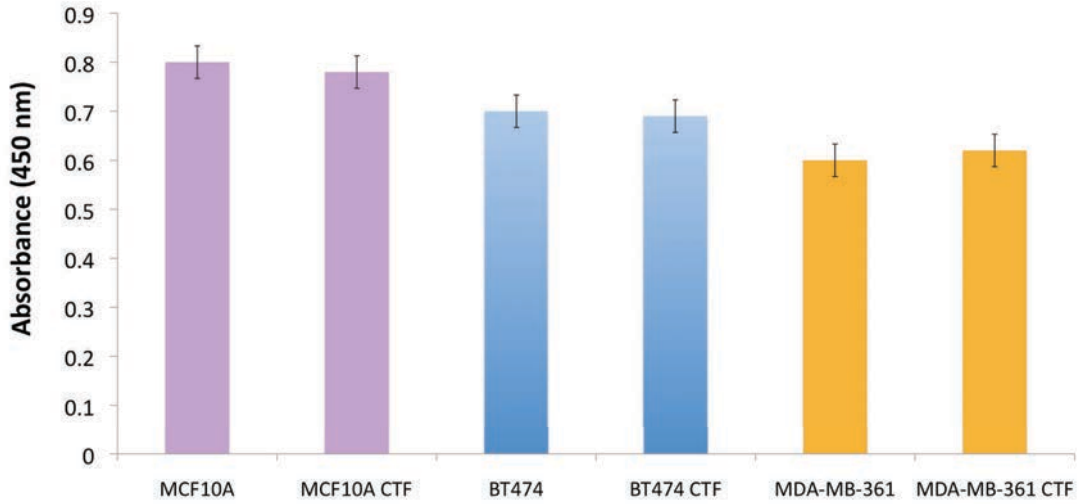

Figure 20. Analysis of the effects of the CTF-based viability assay in the performance of the capture ELISA.

Cells were plated in triplicate directly in 384-well ELISA plates (1 X 10^3 MCF10A cells and 6 X 10^3 MDA-MB-361 or BT474 cells) for 72 hours. ELISA was performed using the anti-NUMB moAb21 as a capture antibody (4 µg/ml) incubated overnight; after 3 washes, a blocking buffer was added for 1 h. The CTF substrate was added before the ELISA substrate to measure cell viability. Data are shown as the mean ± S.D. from 3 independent experiments.

We next used this protocol to measure the response of MCF10A, MDA-MB-361 and BT474 cells to MG-132 treatment. Results from this analysis in a 384-well plate format were similar to those obtained in cells grown in 10-cm plates (see Figure 19), with a maximun increase in NUMB expression observed in MDA-MB-361 cells exposed to 5µM MG-132 for 24 h (Figure 21).

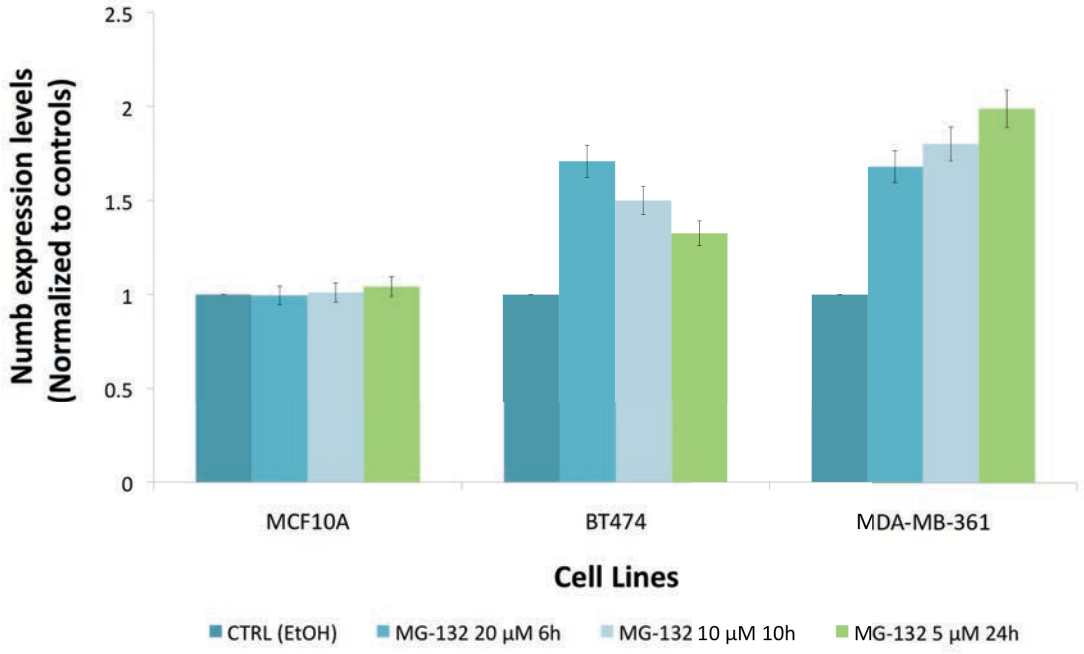

Figure 21. Capture ELISA assay performed in a 384-well plate format to detect NUMB protein levels upon proteasome inhibition.

The effect of MG-132 treatment on NUMB levels in the indicated cell lines was determined by the capture ELISA assay in a 384-well plate using the chromogenic HRP substrate, tetramethylbenzidine. Cells were plated directly in 384-well ELISA plates (1 x 10^3 MCF10A cells and 6 x 10^3 MDA-MB-361 or BT474 cells) and then treated with MG-132 (5/10/20 µM for 24, 10 and 6 h respectively) or with equivalent concentrations of the solvent ethanol (EtOH) as a control (CTRL). ELISA assay was performed using the anti-NUMB moAb21 as a capture antibody (4 µg/ml) incubated overnight; after 3 washes, a blocking buffer was added for 1 h. After another round of washes, cell lysis was performed according to the manufacturer's instructions with cell lysates incubated for 2 h and then, after 3 washes, the biotinylated detection antibody (100 ng/ml) was added and incubated for 2 h. Finally, streptavidin-coniugated to horseradish peroxidase (streptavidin-HRP) and the TMB substrate were added to the plate. Absorbance values from ELISA assay (NUMB protein levels) were normalized to the number of cells/well measured by the Cell Titer Fluor Cell Viability Assay (Promega), performed according to the manufacturer's instructions. Cells from each data point were plated in triplicate. Each data point represents the mean ± S.D. (n = 3) of triplicate experiments. Every treated sample was normalized for control sample in each cell line.

Based on these results, we decided to verify whether we could improve the dynamic range of the ELISA in scoring cellular changes in NUMB expression upon proteasome inhibition, by modifying stepwisely the different steps of the original ELISA protocol.

We started by challenging different concentrations of either the capture (Figure 22A) or the detection antibody (Figure 22B) against standard concentrations of the NUMB recombinant protein (0-1600 pg/ml).

Compared to the concentrations of the capture and detection antibody indicated by the manufacturer's instructions (respectively, 4 µg/ml and 100 ng/ml), we tested in the ELISA protocol four different concentrations (1, 2, 4, 8 µg/ml) of the moAb21 as a capture antibody and of the commercial rabbit polyclonal detection antibody (25, 50, 100, 200 ng/ml), observing no substantial differences across the different concentrations of either the capture or the detection antibodies in the binding of the different dilutions of the NUMB recombinant portein (Figure 22A,B).

In parallel experiments, the same concentrations of capture and detection antibodies were challenged against the lysates used before of MDA-MB-361 plated in 10-cm plates and treated with 5µM MG-132 for 24 h, a condition that, by IB analysis, yielded the most remarkable increase in NUMB (see Figure 19 for comparison). Unfortunately, none of the different concentrations of either capture or detection antibodies were able to provide a better dynamic range in the detection of NUMB increase compared to the experimental conditions of the original ELISA protocol (Figure 23 A,B).

A

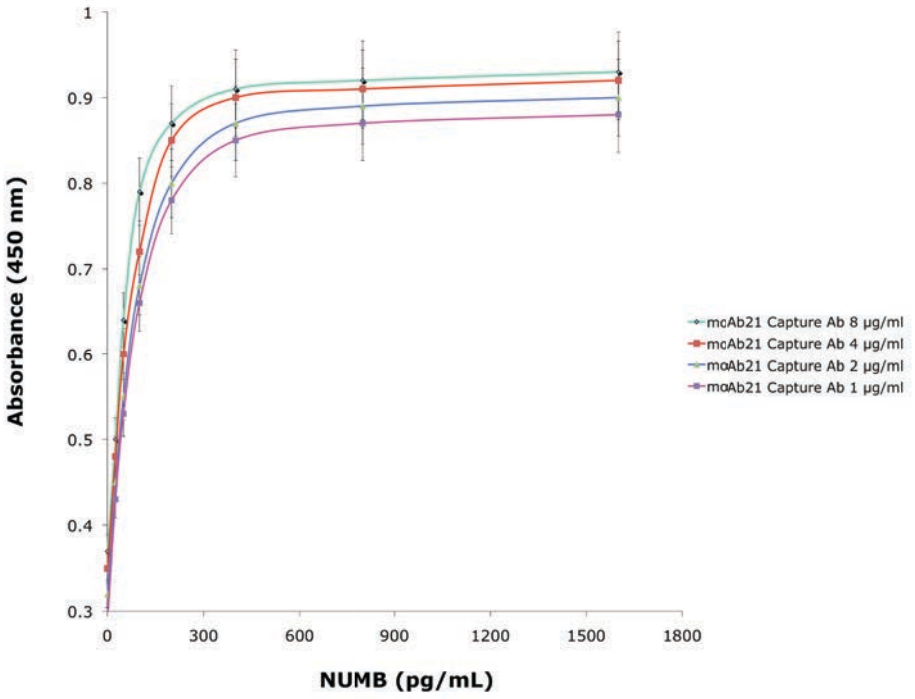

B

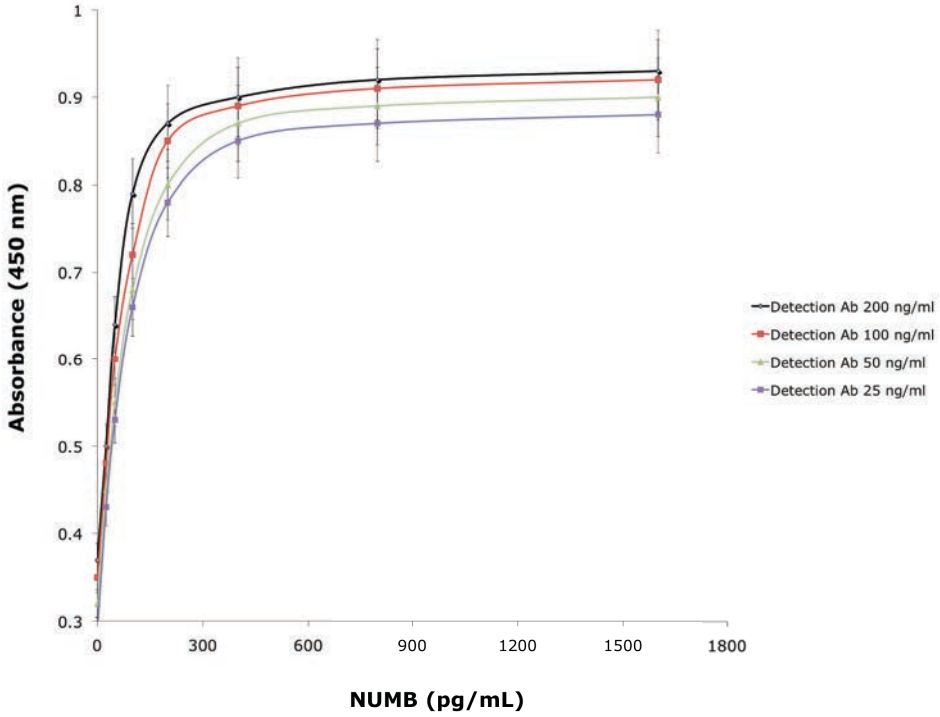

Figure 22. Optimization of the ELISA assay: set-up of capture or detection antibody's concentration. The indicated concentrations of moAb21 as a capture antibody A) or of the detection antibody provided by the ELISA kit B) were tested in the ELISA protocol against the indicated serial dilutions of a recombinant purified human NUMB protein. Data represent the mean ± S.D. of 3 indipendent experiments performed in triplicate.

A

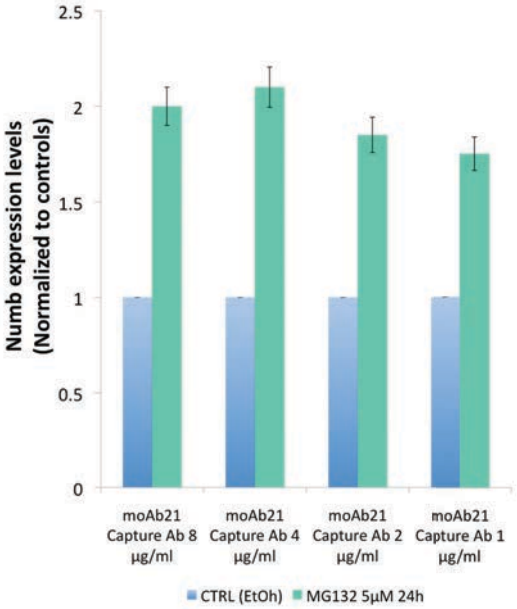

B

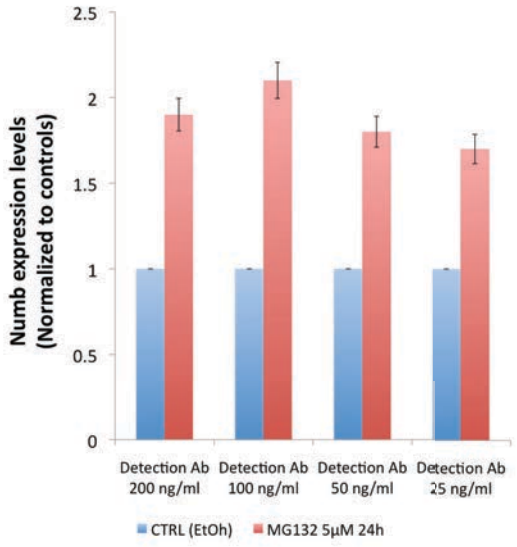

Figure 23. Optimization of the ELISA assay: detection of NUMB protein levels upon proteasome inhibition using different concentrations of capture or detection antibody.

ELISA performed in the presence of the indicated concentrations of moAb21 as a capture antibody A) or of the detection antibody provided by the ELISA kit B) to measure variations in NUMB expression in MDA-MB-361 cells treated with 5µM MG-132, or with equivalent concentrations of EtOH as a control, for 24h. Data represent the mean ± S.D. of 3 indipendent experiments performed in triplicate.

As a further attempt to improve the sensitivity of the ELISA, we decided to substitute the HRP chromogenic substrate with a chemiluminescent substrate (Chemiluminescent Pico ELISA Signal-Luminol-based, Thermo Scientific). We compared the two detection systems using serial dilutions of a purified recombinant human NUMB protein provided by the manufacturer, and observed that the chemiluminescent substrate was more sensitive and displayed a wider dynamic working range than the chromogenic substrate (Figure 24A,B). Indeed, TMB substrate gave linear read-out between 0-200 pg/ml of NUMB protein concentration, before plateuing out, while chemiluminescent substrate was still linear from 100 pg/ml to 1600 pg/ml.

We then repeated the MG-132 treatment experiment with the new chemiluminescent substrate after growing 1 X 10^3 MCF10A cells and 6 X 10^3 MDA-MB-361 and BT474 cells in a 384-well plate. We observed a maximum of three fold-increase in the NUMB protein levels in MDA-MB-361 treated with 5 μM MG-132 for 24 h (Figure 25), which constitutes, albeit to a limited extent, an improvement of the dynamic range of the ELISA compared to the standard manufacturer's protocol. Thus, we decided to use the chemiluminescent, instead of the chromogenic, substrate in our ELISA assay for the siRNA screening.

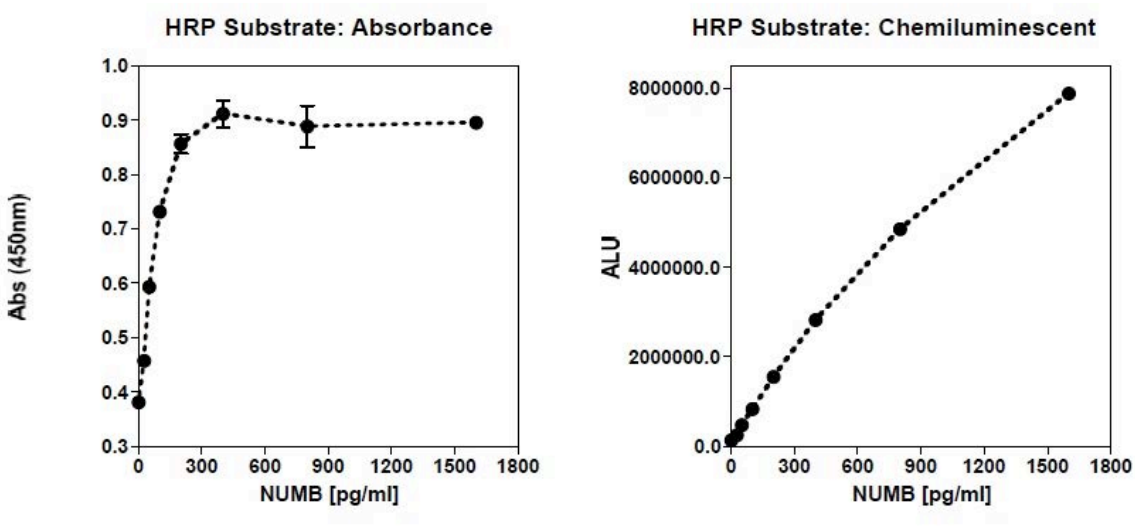

Figure 24. Optimization of the ELISA assay: chromogenic *vs* chemiluminescent substrate.

Comparison of the chromogenic A) and chemiluminescent B) substrates as detection systems in ELISA using standard serial dilutions of a recombinant purified human NUMB protein (0-1600 pg/ml).

ELISA was performed using anti-NUMB moAb21 as a capture antibody (4 µg/ml) and the commercial biotinylated antibody (100 ng/ml) as a detection antibody combined to streptavidin-HRP and to the TMB substrate provided by the kit A) or to the a chemiluminescent substrate (Chemiluminescent Pico ELISA Signal-Luminol-based, Thermo Scientific) B). Data represent the mean ± S.D. from 3 independent experiments performed in triplicate.

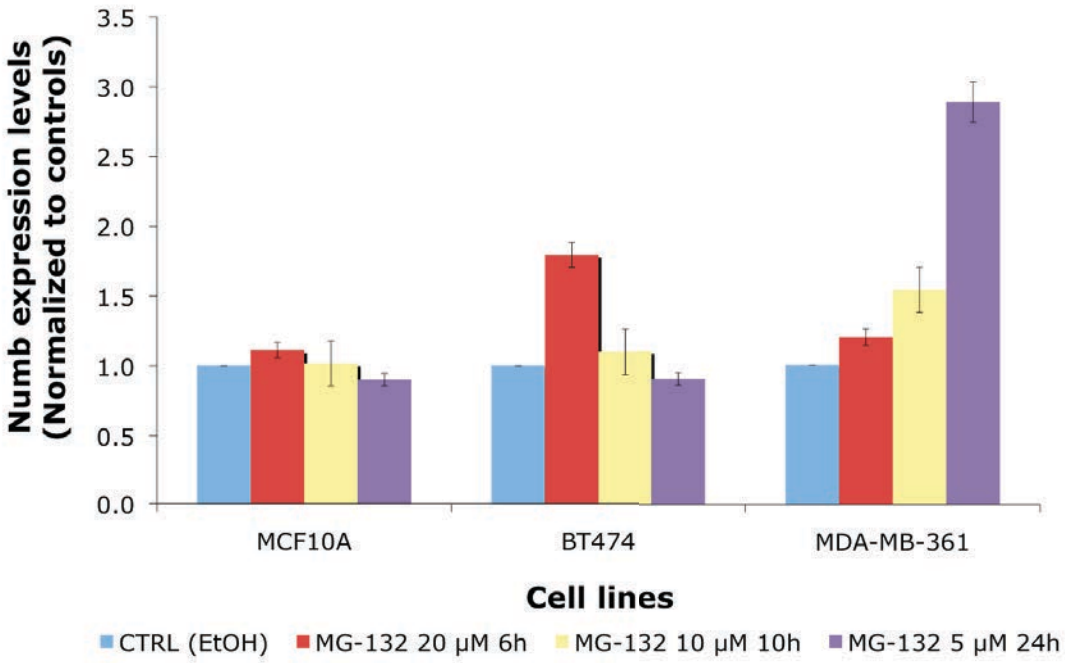

Figure 25. Detection of NUMB restoration following MG-132 treatment using the capture ELISA assay and the chemiluminescent substrate.

The effect of MG-132 on NUMB levels in the indicated cell lines was determined by the capture ELISA assay in a 384-well plate using the chemiluminescent substrate (Chemiluminescent Pico ELISA Signal-Luminol-based). NUMB protein levels were normalized to the number of cells/well measured with the Cell Titer Fluor Cell Viability Assay (Promega). Cells were plated directly in 384-well ELISA plates (1 X 10^3 MCF10A cells and 6 X 10^3 MDA-MB-361 and BT474 cells) and then treated with MG-132 (5/10/20 µM for 24, 10 and 6 h respectively) and control (CTRL) samples received an equivalent volume of solvent Ethanol (EtOH). ELISA assay was performed using mouse anti-NUMB moAb21 as capture antibody (4 µg/ml) incubated overnight; after 3 washes, a blocking buffer was added for 1 h. After another round of washes, cell lysis was performed according to the manufacturer's instructions with cell lysates incubated for 2 h and then, after 3 washes, the biotinylated detection antibody (100 ng/ml) was added and incubated for 2 h. Finally, streptavidin coniugated to horseradish-peroxidase (streptavidin-HRP) and the chemiluminescent substrate were added to the plate. Absorbance values from ELISA assay (NUMB protein levels) were normalized to the number of cells/well measured by the Cell Titer Fluor Cell Viability Assay (Promega), performed according to the manufacturer's instructions. Cells from each data point were plated in triplicate. Each data point represents the mean ± S.D. (n = 3) of a representative experiment of 3 repeats. Every treated sample was normalized for control sample in each cell line.

4.3.2 Optimization of cell growth conditions in 384-well plates.

We next set out to determine optimal cell growth conditions in 384-well plates. To this aim, we plated different amounts of MDA-MB-361 cells in 384-well plates and measured cell growth over 96 h using the aforementioned Cell Titer Fluor kit.

We observed exponential cell growth over 96 h in wells containing a starting concentration of 2.5 – 7.5 x 10^3 cells/well (Figure 26A). From the standard curve, generated by plotting fluorescent content versus cell concentration (Figure 26B), we determined that the doubling time for MDA-MB-361 cells was approximately 72 h, which is consistent with known doubling time for this cell line. Moreover, the signal obtained from wells plated at 7.5 x 10^3 at T = 0, after 72 h (17.5 x 10^3 AFU) was within the linear range. Thus, for the siRNA screening experiments, we chose a starting concentration of MDA-MB-361 cells of $\leq$ 7.5 x 10^3 cells/well.

We next measured NUMB levels in lysates from wells containing different starting amounts of cells using the ELISA assay with the new chemiluminescent detection system and we observed a linear correlation up to 12 x 10^3 cells/well (Figure 27A). From the standard curve generated with recombinant NUMB (Figure 27B), we observed a linear correlation between NUMB concentration and the ELISA read-out up to 800 pg/ml of rNUMB, and determined that 7.5 x 10^3 cells/well corresponds to ~200 pg/ml. Since our aim is to efficiently detect NUMB restoration by ELISA and considering the low dynamic range of this assay, it is necessary to use a cell concentration in the siRNA screening experiments that corresponds to a quantity of NUMB at the lower end of the standard curve, but not too close to background values. Taking into consideration these results we concluded that a suitable starting concentration of cells is 6 - 7.5 x 10^3 cells/well.

A

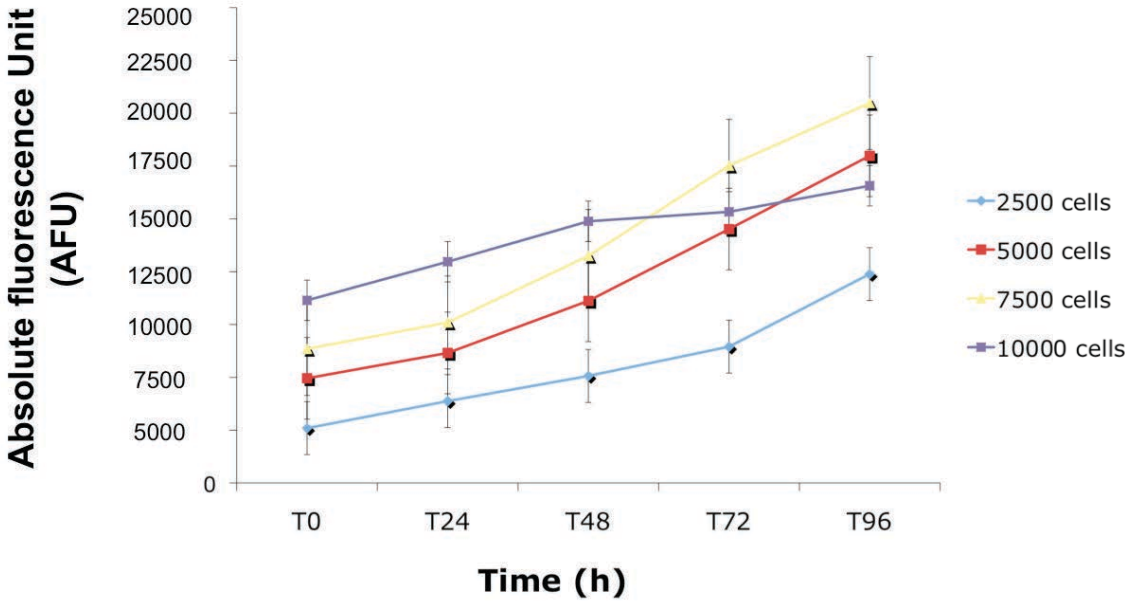

B

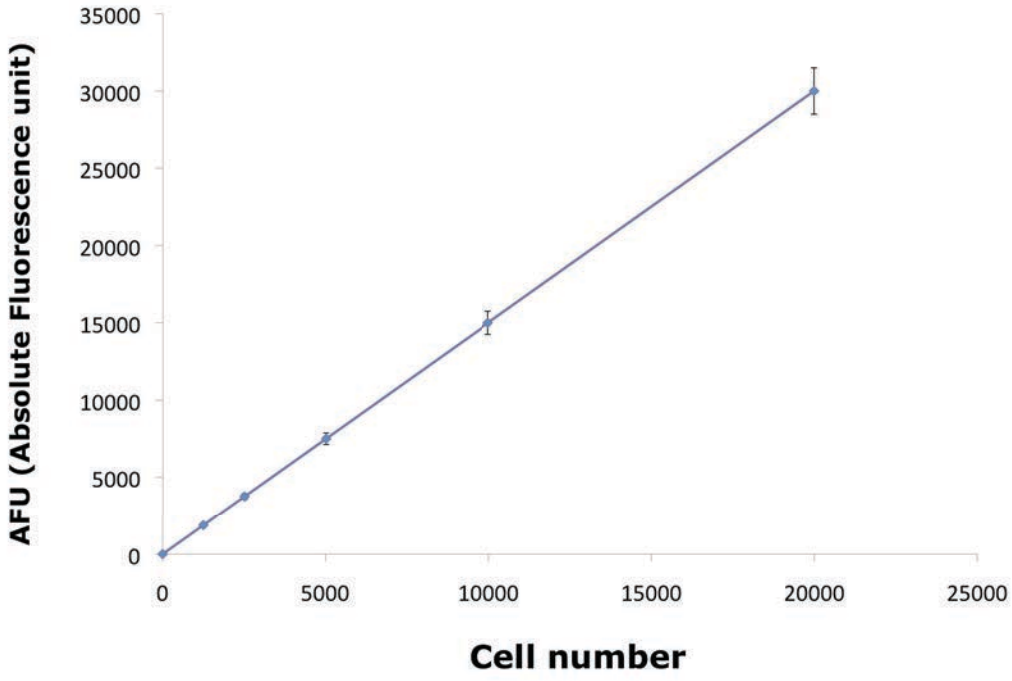

Figure 26. Set up of growth conditions of MDA-MB-361 cells in 384-well plates.

A) MDA-MB-361 cells were plated in quadruplicate in 384-well plates at the indicated concentrations. Cell viability was measured using the Cell Titer Fluor Kit every 24 h over 96 h period. Each data point represents the mean ± S.D. (n = 4) of a representative experiment of 3 repeats. Time 0 (T0) was considered as 3 h after plating, which represents the time required for cells to attach. B) Standard curve showing the relationship between cell number at T0 and fluorescence content determined using the Cell Titer Fluor Kit.

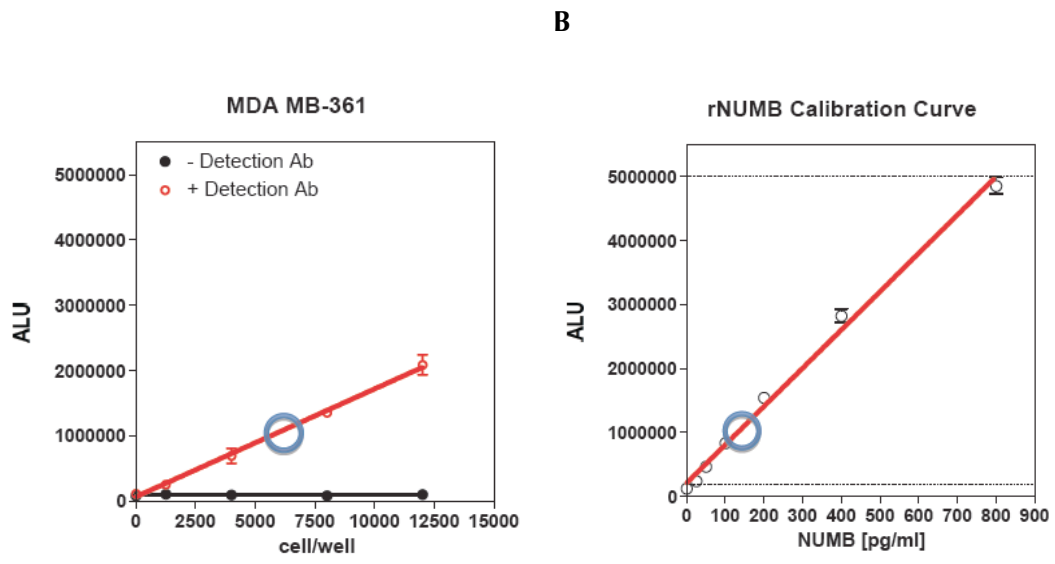

Figure 27. Relationship between cell concentration and NUMB protein levels measured by the capture ELISA assay.

A) MDA-MB-361 cells were plated in quadruplicate in 384-well plates at the indicated concentrations. NUMB levels were determined using ELISA with the chemiluminescent detection system. The blue circle highlights the position on the graph corresponding to 6000 cells/well (A) or 150 pg/ml of NUMB (B). B) Standard curve generated by testing in ELISA increasing concentrations of a purified recombinant NUMB with the use of the chemiluminescent detection system. Data points represent the mean ± S.D. (n = 4) of a representative experiment of 3 repeats.

4.3.3 Optimization of reverse transfection of siRNAs.

We employed a siGENOME SMARTpool siRNA from Dharmacon Technologies (pools of 4 oligos/gene) and a reverse transfection protocol with an incubation time of 72 h. We set up and optimized RNAi conditions using NUMB as the target protein in MDA-MB-361 cells. We used different starting concentrations of cells ranging from 5 to 15x10^3 cells/well and determined that the level of NUMB knockdown was comparable at all concentrations of cells (Figure 28A). Similar results were also obtained with MCF10A cells using the same protocol (Figure 28B). We concluded that the starting MDA-MB-361 cell concentration of 6 to 7.5 x 10^3 cells/well is suitable for protein knockdown in siRNA experiments.

A

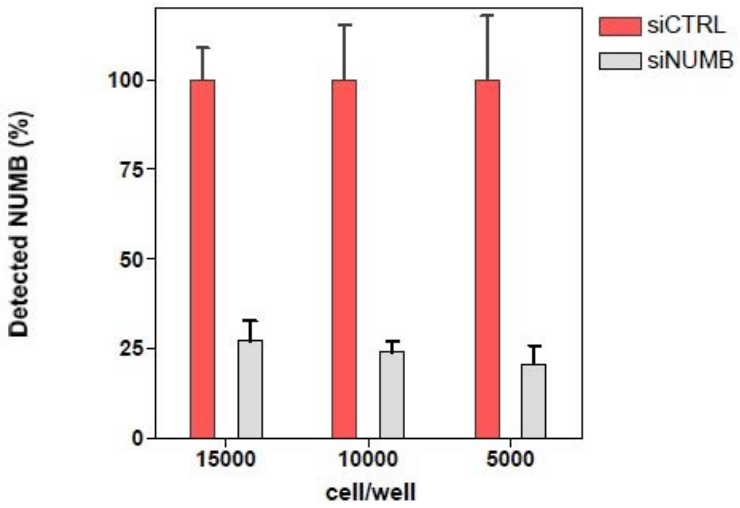

B

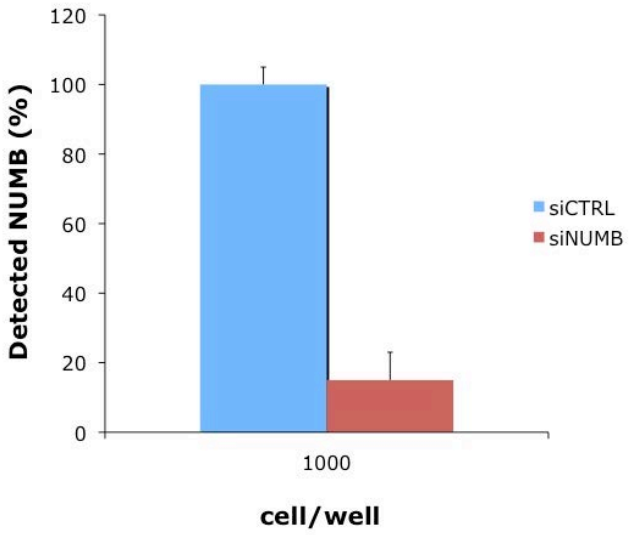

Figure 28. Set up of *RNA-interference* conditions in 384-well plates.

NUMB was knocked down in MDA-MB-361 cells A) and MCF10A cells B), plated in quadruplicate at the indicated concentrations in 384-well plates, using 50 nM anti-NUMB or control siRNA oligo (siNUMB and siCTRL, respectively) for 72 h. NUMB levels were detected using the ELISA assay with the chemiluminescent detection method and the number of cells/well was determined using the Cell Titer Fluor viability assay. NUMB levels are shown normalized to number of cells/well and to controls.

4.4 IDENTIFICATION OF CANDIDATE E3 LIGASES TARGETING NUMB BY siRNA SCREENING

After having identified a suitable cell model system for NUMB-deficient breast cancer, i.e. MDA-MB-361 cells, and optimized conditions for the NUMB capture ELISA assay as well as for the siRNA reverse trasfection protocol in a 384-well plate format, we decided to run the 'high-throughput siRNA phenotypic screening' to identify possible NUMB downregulators among enzymes belonging to E3 ligase family. For that purpose, we used a commercial library from Dharmacon Technology, the Dharmacon siGENOME® SMARTpool® siRNA Library-Human Ubiquitin Conjugation subset 1-3 (G-005615 Lot 08119).

4.4.1 Plate uniformity and signal variability assessment.

We decided to perform the siRNA screening using the automated EVOware platform; all the automation process of the screening was done in collaboration with the Drug Discovery Unit (DDU) at IFOM-IEO Campus.

During the automation process, two main protocol were followed: 1) the siRNA reverse transfection protocol and 2) the ELISA protocol, whose optimization and set-up has already been described in Section 4.3.

1) For all silencing experiments in the screening, we used a final concentration of the siRNA pool of control/gene oligos (siCTRL/siGeneX) of 50 nM; according to the reverse transfection protocol, the first step was the distribution of oligos targeting individual E3 ligases into separate wells of a 384-well plate, followed by cell plating and incubation for 72 h at 37 °C; these steps were automatized through the help of a automatic dispencer. As a negative control of the trasfection we used NUMB knockdown (siNUMB), as assessed in Section 4.3; as a positive control of NUMB restoration after

candidate gene silencing we used MDA-MB-361 cells treated with MG-132 (5μM for 24 h) during all screening experiments, as already assessed in Section 4.2 and 4.3.

2) For the ELISA protocol, we used the in-house-produced moAb21 antibody at a final concentration of 4 μg/ml as capture antibody, the mouse polyclonal detection antibody provided by kit, at a final concentration of 100 ng/ml, and the Chemiluminescent Pico ELISA Signal-Luminol-based as substrate for the detection step. The different steps of the ELISA protocol, such as coating of capture/detection antibodies and distribution of buffer solutions, except for washing steps, had been fully automatized. Cell lysates from treated MDA-MB-361 cells were transferred from siRNA trasfection plates to ELISA plates through the automated dispencer. Initially, we defined the workflow for the automation of the screening by writing two specific scripts for the EVOware platform, in order to complete the two main steps in the protocol: 1) Transfection of siRNA and 2) ELISA. The accuracy of the automation process was evaluated by assessing both plate uniformity and signal variability of the ELISA performed with the EVOware platform. Three 384-well plates were assayed for intra- and inter-plate signal uniformity, performing ELISA assay using recombinant NUMB (rNUMB) protein at two different concentrations, whose optical absorbance values defined, respectively, High (H), corresponding to 800 pg/ml, and Medium (M) signals, corresponding to 400 pg/ml; the optical absorbance value of the buffer alone was considered as Low signal (L). Statistical analysis showed no drift or edge effects throughout the plates. Coefficients of variation (CV) of all the signals (H, M and L), defined as the ratio Standard deviation and mean of each experimental point, were below the acceptance criterion of CV < 20%, which is the standard criterion for these kind of assays (Table 1), indicating that intra- and inter-plate variability was low. A similar experiment was performed with MDA-MB-361 cells treated with siCTRL, siNUMB and MG-132. Also in this case both the intra- and inter-plate CV values were well below the defined threshold of 20% (Table 2).

Signal (Recombinant NUMB)	CV inter	CV intra
High	7.81	5.91
Medium	6.53	6.21
Low	7.12	7.68

Table 1. Assessing plate uniformity of the automated ELISA performed with recombinant NUMB.
Three 384-well plates were assayed for intra- and inter-plate signal uniformity, using in each plate recombinant NUMB (rNUMB) protein at two different concentrations: High (H), corresponding to 800 pg/ml, and Medium (M) signals, corresponding to 400 pg/ml, or buffer alone, considered as Low signal (L). The intra- and inter-plate CV values were calculated using the ratio S.D./mean of each data point in the three different plates. Plates were coated with capture moAb21 antibody (4 µg/ml), washed and blocked before adding rNUMB at H and M concentrations or buffer alone (L); this was done for all wells of the plate. Captured NUMB was detected using biotinylated detection anti-NUMB antibody and streptavidin-HRP system. Luminescence values relative to rNUMB levels were measured with Chemiluminescent Supersignal PICO Luminol (Thermo Scientific).

Signal (NUMB levels)	CV inter	CV intra
siCTRL	9.81	5.45
siNUMB	11.21	6.51
MG-132	10.2	7.25

Table 2. Assessing plate uniformity of the automated siRNA trasfection and ELISA performed with MDA-MB-361 cells.
Three 384-well plates were assayed for intra- and inter-plate signal uniformity on MDA-MB-361 cells, using siCTRL, siNUMB and MG-132 as controls. MDA-MB-361 cells were plated (6000 cells/well) onto siRNA oligos following the reverse trasfection protocol for 72 h at 37°C. Oligos, trasfection reagent (Dharmacon) and cells were dispensed in an automatized way. After 72 h, cell lysates were transferred automatically into the ELISA plate.
The intra- and inter-plate CV values were calculated using the ratio S.D. /mean of each data point in the three different plates, as reported in the table. Plates were coated with capture moAb21 antibody (4 µg/ml), washed and blocked before adding cell lysates from reverse transfection plates. This was done for all wells of the plate. Captured NUMB was detected using biotinylated detection anti-NUMB antibody and streptavidin-HRP system. Cell counting was measured with Cell Titer Fluor cell viability assay (Promega), while luminescence for detection of NUMB levels was measured with Chemiluminescent Supersignal PICO Luminol system (Thermo Scientific).

4.4.2 E3 ligase siRNA screening

The siRNA library (Dharmacon siGENOME® SMARTpool® siRNA Library - Human Ubiquitin Conjugation subset 1-3) was provided in 9 x 96-well plates. Each well contains 40 µl of a 2.5 µM concentration of siRNA smart pool oligos (4 oligos/gene) in 1x siRNA buffer, for a total of 600 target genes. In each plate, columns 1 and 11 do not contain any target gene siRNA oligo and are filled with 40 µl of 1x siRNA buffer, being available for eventual additional controls. From each original 96-well plate, three 384-well pre-spotted "daughter" plates, containing quadruplicate wells, were prepared and used in the screening. We decided to design each plate in a way that all controls were included among test wells, following the scheme showed below (Figure 29).

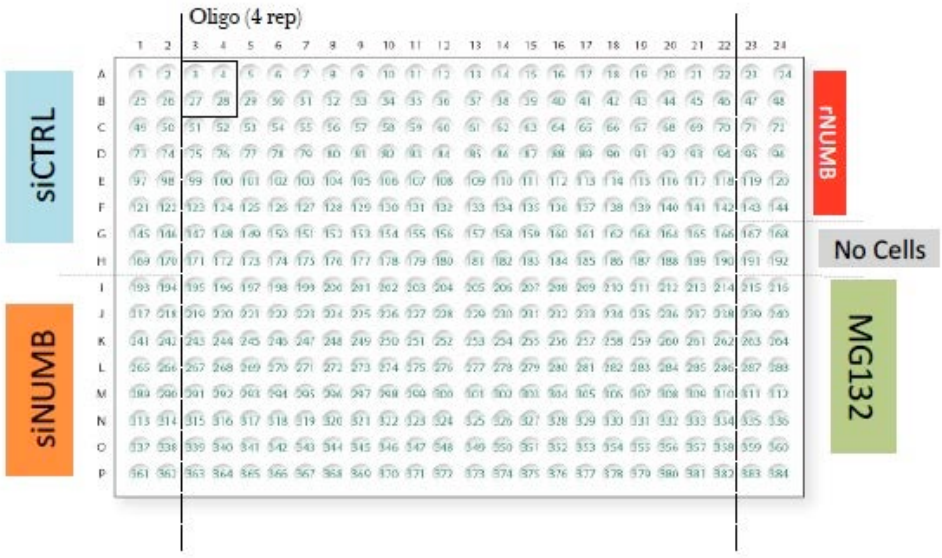

Figure 29. Schematic representation of the 384-well plate format for the E3 ligase screening.
The siRNA library (Dharmacon siGENOME® SMARTpool® siRNA Library Human Ubiquitin Conjugation subset 1-3) purchased from Dharmacon was provided in 9 x 96-well plates. Each 96-well plate was pre-spotted in three 384-well plates, according to the experimental design indicated in the figure. Positive control for NUMB restoration (MG-132), the standard curve performed with the recombinant NUMB (rNUMB), the positive (siNUMB) and the negative control (siCTRL) of the transfection were spotted at both sides of each plate.

Three independent screening experiments were performed, referred to as the Pilot experiment, and the 1st and 2nd rounds of screening.

The Pilot experiment differed from the 1st and 2nd rounds of screening in the sense that it was performed using only two 384-well plates containing the target genes. This Pilot experiment was instrumental to assessing the global assay performance of the overall optimized procedure described at the beginning of this section, which was then used for the two subsequent rounds of screening (termed as 1st and 2nd rounds).

After removing outliers the final intra- and inter-plate variability was below the 20% threshold, both in the Cell Titer Fluor viability assay (Figure 30A) and in the ELISA assay (Figure 30B).

Based on overall results from this initial testing, we decided to perform two additional screening rounds with the remaining plates, which also showed a final intra- and inter-plate variability below the 20% threshold either in the Cell Titer Fluor viability assay (Figure 30A) and in the ELISA assay (Figure 30B).

In the pilot experiment and in the subsequent two screening rounds, the fold-increase in NUMB expression following MG-132 treatment (positive control) varied from 1.5 to 2.5 relative to siCTRL cells, while NUMB downregulation after NUMB silencing (negative control) was from 60 to 80% relative to control silenced cells (siCTRL).

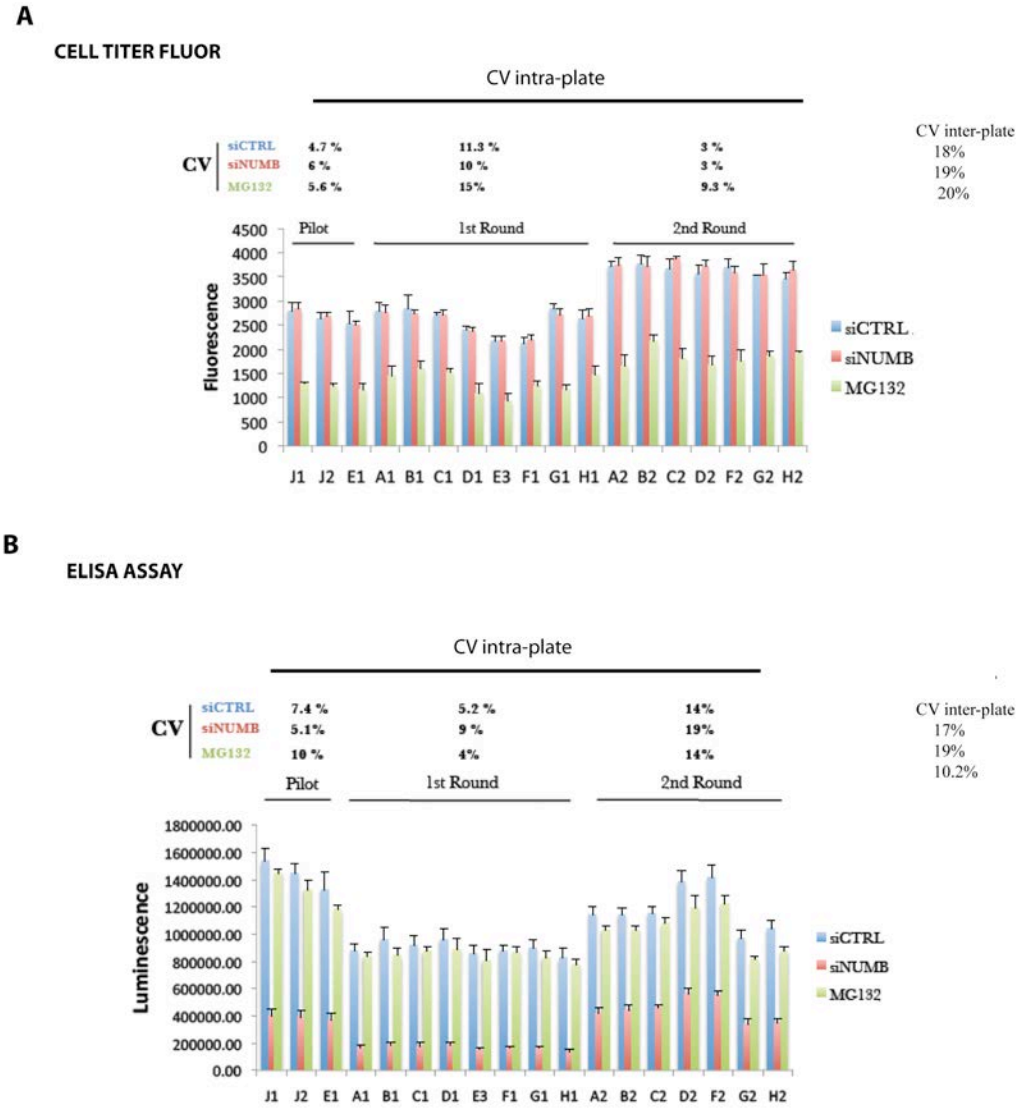

Figure 30. Assessing plate uniformity of the automated siRNA trasfection and ELISA performed with MDA-MB-361 cells.

The 384-well plates (A-J) from the Pilot experiment (J1, J2 and E1 plates), from the 1st (A1-D1, F1-H1 plates) and 2nd screening round (A2-D2, F2-H2 plates) were assayed for intra- and inter-plate signal uniformity performed on MDA-MB-361 cells, using siCTRL, siNUMB and MG-132 as controls, in the Cell Titer fluor cell viability assay Performance (A) and in the ELISA assay performance (B). All plates were run in triplicate in Pilot and screening rounds. The intra- and inter-plate CV values were calculated using the ratio S.D./mean of each data point in the three different plates. MDA-MB-361 cells were plated (6000 cells/well) onto pre-spotted siRNA oligos to allow reverse trasfection for 72 h at 37°C. Oligos, trasfection reagent (Dharmacon) and cells were dispensed in an automatized way. After 72 h, cell lysates were transferred automatically into the ELISA plate. Plates were coated with capture moAb21 antibody (4 µg/ml), washed and blocked before adding cell lysate from reverse transfection experiment. This procedure was followed for all wells of the plate. Captured NUMB was detected using biotinylated detection anti-NUMB antibody and streptavidin-HRP system and fluorescence; cell counting was measured with the Cell Titer Fluor cell viability assay (Promega), while luminescence for detection of NUMB levels was measured with Chemiluminescent Supersignal PICO Luminol system (Thermo Scientific).

From the combination of results from the Pilot experiment and from the 1st and 2nd rounds of screening, we identified a number of E3 ligases that negatively regulate NUMB expression: i.e., E3 ligases whose ablation resulted in increased NUMB expression in MDA-MB-361 cells (Table 3). Data were analyzed by performing a three-step analysis: 1) Self-Normalization, 2) Normalization and 3) Hit identification (for details on step 1 and 2 see Section 6.13.2 of Material and Methods).

Normalized data were processed for hit identification using a Median Absolute Deviation approach (MAD). MAD can be defined as follows: MAD: = Median ($|X_i$ – median(X)|), where X indicates all the normalized values in the sample wells of a plate and Xi indicates the sample at position *i* in the plate.

To score for potential hits, we applied a threshold of

$$\text{Median}(X) \pm 3 \times \text{MAD},$$

where MAD (Median Absolute Deviation) is defined as

$$\text{Median}(|X_i - \text{median}(X)|)$$

X indicates all the normalized values in the sample wells of a plate and X_i indicates the sample at position *i* in the plate.

Using these criteria, we identified 15 candidate E3 ligases that negatively regulate NUMB. By lowering the threshold (Median(X) ± 2 x MAD) and by matching positive candidates common to the pilot experiment and to the two rounds of screening, we obtained 21 candidate E3 ligases that target NUMB (Table 3).

Threshold applied	Gene symbol (NCBI*)	Full name (NCBI*)
3XMAD	RBX1	ring-box 1, E3 ubiquitin protein ligase
	TRIP12	thyroid hormone receptor interactor 12
	UBE2G1	ubiquitin-conjugating enzyme E2G 1
	WHSC1L1	Wolf-Hirschhorn syndrome candidate 1-like 1
	JHDM1D	jumonji C domain containing histone demethylase 1 homolog D (S. cerevisiae)
	LOC642446	tripartite motif containing 64B
	FBXW8	F-box and WD repeat domain containing 8
	UBR3	ubiquitin protein ligase E3 component n-recognin 3 (putative)
	DTX1	deltex homolog 1 (Drosophila)
	FBXL13	F-box and leucine-rich repeat protein 13
	FBXO38	F-box protein 38
	KRTAP5-9	keratin associated protein 5-9
	BRPF1	bromodomain and PHD finger containing, 1
	MDM2	MDM2 oncogene, E3 ubiquitin protein ligase
	UBE2Q2	ubiquitin-conjugating enzyme E2Q family member 2
2XMAD (and confirmed in two experimental replicates)	UBA7	ubiquitin-like modifier activating enzyme 7
	FBXO9	F-box protein 9
	FBXO28	F-box protein 28
	FBXO42	F-box protein 42
	LOC652859	similar to tripartite motif protein 27
	UBE2F	ubiquitin-conjugating enzyme E2F (putative)

* http://www.ncbi.nlm.nih.gov/

NA = Not Available

Table 3. List of candidate E3 ligases involved in the negative regulation of NUMB, identified through a high-throughput phenotypic siRNA screening.

Positive hits from the ELISA-based high-throughput screening were selected using a Median Absolute Deviation (MAD) approach. We used a threshold of Median(X) ± 3 x MAD to identify the top 15 candidate hits and a threshold of Median(X) ± 2 x MAD to identify additional hits that were confirmed in the 1st and 2nd rounds of screening. This analysis yielded a total number of 21 candidate E3 ligases.

4.5 FUNCTIONAL VALIDATION OF CANDIDATE E3 LIGASES RESPONSIBLE FOR NUMB DEGRADATION.

4.5.1 Validation of the top six candidate E3 ligases identified by high-throughput siRNA screening.

Despite the extensive troubleshooting performed in the preliminary set-up phase of this work, the ELISA platform we developed remained affected by the intrinsic problem of a low degree of sensitivity, as witnessed by the fact that, throughout the screening, even in the case of our positive control (MDA-MB-361 cells exposed to 5 μM MG-132 for 24h), we could never score NUMB increases greater than two fold. The fact that all the candidate hits from the screening were therefore comprised within a low dynamic range unavoidably reflects in the occurrence of either false positive or false negative hits. We therefore embarked on a stepwise validation process starting with the top six candidates, (RBX1, TRIP12, KIAA1718, UBE2G1, WHSC1L1, LOC642446) identified in the screening. Initially, we verified by q-RT PCR the efficiency of the individual SMARTPool siGENOME siRNA oligo pools (4 oligos/gene, Dharmacon Technologies), used in the screening to silence the target gene. Using the same experimental conditions to perform siRNA reverse transfection as in the high-throughput screening, we observed that all six target genes were efficiently silenced by their respective siRNA pool (Figure 31A). We then assessed by IB the restoration of NUMB protein upon candidate gene silencing (Figure 31B). We observed that NUMB levels increased only after silencing of RBX1 and WHSC1L1, with no substantial changes in the case of the other genes. From this first validation step, we were therefore able to confirm that silencing of RBX1 and WHSC1L1 lead to restoration of NUMB protein levels in a model of NUMB-deficient tumor breast cells (Figure 31B), suggesting that these two genes might be involved in the negative regulation of NUMB cellular levels.

A

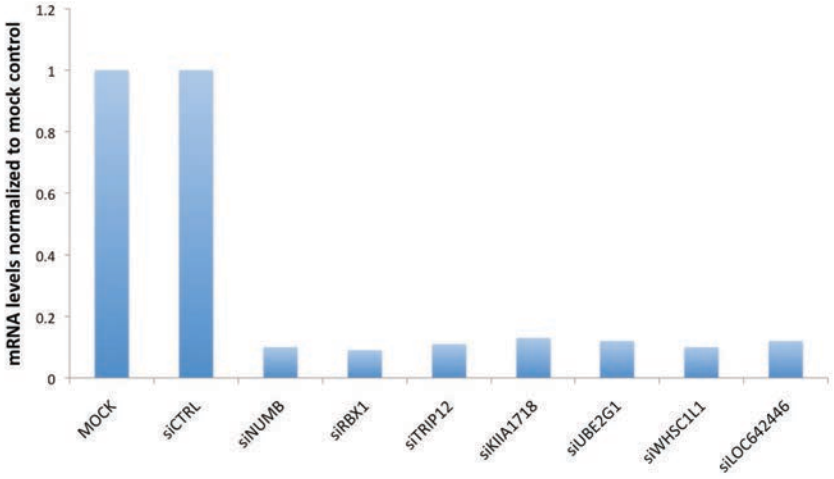

B

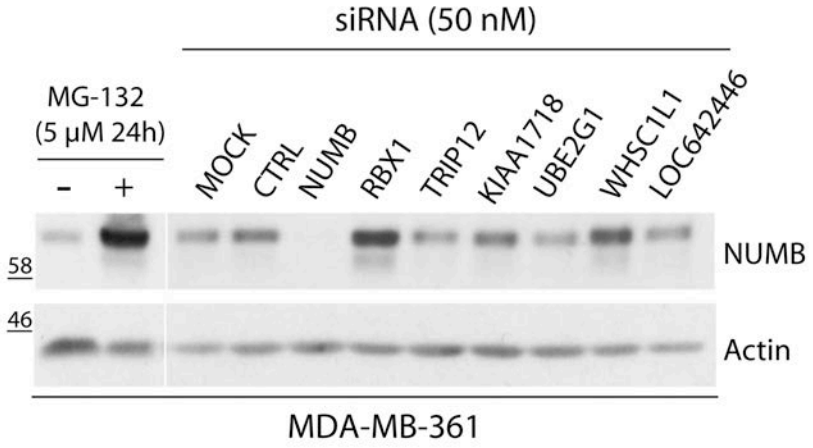

Figure 31. Validation of candidate E3 ligases in MDA-MB-361 cells.

A) The efficiency of the individual siRNA pools in silencing the corresponding target gene was evaluated for the top six candidate E3 ligases by q-RT PCR. MDA-MB-361 cells ($3X10^5$) were transfected with 50 nM of oligo pool and incubated for 72 hours using Lipofectamine RNAiMAX (Invitrogen) technologies. Total RNA was extracted and q-RT PCR performed as described in Material and Methods (Section 6.5, 6.7, 6.8). Results for each gene from siRNA transfected cells were normalized to the MOCK (not transfected) control cells. siCTRL: non-targeting siRNA oligo (Dharmacon Technologies). Results are representative of 3 independent experiments. B) The effect of silencing the top six candidate E3 ligases on NUMB protein levels in MDA-MB-361 cells was determined by immunoblotting. MBA-MB-361 cells ($3X10^5$) were transfected with 50 nM siRNA oligo pools using Lipofectamine RNAiMAX protocol (Invitrogen) and incubated for 72 h, before cell lysis (see section 6.5 of Material and Methods). MG-132 treatment (5 μM) was started 48 h after transfection and cells were then harvested 24h after the beginning of the treatment. Total cell lysate (20 μg) was loaded on gel for IB analysis. A non-targeting siRNA oligo (Dharmacon Technologies) was used as a negative control (CTRL). An anti-NUMB siRNA was used as a positive control for transfection efficiency. MG-132 treatment (5 μM for 24 h) was used as a positive control for NUMB restoration. Protein loading was assessed using an anti-actin antibody. MW markers are shown to the left of the blot. Blot is representative of 3 independent experiments.

4.5.2 Development of a NUMB-GFP based system for measuring NUMB restoration

As a complementary approach for the validation of candidate positive hits, we devised a strategy based on the use of a NUMB fusion protein conjugated to the Green Fluorescent Protein (NUMB-GFP). To this aim, we used a lentiviral vector (pLVX-Puro) to deliver a NUMB-GFP protein into MDA-MB-361 and MCF10A cells, yielding cells stably expressing the fusion protein (respectively, MDA-MB-361/NUMB-GFP and MCF10A/NUMB-GFP cells). We next checked whether the behavior of ectopic NUMB-GFP in these cells mimics the one of the endogenous protein in the corresponding parental cell lines. We therefore monitored by IB and immunofluorescence analysis (IF) the expression of NUMB-GFP in MDA-MB-361/NUMB-GFP and MCF10A/NUMB-GFP cells under basal and MG-132 or MG-341-treated conditions (Figure 32A,B,C). Faithfully recapitulating the situation of endogenous NUMB in control parental cells, we observed, either by IB or IF analysis, basally low NUMB-GFP levels in MDA-MB-361/NUMB-GFP cells, which could be promptly restored by MG-132 (Figure 32A,B) or MG-341-mediated proteasome inhibition (Figure 32C), while no differences could be observed in in MCF10A/NUMB-GFP cells. We concluded that MDA-MB-361/NUMB-GFP cells are a suitable cell model system for the validation of our top candidates from the siRNA screening.

We therefore used the MDA-MB-361/NUMB-GFP model system to silence individually the top six candidates with the corresponding siRNA oligo pools and evaluate the effect of this treatment on NUMB-GFP levels by IB and IF analysis (Figure 33A,B). In these experiments, RBX1 was confirmed as the most potent negative regulator of NUMB expression. Of note, the modest restoration of NUMB expression observed upon silencing of WHSC1L1 and TRIP12 in MDA-MB-361/NUMB-GFP cells could not be reproducibly observed in other replicates using this model system, nor was it reproducible for the endogenous NUMB protein in parental MDA-MB-361 cells.

We therefore decided to focus on RBX1 as a candidate hit to be subjected to thorough biochemical and functional validation.

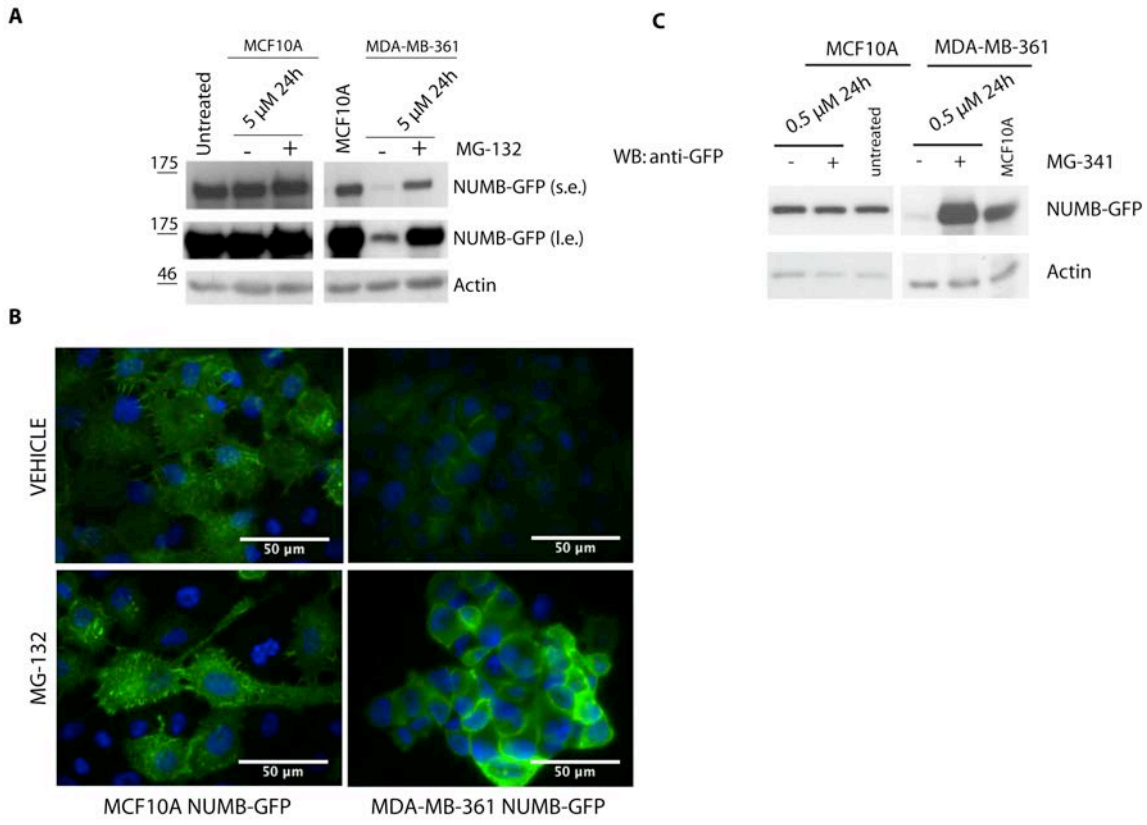

Figure 32. Characterization of the MDA-MB-361/NUMB-GFP and MCF10A/NUMB-GFP model system.

MDA-MB-361 and MCF10A cells were stably infected with a lentiviral vector expressing NUMB-GFP. The effect of MG-132 treatment (5 μM for 24 h) and of MG-341 (0.5 μM for 24h) on NUMB-GFP levels in the two infected cell populations was determined by IB (A, C) and fluorescence microscopy (B). A,C) Actin was used as a loading control. s.e., short exposure; l.e., long exposure. B) DAPI was used to stain nuclei (blue), NUMB-GFP (green). Scale bar, 50 μm.

A

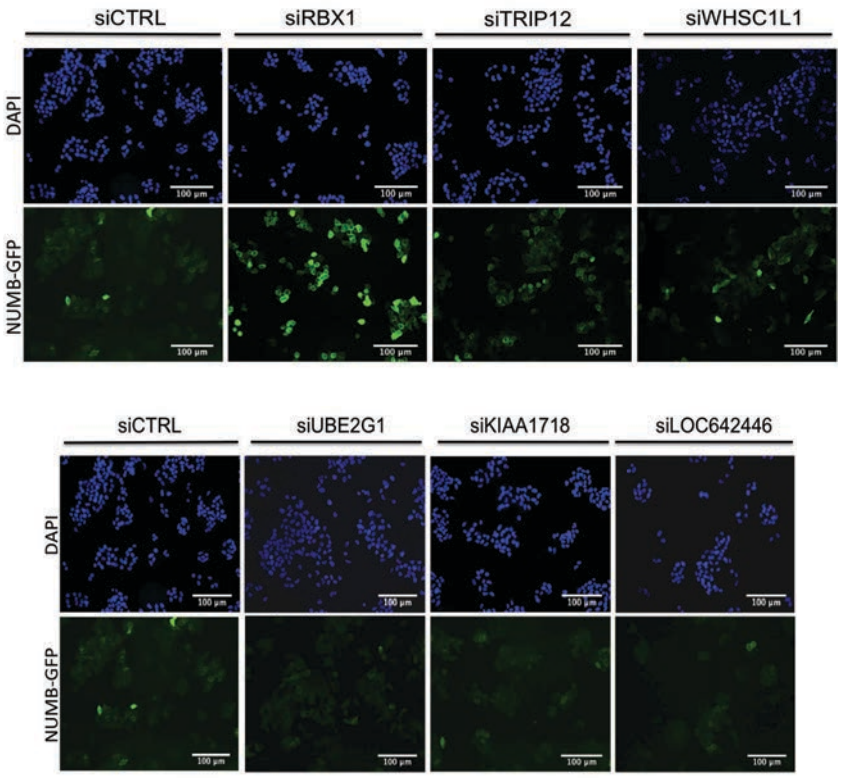

B

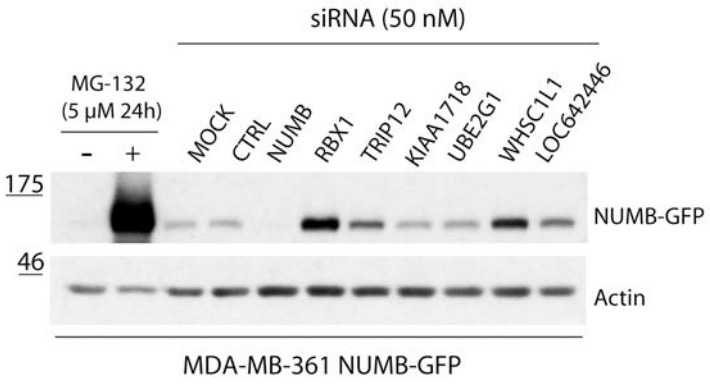

Figure 33. Analysis of the effects of silencing the six top candidate E3 ligases in MDA-MB-361 cells stably expressing NUMB-GFP.

The effect of silencing the six candidate E3 ligases on NUMB-GFP levels was assessed in MDA-MB-361/NUMB-GFP by (A) IF and (B) IB analysis. MDA-MB-361/NUMB-GFP cells (3 X 10^5) were transfected with 50 nM siRNA oligo pools using Lipofectamine RNAiMAX protocol (Invitrogen) and incubated for 72 h (see section 6.5 of Material and Methods), before IF analysis (A) and cell lysis for IB (B). MG-132 treatment (5 μM) was performed 48 h after transfection and cells were harvested 24 h post-treatment. A) A non-targeting siRNA oligo (Dharmacon Technologies) was used as a negative control (siCTRL). Nuclei are shown in blue (DAPI staining) and NUMB-GFP in green. Scale bar, 100 μm. B) Total cell lysate (20 μg) was loaded on gel for IB analysis. MG-132 treatment (5 μM for 24 h) was used as a positive control for NUMB-GFP restoration. Actin was used as a loading control. MW markers are shown to the left of the blots. Results are representative of 3 independent experiments.

4.5.3 Deconvolution of the pool of anti-RBX1 siRNA oligos.

We next went on to verify the individual efficiencies of the four anti-RBX1 siRNA oligos comprised in the pool originally used in the high-throughput screening.

We observed by IB that, albeit to a different extent, all four oligos caused an increase in NUMB levels in MDA-MB-361 cells, with oligo #03 being the most efficient and comparable to MG-132 treatment in its effect (Figure 34A).

Remarkably, when the same experiment was performed in MCF10A cells or in MDA-MB-231 cells as models of, respectively, normal and tumor breast cell lines with proficient NUMB levels and insensitive to MG-132 treatment, none of the four siRBX1 oligos yielded any modification of NUMB expression over the basal cellular levels (Figure 34B).

We therefore concluded that silencing of RBX1 is able to restore NUMB expression only when the NUMB protein is hyper-degraded by the UPS, thereby placing RBX1 as a key player in the molecular pathogenetic setting of NUMB-deficient breast tumors.

A

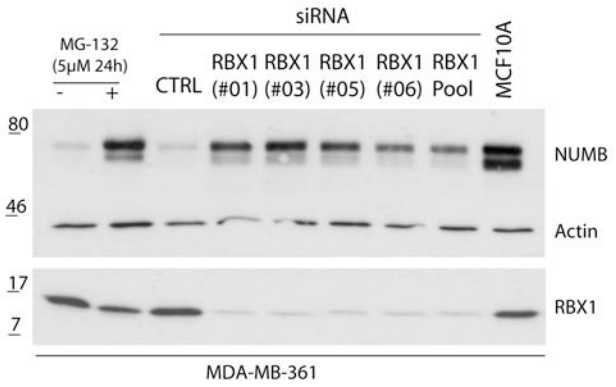

B

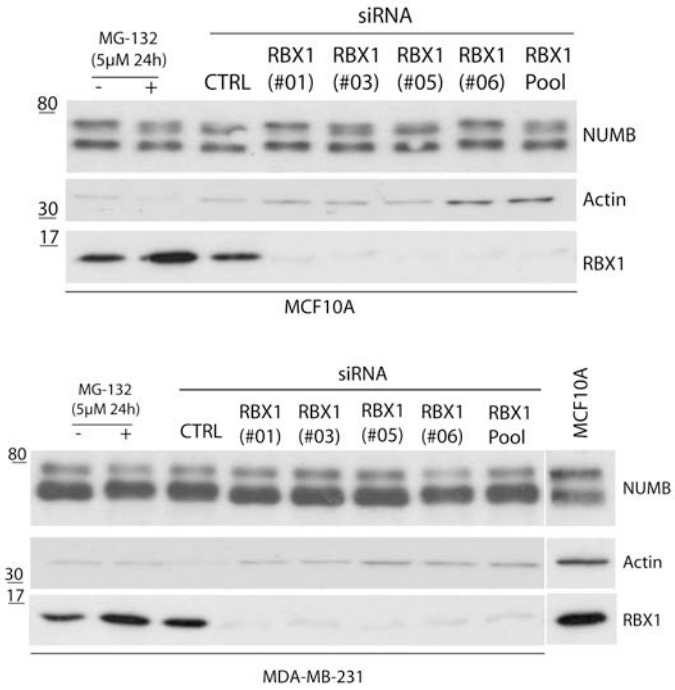

Figure 34. The effect of individual anti-RBX1 siRNA oligos on NUMB levels in breast epithelial cell lines.

The effect of the four anti-RBX1 siRNA oligos, singularly (RBX1 #01/03/05/06) or pooled (RBX1 pool) on NUMB expression levels in MDA-MB-361 cells (A) and in MCF10A and MDA-MB-231 cells (B) was determined by IB analysis. Cells (3 X 10^5 MDA-MB-361 and 1 X 10^5 MDA-MB-231 and MCF10A) were transfected with 10 nM of each siRNA oligo (50 nM siRNA oligo pool) using Lipofectamine RNAiMAX protocol (Invitrogen) and incubated for 72 h, before cell lysis (see section 6.5 of Material and Methods). MG-132 treatment (5 μM) was performed 48 h after transfection and cells were harvested 24 h after treatment. Total cell lysate (20 μg) was loaded on gel for IB analysis. A non-targeting siRNA oligo provided by Dharmacon (CTRL) was used as a negative control. The efficiency of RBX1 silencing was assessed by anti-RBX1 immunoblotting. NUMB basal expression levels are compared to those in MCF10A cells. MG-132 treatment (5 μM for 24 h) was used as a positive control of NUMB restoration levels. Actin was used as a loading control. MW markers are shown on the left. Results are representative of 3 independent experiments.

4.5.4 RBX1 silencing restores NUMB protein levels in primary tumor cells from breast cancer patients.

These results prompted us to directly assess the relevance of RBX1 to human cancer. To this aim, we set out to determine the effects of RBX1 silencing on NUMB levels in primary tumor epithelial cells derived from breast cancer patients. We have previously established that these primary tumor cells faithfully recapitulate the biology of the original tumor [105]. We therefore initially characterized a set of primary tumor cells for their intrinsic NUMB status and for their response to MG-132. We defined NUMB–proficient tumors as those with basal levels of NUMB higher or at least comparable to those in their normal counterpart and NUMB-deficient tumors as those with low basal levels of NUMB relative to their normal counterpart, which could be restored by MG-132 treatment.

We took andvantage of having in our lab one sample, used for other research lines in the lab, from human mammary tumor epithelial cells already characterized for NUMB levels as a NUMB-proficient tumor (12-M-176T) and one selected as a NUMB-deficient tumor (12-B1-54P). We used these samples for the analysis of the effects of RBX1 silencing.

We first optimized conditions for silencing RBX1 in 12-M-176T and 12-B1-54P samples, using the four anti-RBX1 oligos (singularly and pooled) used for the original screening. We decided to adopt the same conditions used for *RBX1* silencing in MDA-MB-361, MCF10A and MDA-MB-231 cells. Briefly, we performed the reverse trasfection protocol by plating cells after oligos seeding and incubating them for 72 h at 37°C. From this optimization, we identified siRNA oligos #01 and #03 as the most efficient at silencing RBX1 (Figure 35).

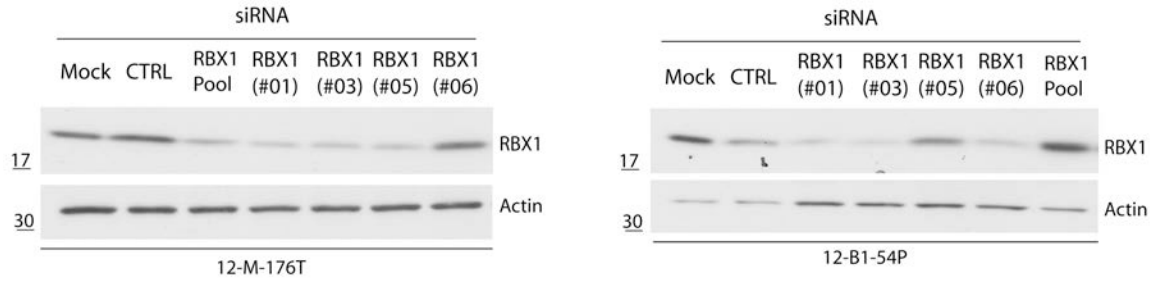

Figure 35. Test of the silencing efficiency of anti-RBX1 siRNA oligos in primary human tumor breast epithelial cells.

The effect of the four anti-RBX1 siRNA oligos, singularly (RBX1 #01/03/05/06) in two samples of human tumor breast epithelial cells derived from breast cancer patients (12-M-176T and 12-B1-54P) was determined by IB analysis. Cells (3 X 10^5) were transfected with 10 nM of each siRNA oligo or with 40 nM of the siRNA oligo pool, using Lipofectamine RNAiMAX protocol (Invitrogen) and incubated for 72 h, before cell lysis (see section 6.5 of Material and Methods). Total cell lysate (20 μg) was loaded on gel for IB analysis. A non-targeting siRNA oligo provided by Dharmacon (CTRL) and not transfected cells (Mock) were used as negative controls. The efficiency of RBX1 silencing was assessed by anti-RBX1 IB. Actin was used as a loading control. MW markers are shown on the left. Results are representative of 3 independent experiments.

We then transiently silenced RBX1 in the NUMB-proficient (12-M-176T) and the NUMB-deficient (12-B1-54P) primary tumor cell cultures. We observed that upon RBX1 silencing in the NUMB-deficient tumor, NUMB protein levels were restored to levels comparable to those following MG-132 treatment (Figure 36). In contrast, in the NUMB-proficient tumor, RBX1 silencing had no effect on NUMB levels (Figure 36). These data confirm an involvement of RBX1 in the downregulation of NUMB in NUMB-deficient human breast cancers.

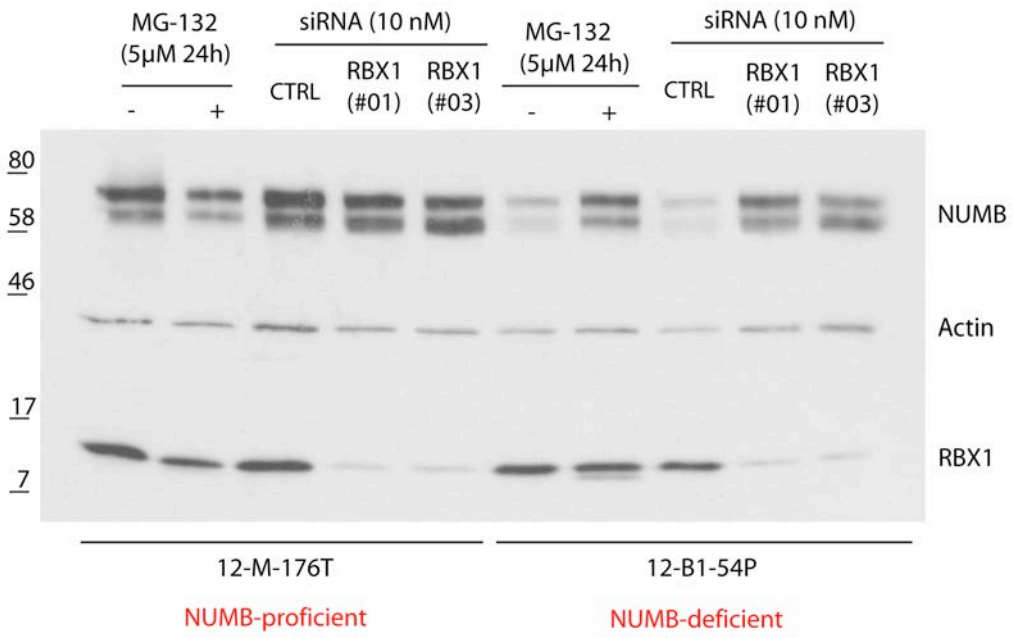

Figure 36. Assessment of the effect of RBX1 silencing on NUMB levels in NUMB-deficient and NUMB-proficient human primary breast tumor epithelial cells.

The effect of anti-RBX1 siRNA oligos #01 and #03 on NUMB protein levels in NUMB-deficient (12-B1-54P) and NUMB-proficient (12-M-176T) primary breast tumor cells was determined by IB. Cells (1 X 10^5) were transfected with 10 nM of each siRNA oligo using Lipofectamine RNAiMAX protocol (Invitrogen) and incubated for 72 h, before cell lysis (see section 6.5 of Material and Methods). MG-132 treatment (5 μM) was performed 48 h after transfection and cells were harvested 24 h post MG-132 treatment. Total cell lysate (20 μg) was loaded on gel for IB analysis. The efficiency of RBX1 silencing was controlled using an anti-RBX1 antibody. A non-targeting siRNA oligo (CTRL) was used as a negative control. Treatment with 5 μM MG-132 for 24 h was used as a positive control for NUMB restoration. Actin was used as a protein loading control. MW markers are shown on the left. Blots are representative of 2 independent experiments.

4.5.5 RBX1 silencing restores NUMB protein levels in primary tumor cells from lung cancer patients.

To extend our findings to other human malignancies in which loss of NUMB expression has been shown to be pathogenetically relevant, we analyzed the involvement of RBX1 in regulating NUMB levels in primary cells derived from non-small cell lung cancer (NSCLC).

We took andvantage of having in our lab the following types of samples: one sample, used for other research lines in the lab, of human lung tumor epithelial cells already characterized for NUMB levels as NUMB-proficient (12-P-36T), one as normal (12-L-303NP) and four selected as NUMB-deficient (12-L-313P, 12-L-302P, 12-L-311P and 12-L1-3P). We decided to analyze the effects of RBX1 silencing on NUMB levels on these samples by IB. To do this, we silenced RBX1 using siRNA oligos anti-RBX1 oligos R#01 and R#03 used for the original screening. We decided to use the same conditions used for RBX1 silencing in primary tumor breast cancer cells. As with primary breast cancer cells, we observed an increase in NUMB protein levels only in the NUMB-deficient cells (Figure 37). These data suggest that RBX1-dependent downregulation of NUMB could be a phenomenon common to different types of NUMB-deficient cancers.

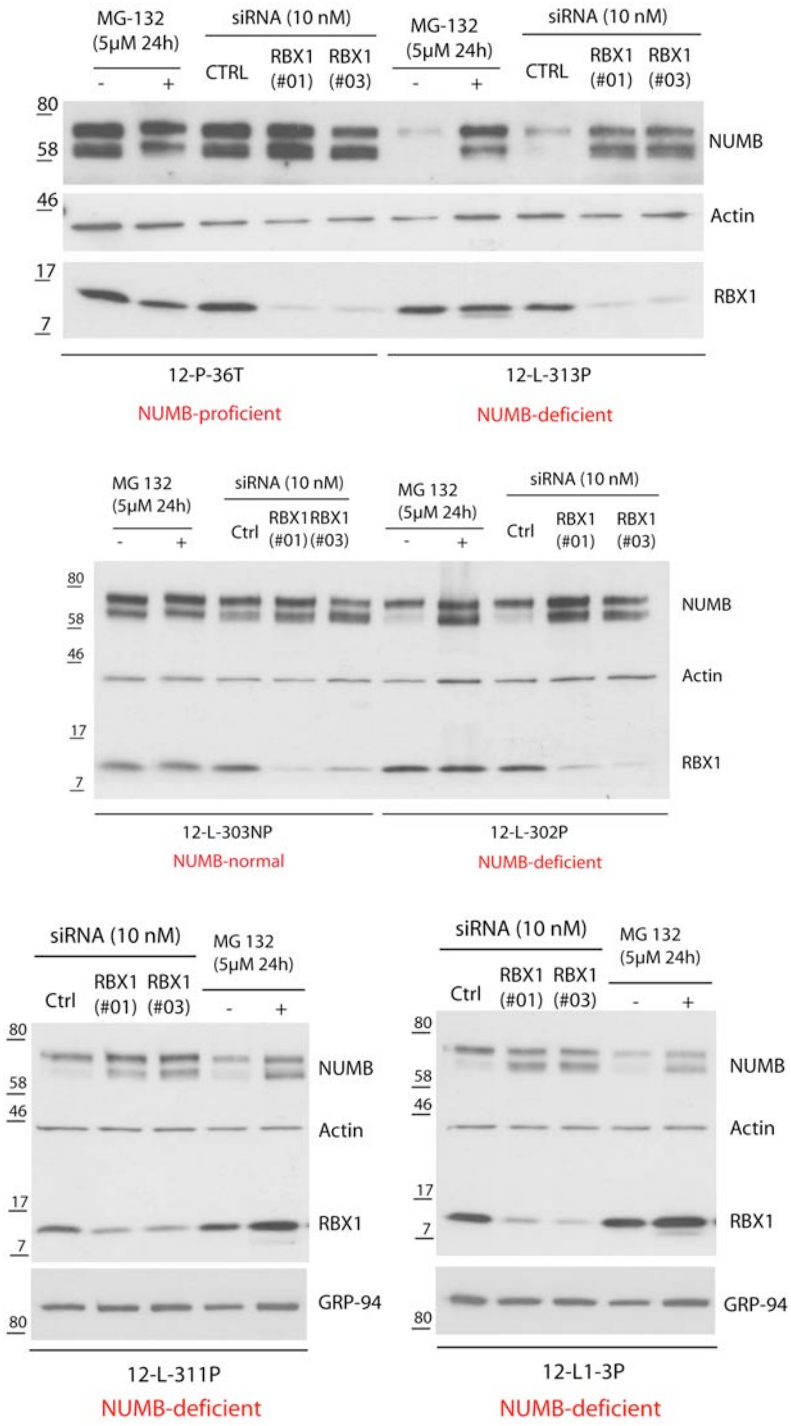

Figure 37. The effect of RBX1 silencing on NUMB protein levels in NUMB-deficient and NUMB-proficient human primary tumor cells from NSCLCs.

The effect of anti-RBX1 siRNA oligos #01 and #03 on NUMB protein levels in the NUMB-deficient (12-L-313P, 12-L-302P, 12-L-311P and 12-L1-3P), NUMB-proficient (12-P-36T) and NUMB normal (12-L-303NP) NSCLC tumor samples was determined by IB analysis. The efficiency of RBX1 silencing was controlled using an anti-RBX1 antibody. A non-targeting siRNA oligo (CTRL), provided by Dharmacon, was used as a negative control. Treatment with 5 μM MG-132 for 24 h was used as a positive control for NUMB restoration. Actin and GRP-94 were used as a protein loading controls. MW markers are shown on the left. Blot is representative of 2 independent experiments.

4.5.6 Characterization of the molecular mechanism responsible for enhanced RBX1-dependent NUMB degradation in NUMB-deficient cancers

We hypothesized that overexpression of RBX1 in tumors could be responsible for the hyper-ubiquitination and excessive degradation of NUMB in NUMB-deficient tumors. To test this hypothesis, we compared RBX1 protein levels in NUMB-deficient and NUMB-proficient primary tumor epithelial cell cultures from breast and lung tumors by IB (Figure 38). In this preliminary analysis, we observed no differences in RBX1 protein levels between the NUMB-deficient and NUMB-proficient tumors.

One possibility is that RBX1 mutations, which have also been detected in several types of human cancercs (source TCGA), might result in deranged activity of the RBX1 protein. While this speculation deserves experimental addressing, we noted that RBX1 is a component of the SCF multi-protein E3 ligase complex that contains proteins, such as cullins and F-box proteins, which cooperate with RBX1 in the ubiquitination process. We therefore reasoned that other SCF complex proteins could be deregulated/mutated in NUMB-deficient tumors, for the activity of which RBX1 represents a key component.

Of note, in the process of ubiquitination and ensuing proteasomal degradation through the SCF E3 ligase complex, the specificity towards the protein substrate rests on the F-box component of the SCF multi-protein complex. Intriguingly, we noted that the F-box protein FBXW8 was one of the top hits in the list of candidates identified from our screening (Table 3). This F-box protein has been described to form heterodymers and to be responsible for the binding of CUL1-RBX1 to CUL7-RBX1, enhancing the ubiquitination of CUL1 substrates [215].

We therefore decided to test the effects of silencing FBXW8 on NUMB protein levels in NUMB-deficient (MDA-MB-361) and NUMB-proficient (MCF10A and MDA-MB-231) breast epithelial cells. We used the four anti-FBXW8 siRNA oligos employed in the high-throughput screening, individually or pooled together, to silence FBXW8. Initially, we verified the efficiencies of these siRNAs at silencing FBXW8 in the three cell lines by q-

RT PCR (Figure 39A). We then assessed NUMB protein levels by IB and observed that, in MDA-MB-361 cells, all four oligos were able to restore NUMB to levels comparable or greater than MG-132 treatment (Figure 39B). In contrast, we did not observe any effects on NUMB levels in NUMB normal and NUMB-proficient tumor epithelial cells, MCF10A and MDA-MB-231, respectively (Fig. 39B). These data suggest that FBXW8 could be involved in the hyper-degradation of NUMB in NUMB-deficient tumors, most likely cooperating with RBX1 in the contest of a SCF multiprotein complex.

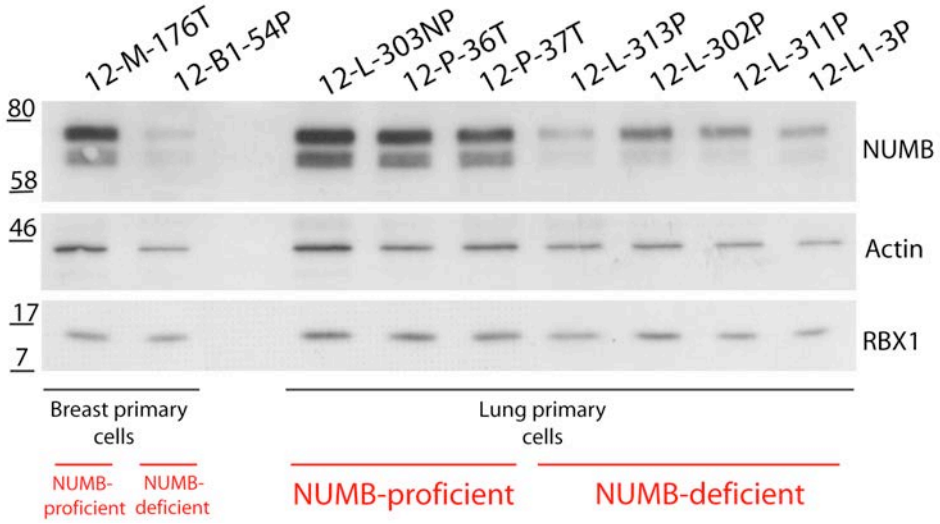

Figure 38. Analysis of RBX1 protein levels in NUMB-deficient and NUMB-proficient primary tumor epithelial tumor cells from lung and breast cancer.

NUMB and RBX1 expression levels in NUMB-deficient and NUMB-proficient breast and lung primary tumor cells were determined by IB analysis using specific antibodies. Actin was used as a loading control. MW markers are shown on the left. Blots are representative of 2 indipendent experiments.

A

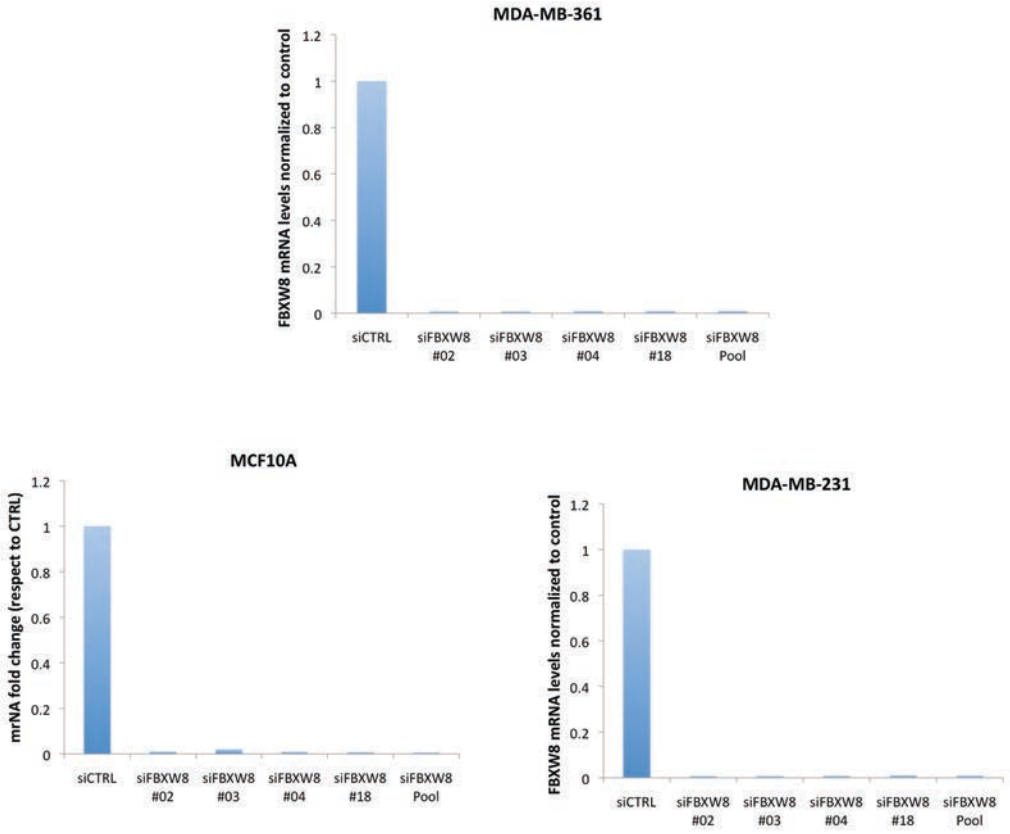

B

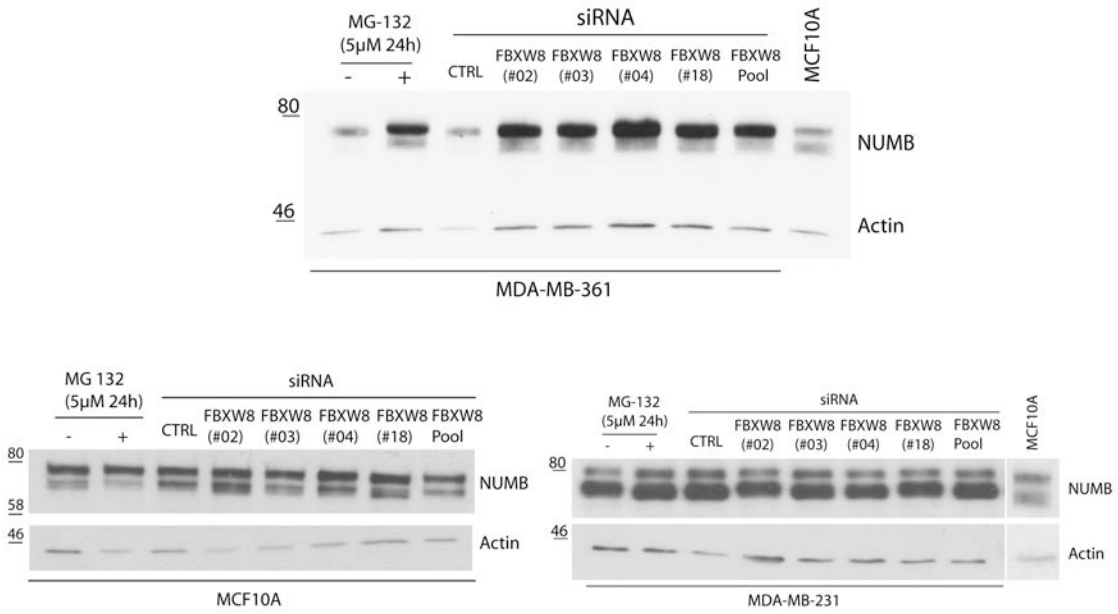

Figure 39. Analysis of the effects of *FBXW8* silencing on NUMB levels in breast cancer cell lines.

The efficiency of FBXW8 silencing was assessed by q-RT PCR analysis in all the three cell lines (A). The effect of the four anti-FBXW8 siRNA oligos employed in the high-throughput screening, singularly (FBXW8 #02/#03/#04/#18) or pooled (FBXW8 pool) on NUMB expression levels, in MDA-MB-361, MCF10A and MDA-MB-231 cells was determined by IB (B). A non-targeting siRNA oligo (CTRL), provided by Dharmacon, was used as a negative control. MG-132 treatment (5 μM for 24 h) was used as a positive control for NUMB restoration. NUMB basal expression levels are compared to those of MCF10A cells. Actin was used as a loading control. MW markers are shown on the left. Results are representative of 3 independent experiments.

4.5.7 NUMB and RBX1 physical interact in MDA-MB-361 cells.

The process of ubiquitination by SCF E3 ligases requires binding of the substrate within the multi-protein machinery. We therefore decided to investigate the possibility that NUMB and RBX1 might physically interact by performing immunoprecipitation experiments in MDA-MB-361 cells. To this aim, considering that E3 ligase/substrate interactions might be transient and notably difficult to detect, we decided to overexpress a FLAG-tagged NUMB protein in MDA-MB-361 cells and to perform IP experiments in the presence of MG-132 to stabilize the NUMB-FLAG protein and enhance the eventual NUMB-RBX1 interaction. We therefore generated a lentiviral construct to overexpress NUMB in mammalian cells using the lentiviral backbone pLentilox 3.7 (pLL 3.7), which allows achieving high and constitutive expression of genes of interest, due to the presence of the human cytomegalovirus immediate early promoter. Using this lentiviral vector, we generated a construct for the human FLAG-tagged full length (FL) NUMB (NUMB FL-FLAG) and for a FLAG-tagged NUMB mutant lacking the Phospho-Tyrosine Binding (PTB) domain of NUMB (NUMB ΔPTB-FLAG), an adaptor domain mediating NUMB interaction with many binding partners [216].

We therefore transfected 293T packaging cells with these constructs to produce viruses to infect MDA-MB-361 cells. Not infected cells were used as a negative control (NI).

We performed an anti-FLAG immunoprecipitation experiment using the anti FLAG M2 affinity gel (Sigma Aldrich), a purified murine IgG1 monoclonal antibody covalently attached to agarose. Analysis of the immunoprecipitates by IB revealed that RBX1 co-immunoprecipitates with NUMB FL-FLAG, but not with NUMB ΔPTB-FLAG (Figure 40). This result suggests a putative interaction between NUMB and RBX1, possibly mediated through the PTB domain of NUMB.

We also verified that the NUMB ΔPTB-FLAG protein was still able to bind to other known interactors of NUMB, by analyzing the interaction of this NUMB mutant with the

endocytic proteins Eps15 and AP2, that are known to interact with the C-terminal region of NUMB [10,30]. We found that both Eps15 and AP2 were enriched in both the NUMB FL-FLAG and NUMB ΔPTB-FLAG IP samples, arguing for the specificity of the interaction between NUMB and RBX1 through the PTB domain (Figure 40).

We are now verifying whether we can observe an interaction between NUMB and RBX1 following IP of the endogenous proteins and whether this interaction is direct or mediated by the participation of other components of the SCF complex, first and foremost, FBXW8.

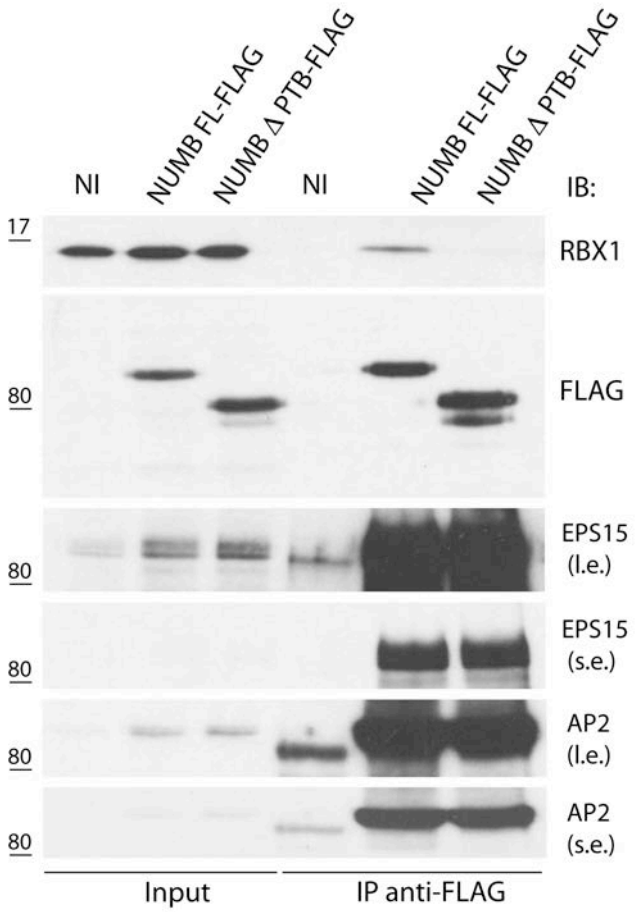

Figure 40. Analysis of the physical interaction between NUMB and RBX1 in MDA-MB-361 cells.

MDA-MB-361 cells were infected with NUMB FL-FLAG or NUMB ΔPTB-FLAG. Not infected (NI) MDA-MB-361 cells were used as a negative control. The cells were treated with MG-132 (5 μM for 24 h) two days after cells infection and lysed at the end of the treatment. FLAG-tagged NUMB proteins were immunoprecipitated from total cell lysates (30 mg) with anti FLAG M2 affinity gel (120 μl) and immunoprecipitates were analysed by IB using the indicated antibodies. Blot shows input of the IP reaction (25 μg) and a half of the anti FLAG immunoprecipitates. s.e., short exposure; l.e., long exposure. MW markers are reported to the left of the blots. Experiment is representative of two repeats.

4.6 TARGETING LOSS OF NUMB AS AN ANTI-CANCER THERAPY FOR NUMB-DEFICIENT BREAST CANCERS.

The overall rationale of this thesis work is based on the notion that loss of NUMB in human cancer is the consequence of its exaggerated ubiquitination and ensuing degradation. A clinically relevant corollary of this view is that targeting the upstream mechanisms responsible for NUMB degradation in tumors might represent an effective therapeutical strategy. While the bulk of this thesis work was aimed at identifying such mechanisms through a high-thoughput siRNA-based screening focused on the family of E3 ligases, we also decided to perform experiments to provide proof-of-concept that restoring NUMB expression is an effective anti-cancer strategy. To do this, we decided to exploit MDA-MB-361 and MDA-MB-231 cells as models of, respectively NUMB-deficient and NUMB-proficient tumor cells, and to verify the effects of proteasomal inhibition by MG-132 on their tumorigenic potential *in vivo*. To this aim, we orthotopically xenografted 1.5 x 10^6 MDA-MB-361 or 1.5 x 10^5 MDA-MB-231 cells into the inguinal mammary fat pads of NOD/SCID IL2R gamma-chain null female mice. Once tumors had reached ~150 mm^3 volume (~4 weeks after injection), as assessed by *in vivo* caliper measurements, mice were treated every three days with MG-132 at a dose of 1 mg/kg intravenously. Control mice received and equivalent dose of vehicle, ethanol. Two weeks after the first treatment, mice were sacrificed and tumors were explanted and weighed. Tumor explants were also lysed for protein extraction and IB analysis to control for the efficiency of MG-132 treatment and NUMB restoration, by monitoring beta-catenin and NUMB protein levels. We observed that tumor outgrowths generated by MDA-MB-361 cells in MG-132 treated mice were ~50% smaller in size compared to tumors generated in control mice (Figure 41A, C). IB analysis of beta-

catenin and NUMB confirmed that the proteasome was efficiently inhibited and NUMB restored in MG-132 treated MDA-MB-361 tumors (Figure 41B).

In contrast, tumor outgrowths generated by MDA-MB-231 cells in MG-132 treated mice were comparable in size to tumors generated in control mice (Figure 42A, C). IB analysis confirmed that MG-132 treatment was efficient as beta-catenin levels were higher in MG-132 treated mice compared with controls (Figure 42B). Altogether, these results indicate that NUMB restoration upon proteasome inhibition results in a significant reduction of the tumorigenic potential of NUMB-deficient tumor cells. This effect is specific and directly dependent on the restoration of NUMB expression, rather than related to off-target effects of the MG-132 treatment, as witnessed by evidence that the growth inhibitory effect could not be observed in NUMB-proficient tumor cells. Therefore, targeting proteosomal degradation of NUMB in NUMB-deficient tumors can represent an effective anti-cancer strategy. Remarkably, by this experiments, we have also established an amenable *in vivo* model to assess the potential of RBX1/FBXW8 inhibition in affecting tumor growth of NUMB-deficient cancers.

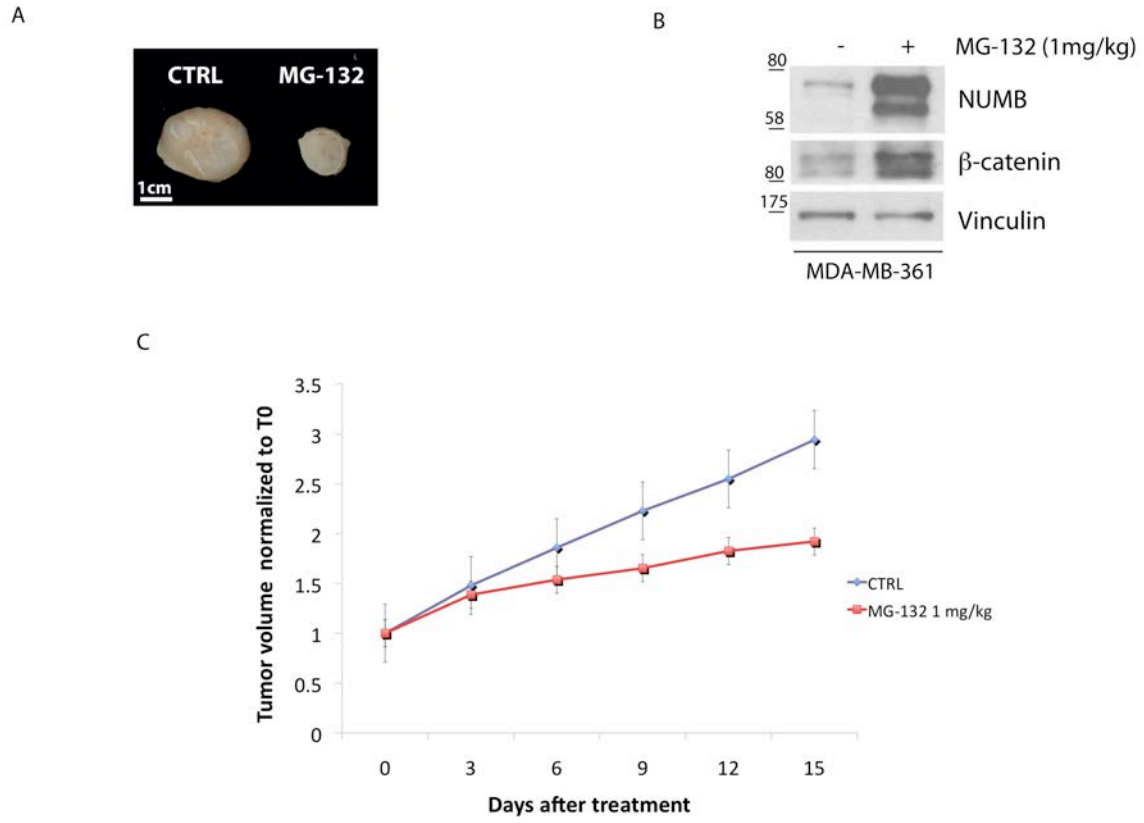

Figure 41. Effects of MG-132 treatment on the tumorigenicity of NUMB-deficient MDA-MB-361 cells *in vivo*.

Mammary tumors were generated by injecting 1.5 x 10^6 MDA-MB-361 cells into the inguinal mammary fat pads of NOD/SCID IL-2R gamma chain null mice. Tumors were allowed to develop until they reached 150 mm^3 before starting the treatment of mice every 3 days with MG-132 (1 mg/kg) or ethanol (1 mg/kg), in controls (CTRL). Two weeks after the first treatment, animals were sacrificed and tumors explanted and weighed. A) Representative images of tumor outgrowths obtained from MG-132-treated and CTRL mice. Scale bar, 1 cm. B) IB analysis of NUMB and beta-catenin expression in MG-132-treated and CTRL tumors. Vinculin was used as a protein loading control. MW markers are shown on the left. C) Kinetic evaluation of tumor growth in MG-132-treated and CTRL mice. Tumor volume was assessed by *in vivo* caliper measurements after the first treatment (Day 0) and then every 3 days for a period of 15 days. Results are plotted as fold-increase with respect to Day 0 and are the mean ± S.D. of 3 independent experiments (n = 9).

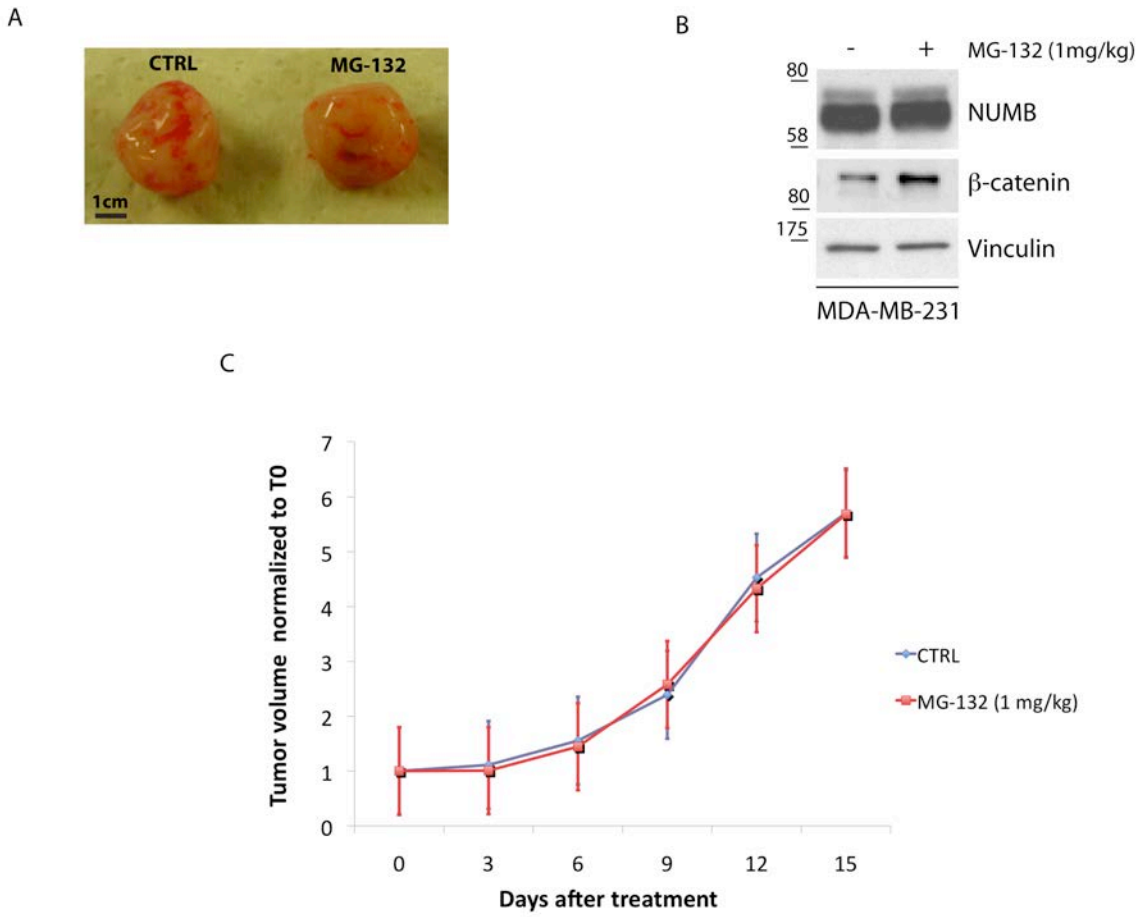

Figure 42. Effects of MG-132 treatment on the tumorigenicity of NUMB-proficient MDA-MB-231 cells *in vivo*.

Mammary tumors were generated by injecting 1.5 x 10^5 MDA-MB-231 cells into the inguinal mammary fat pads of NOD/SCID IL-2R gamma chain null mice. Tumors were allowed to develop until they reached 150 mm^3 before starting the treatment of mice every 3 days with MG-132 (1 mg/kg) or ethanol (1 mg/kg), in controls (CTRL). Two weeks after the first treatment, animals were sacrificed and tumors explanted and weighed. A) Representative images of tumor outgrowths obtained from MG-132 treated and CTRL mice. Scale bar, 1 cm. B) IB analysis of NUMB and beta-catenin expression in MG-132 treated and CTRL tumors. Vinculin was used as a protein loading control. MW markers are shown on the left. C) Kinetic evaluation of tumor growth in MG-132-treated and CTRL mice. Tumor volume was assessed by *in vivo* caliper measurements after the first treatment (Day 0) and then every 3 days for a period of 15 days. Results are plotted as fold-increase with respect to Day 0 and are the mean ± S.D. of 3 independent experiments (n = 9).

5 DISCUSSION

5.1 RNAi HIGH-THROUGHPUT SCREENING TO IDENTIFY NUMB NEGATIVE REGULATORS IN NUMB-DEFICIENT TUMORS

In the human genome project era, it has become clear that the identification of genetic networks regulating cellular homeostasis such as cell differentiation and transformation, cell growth and apoptosis, is fundamental to understanding their complexity and, moreover, the complexity of their dysfunction, which leads to pathological situations, first and foremost cancer.

In the last decades, the employment of high-throughput screening approaches combined with traditional cell culture techniques, has opened the way to functionally profile the biological processes of thousands of genes in live cells through the invention of innovative cellular-genomics methodologies. Among these, RNA interference (RNAi) has the potential to perform rapid genome-wide loss-of-function (LOF) screens in mammalian systems, which until recently has been applied only to lower organisms.

In this thesis, we developed a strategy to perform a high-throughput screening aimed at analyzing, in a rapid and homogeneous manner, hundreds of putative candidate genes involved in NUMB downregulation in live cells.

The screening assay employs: i) a NUMB-deficient cell model system (the MDA-MB-361 cell line) that recapitulates NUMB-deficient human cancers, in which NUMB protein is excessively ubiquitinated and degraded by the proteasome; ii) a siRNA library (Dharmacon Technologies) targeting families of potential NUMB regulators (e.g. E3 ligases), in which each gene is targeted by a pool of 4 siRNA oligos to guard against potential off-target effects; iii) an ELISA capture assay, employing an in-house produced monoclonal NUMB antibody, which measures NUMB protein levels in cell lysates (see section 4.3).

Using this assay, we screened an E3 ligase siRNA library targeting ~600 E3 ligases (see section 4.4) and derived a list of 21 candidate ligases that potentially downregulate NUMB protein levels (see Table 3) in human cells. This list included: i) HECT-type ligases, e.g. TRIP12; ii) monomeric RING finger E3 ligases, such as MDM2; and iii) multisubunit RING finger E3 ligases and F-box proteins belonging to SCF complexes.

Upon validation of the top six candidates (see sections 4.5), we were able to verify only one hit, RBX1, as a negative regulator of NUMB. Based on this finding, we also investigated FBXW8, which is known to interact with RBX1 in an SCF complex [215], and verified its involvement in NUMB downregulation. Thus, from 7 candidates tested, only two were validated as true NUMB regulators. From this initial validation, it appears that the screening assay we developed is intrinsically affected by a high rate of false positive results. This high false positive hit rate is likely attributable to the limited dynamic range of the ELISA screening assay, in which only a 2.5-fold difference in NUMB levels was obtained in the positive control (MG-132 treated samples) over basal levels. Nevertheless, despite the limitations of the screening assay, we were able to successfully identify and validate two components of an SCF multi-component E3 ligase complex, RBX1 and FBWX8, that mediate proteasomal degradation of NUMB.

These results demonstrate that the high-throughput siRNA screening assay is a valid assay for identifying genes involved in NUMB downregulation and we are now using this system to screen other siRNA libraries targeting potentially interesting gene families, such as kinases.

5.2 CHARACTERIZATION OF THE UPS MACHINERY REGULATING NUMB

RBX1 is a 15 kDa protein containing a RING finger domain that together with the scaffold protein Cullin, determines the catalytic activity of SCF ligases. FBXW8, on the other hand, is one of the F-box protein that determines substrate specificity of SCF ligases. FBXW8 belongs to the Fbw class of F-box proteins that contain a WD-40 domain, which mediates binding to the substrate [165].

We validated both RBX1 and FBXW8 as a negative regulators of NUMB in breast cancer cell lines, and, in the case of RBX1, also in primary tumor cells derived from NUMB-deficient human breast and lung cancers (see section 4.5). Moreover, we demonstrated that NUMB and RBX1 physically interact in MDA-MB-361 cells (see section 4.5.7), supporting the idea that RBX1 directly regulates NUMB.

Based on these data, it is tempting to speculate that an SCF complex containing RBX1 and FBXW8 mediates NUMB downregulation. Indeed, published data indicate the existence of an SCF complex comprised of RBX1, CUL7, FBXW8 and Skp1 [215]. This ligase complex is critical for correct intrauterine growth and placental development due to its role in the regulation of cell differentiation and vascular morphogenesis. Consistently, dysfunction of the CUL7-SCF complex has been linked to pre- and post-natal growth retardation in mice and humans [217-219].

Interestingly, FBXW8 is the only F-box protein that has been shown to bind to the CUL7, and only a few CUL7 E3 ligase substrates have been identified, including cyclin D1 and insulin receptor substrate 1 (IRS-1) [220], suggesting a role for this ligase in cell proliferation and survival, as well as the Golgi reassembly stacking protein 1 (GRASP65) [215].

However, there is evidence that CUL7-RBX1 can promote the ubiquitination of CUL1 substrates by forming high order complexes with CUL1-RBX1, via the heterodimerization of FBXW8 with other F-box proteins [215]. Thus, it is conceivable that NUMB could be a novel substrate of a RBX1-CUL7 SCF complex that is recruited by FBXW8, or of a RBX1-CUL7/RBX1-CUL1 high order complex in which FBXW8 mediates heterodimerization of the complex. In this latter case, another F-box protein recruits NUMB. Further experiments are therefore required to define the exact nature and composition of the SCF complex mediating NUMB downregulation. Transient silencing of CUL7 and CUL1 in the NUMB-deficient MDA-MB-361 cell line should allow us to determine the involvement of these proteins in NUMB degradation. The precise definition of the SCF complex is relevant, not only from a scientific point-of-view, but also from a translational point-of-view, as it could lead to the identification of novel molecular targets for therapeutic intervention in NUMB-deficient cancers.

5.3 RELEVANCE OF SCF E3 LIGASES TO CANCER

By promoting a variety of short-lived regulatory proteins for targeted degradation, SCF E3 ligases play an essential role in many biological processes, including cell cycle progression, DNA replication, signal transduction, gene transcription, and development, among others [149,172]. It is not surprising therefore that the deregulation of SCF activity, due to alterations of one of its components, leads to subversion of molecular circuitries and contributes to pathological conditions, including cancer.

Indeed, several SCF components are known to be deregulated in cancer. Among the cullins, CUL1 is overexpressed in 40% of lung cancers, with active neddylated forms specifically expressed in high-grade neuroendocrine lung tumor tissues [221], whereas CUL2 frameshift mutations have been detected in two out of 41 colon cancers [222]. CUL5

is a putative tumor suppressor that blocks Src activity [223] and inhibits breast cancer cell growth upon overexpression [224], while CUL4A is overexpressed in a number of human cancers, including poor prognosis breast cancers [225-227].

Among the ~70 F-box proteins encoded by the human genome, only three have been linked to cancer: i) Skp2, which was shown to be oncogenic in hormone-dependent breast cancer cells [228] and in human prostate cells where it led to an increase in p27 degradation and increased proliferation [229,230], while it exerted a tumor suppressor role by regulating the activity of CDKs by the degradation of p27 [231,232]; ii) Fbxw7, which is a tumor suppressor in breast and endometrial cancers [233] and has a high rate of mutations in gastric, colon and prostate cancers [234-237] ; III) β-TrCP, which is either an oncogene or a tumor suppressor, depending on its target substrates in colorectal, pancreatic and breast cancers or melanoma [238-241]. Moreover, ectopic expression of CUL7 increased cell proliferation in U2OS cells expressing functional p53, by antagonizing p53 function [247] and CUL7 is a key factor in regulating the EMT of the trophoblast cells [248].

Of the proteins involved in NUMB degradation, RBX1 has been shown to be overexpressed in carcinomas of the lung, liver and breast [242]. Notably, siRNA silencing of RBX1 in multiple cancer cell lines, such as breast, lung, colon, cervical carcinoma, pancreas and glioblastoma cancer cell lines, suppressed tumor cell growth in monolayer culture, reduced clonogenic potential, and impaired anchorage-independent growth in soft agar, a hallmark of transformed cells [243]. These effects were accompanied by the induced G2/M cell cycle arrest, senescence and apoptosis in a p53-independent manner, leading to suppression of cancer cell growth [242,243]. Thus, RBX1 appears to be required for cancer cell proliferation and survival, as well as for the maintenance of the transformed phenotype *in vitro* [244].

FBXW8 has also been linked to cancer in preliminary studies. It has been demonstrated

that silencing of FBXW8 expression by siRNA inhibited the growth of choriocarcinoma JEG-3 cells, inducing cell growth arrest at G2/M phase through decreasing the levels of CDK1, CDK2, cyclin A and cyclin B1 and upregulation of p27 at protein level [245]. In colon cancer and glioblastoma cell lines, depletion of FBXW8 caused a significant accumulation of cyclin D1, as well as sequestration of CDK1 in the cytoplasm. This resulted in a severe reduction of cell proliferation. Thus, FBXW8 appears to have an essential role in colon cancer and glioblastoma cell proliferation through proteolysis of cyclin D1 [246]. However, no evidence has so far been provided for role of FBXW8 in breast and lung cancer.

In order to causally link RBX1 and FBXW8 (if validated in primary tumor cells) to breast and lung tumorigenesis, it is important to define the mechanism(s) leading to their deregulation. At variance with previous studies reporting overexpression of RBX1 in breast and lung cancers [242], data from our preliminary screening in primary cells do not point to major differences in basal RBX1 protein levels between NUMB-proficient and NUMB-deficient tumors (see section 4.5). However, a more in-depth characterization of the correlation between NUMB status and RBX1 levels is required to determine whether overexpression could be a mechanism leading to deregulated RBX1 activity in NUMB-deficient cancers.

Alternative mechanisms that could result in RBX1-FBXW8-SCF dysfunction in cancer, include activating mutations in the *RBX1* gene, overexpression of FBXW8 (if confirmed as the F-box protein recruiting NUMB), or deregulation of upstream regulators of SCF complexes. Indeed, SCFs have been shown to be regulated by kinases, which phosphorylate the F-box protein and promote their dimerization and consequently SCF ligase activity [245,249]. Moreover, Cullin neddylation is known to be important for the activation of SCF ligases, as it causes dissociation of the ligase assembly inhibitor Cand1, promoting E2 recruitment and ubiquitin transfer [250,251].

5.4 SCF AS A NOVEL TARGET FOR THERAPEUTIC INTERVENTION IN NUMB-DEFICIENT CANCERS

Considering that re-expression of NUMB, or inhibition of the downstream consequences of loss-of-NUMB (such as Notch activation and p53 suppression) in NUMB-deficient tumor cells, impairs tumorigenic phenotypes *in vitro* and *in vivo* [103,107] (Pece, unpublished data), inhibition of the UPS components responsible for NUMB degradation could represent an effective strategy for therapeutic intervention in NUMB-deficient cancers.

We demonstrated that both MG-132 and Bortezomib were able to restore NUMB protein levels in NUMB-deficient breast cancer cell lines to levels comparable to MCF10A cells. Moreover, we observed that MG-132 *in vivo* is able to inhibit growth of NUMB-deficient tumors. Thus, inhibiting the proteasome could be an effective therapeutic strategy for the treatment of NUMB-deficient cancers. Given the availability of a clinically approved proteasome inhibitor, Bortezomib, a full pre-clinical evaluation of this inhibitor in NUMB-deficient cancers is merited.

However, targeting downstream components of the UPS, i.e., the proteasome, is unspecific and could lead to toxic side effects. Indeed, numerous side effects resulting from Bortezomib treatment have been described, such as asthenic conditions, gastrointestinal events, hematological toxicity and peripheral neuropathy [252].

Targeting the upstream components in the UPS should be a more specific strategy as it will affect a smaller set protein substrates, instead of all proteins subject to proteasomal degradation.

In this context, an investigational small molecule inhibitor of the NEDD8-activating enzyme, MLN4924, has recently been developed, which inhibits SCF activation by preventing neddylation of the Cullin subunit [253,254].

This inhibitor causes accumulation of SCF E3 ligases substrates and suppresses growth of colon, NSCLC and breast tumor cells both *in vitro* and *in vivo* by inducing apoptosis [254]. In line with the increased specificity of this drug, MLN4924 was well-tolerated in mice and is now being assessed in Phase I clinical trials against a number of human malignancies [254-257]. Based on the data presented in this thesis, it would be interesting to test the efficacy of this inhibitor against NUMB-deficient cancers.

5.5 CONCLUDING REMARKS

The tumor suppressor protein NUMB has been found to be downregulated in several types of cancers, such as breast, lung and salivary gland tumors [103,106,107]. The mechanism leading its downregulation in breast and lung cancers is excessive ubiquitination and, consequently, proteasomal degradation, in the absence of lesions at the level of the *NUMB* locus, such as loss-of-heterozygosity or primary inactivating mutations affecting the NUMB protein [103,107]. Since we have shown that restoration of NUMB in NUMB-deficient tumors inhibits their growth *in vivo* in immunocomprimised mice (unpublished data), then targeting the UPS machinery responsible for NUMB degradation in human cancers could be an effective therapeutic strategy.

Thus, in the present study, we aimed to identify enzymes involved in NUMB degradation. We employed an ELISA-based RNAi high-throughput screening of ~600 genes of the E3 ligases families and identified and validated the SCF E3 ligase components, RBX1 and FBXW8, as novel negative regulators of NUMB. RBX1 was

validated in primary breast and lung tumor cells, indicating that this protein and its SCF complex could be a valid therapeutic targets in human cancers.

To complete the study, we will now validate FBXW8 in primary tumor cells derived from NUMB-deficient breast and lung cancers. We also plan to define the SCF complex responsible for NUMB degradation by silencing candidate components such as CUL7 and CUL1. Furthermore, we will determine the effects of silencing NUMB-specific SCF components on the tumorigenic potential of NUMB-deficient primary tumor cells *in vivo*. These experiments will provide a preliminary preclinical evaluation of the efficacy of targeting upstream component of the UPS in NUMB-deficient tumors. If these experiments prove successful it would be interesting to test the novel NEDD8-activating enzyme inhibitor, MLN4924, in preclinical *in vivo* models of NUMB-deficient tumors.

Eventually, it will be of great interest to determine the mechanisms regulating the activity of the NUMB-specific SCF complex, e.g. neddylation or phosphorylation, as these events could be deregulated in cancer. We will also determine whether RBX1 and FBXW8 are overexpressed in NUMB-deficient tumors or whether their genes harbor mutations that affect their activity, by performing a deep-sequencing analysis.

Then, we will further investigate the NUMB/RBX1/FBXW8 interaction in order to see if it is direct and if other SCF complex proteins are required.

Moreover, we will perform *in vivo* xenotransplantation studies to assess the potential of RBX1/FBXW8 inhibition in affecting tumor growth of NUMB-deficient cancers.

These investigations should open new avenues in the development of novel therapies for NUMB-deficient cancers.

6 MATERIALS AND METHODS

6.1 GENERATION OF AN ANTI-NUMB MONOCLONAL ANTIBODY

An antigenic peptide corresponding to a unique sequence within NUMB (amino acid residues 537–551), as described in [30], was selected and used to immunize mice in the form of a GST-fusion protein, in collaboration with the Antibody Biochemistry Facility at the IFOM-IEO Campus, Milan. The moAb21 monoclonal antibody was selected and affinity-purified using GE Healthcare columns. The final concentration of the antibody was 1.99 μg/ μl.

6.2 CELL LINES

All human breast cell lines were from the American Type Culture Collection (ATCC). MDA-MB-361, BT474, MDA-MB-231, MDA-MB-415, MDA-MB-453, MCF7, SK-BR3, T-47D and BT549 cell lines were cultured in DMEM medium (from Lonza), supplemented with 10% Fetal Bovine serum (FBS, HyClone), 4 mM L-Glutamine (Euroclone). HCC1569, HCC1954 and AU565 cell lines were cultured in RPMI medium (from Lonza), supplemented with 10% FBS and 4 mM L-Glutamine. ZR-75-1 cell line was cultured in RPMI, supplemented with 10% FBS, 4 mM L-Glutamine, 1 mM Sodium Pyruvate (Life Technologies) and 10 mM Hepes (Life Technologies). BT-20 cell line was cultured in EMEM medium (from Lonza), supplemented with 10% FBS, 1 mM Sodium Pyruvate (Life Technologies), Non-Essential Amino Acids (100X, Gibco, Life technologies,). MDA-MB-175VII cell line was cultured in Leibovitz L-15 medium (Invitrogen, Life Science Technologies), supplemented with 10% FBS and 1% Penicillin/Streptomycin (from Sigma). MDA-MB-468 cell line was cultured in 1:1 mixture of DMEM and Ham's F12 medium, 4 mM L-Glutamine and 10% FBS.

MCF10A cell line was cultured in 1:1 mixture of DMEM and Ham's F12 medium (Gibco, Life Technologies), 20 ng/ml Epidermal Growth Factor (EGF), and 5% Horse Serum (all from Invitrogen), 100 ng/ml Cholera Toxin, 10 μg/ml Insulin, 500 ng/ml Hydrocortisone (all from Sigma).

6.3 PRIMARY EPITHELIAL CELLS

All breast and lung primary epithelial cells were from Institute of European Oncology (IEO, Milan, Italy) and were cultured in a 1:1 mixture of DMEM and Ham's F12 medium, 1% L-glutamine, 1% FBS, 1% Penicillin/Streptomycin (Sigma), 0.2% Gentamicin (Sigma), 0.2% Amphotericin (Sigma), 10 μg/ml Transferrin (Invitrogen), 1 μg/ml Insulin (from Sigma), 1 μg/ml Hydrocortisone (Sigma), 10 mM Hepes pH 7.5 (Life Technologies), Ascorbic Acid 50μM, 15 nM Sodium Selenite, 0.1 mM Ethanolamine and 50 ng/μl Cholera Toxin 10 ng/ml Epidermal Growth Factor (EGF) 35μg/ml, Bovine Pituitary Extract (BPE), 10 nM T3 and, only for breast epithelial cells, 10 nM Beta-Estradiol (all from Sigma). All cells were cultured at 37°C with 5% CO_2.

6.4 CELL TRANSFECTION

Transfections were performed using calcium phosphate, according to manufacturer's instructions. For lentiviral production cells were transfected with calcium phosphate (293T cells).

6.5 SILENCING CANDIDATE GENES EXPRESSION BY siRNA

Transient knock down (KD) of candidate genes was achieved using a specific pre-designed siRNA and the corresponding non-targeting universal control siRNA (Dharmacon Technologies). Briefly, for a 6-wells plate, 5 µl of Lipofectamine RNAiMAX (Invitrogen, Carlsbad, CA) and siRNA oligos diluted at a final concentration of 50 nM for single oligo and 250 nM for pooled oligos (referred to a 2.5 ml final volume), were added to 500 µL OptiMEM (Invitrogen-Gibco Carlsbad, CA), for each well to be transfected. The mix was incubated at room temperature for 20 min. Then cells were counted for plating (3 X 10^5/well for MDA-MB-361 1,5 X 10^5 for MCF10A and MDA-MB-231 and 1 X 10^5 for primary epithelial cells) and were diluted in 2 ml of complete medium without antibiotics in order to obtain the appropriate number to give 50% confluence 24 hours after plating; diluted cells were added to oligos/Lipofectamine RNAiMAX complexes. This gives a final volume of 2.5 ml and a final RNA concentration of 10 nM for single oligo and 50 nM for pooled oligos. 24 hours after trasfection, 2 ml complete medium with 10% FBS was added to cells. After 72 hours, the cells were harvested for WB or IF analysis.

For 384-well format 50 nM of pooled oligos (final concentration) was used and 6000 cells/wells were plated.

6.6 INFECTIONS

Lentivirus was generated by co-transfection of third generation helper vectors together with lentiviral vectors, pLentilox 3.7 (pLL 3.7), in 293T cells. Twenty-four hours after transfection the supernatant was concentrated to 5 ml for each 10 cm plate.

After an additional 24 hours, supernatant was collected, filtered through 45 μm filters, and added to the target cells at 40-50% confluency. Cells were then incubated at 37°C for 12 hours. Forty-eight hours after infection, cells were split and MG-132 (5μM) was added 24 hours before cell harvesting.

6.7 mRNA EXTRACTION AND cDNA SYNTHESIS

RNA was extracted from the control and test cell lines with RNA-ase Mini Kit (Qiagen), according the manufacturer's protocol.

First-strand cDNA synthesis was performed using SuperScript VILO cDNA Synthesis Kit (Invitrogen), following manufacturer's instructions. Briefly, 1 μg of total RNA was mixed with 5X VILO reaction buffer containing random primers (250 ng), dNTPs mix (0.5 mM final concentration) and $MgCl_2$; 1 μl of SuperScript III reverse transcriptase were added to the mix (20 μl final volume) in RNase-free water and the reaction was first incubated at 25°C for 10 min and then at 42°C for 1 hour. Finally, the reaction was inactivated by heating at 85°C for 5 min.

6.8 q-RT PCR

q-RT PCR was performed using the following TaqMan Gene Expression Assays (Applied Biosystems): NUMB (Hs00269398_s1), TRIP12 (Hs00188505_m1), UBE2G1 (Hs00163320_m1), RBX1 (Hs00360274_m1), WHSC1L1 (Hs00256555_m1), KIAA1718 (Hs01398501) and LOC642446 (Hs04190563_mH).

6.9 PROTEIN PROCEDURES

6.9.1 Cell lysis and protein purification

Cells were washed in PBS and lysed in RIPA lysis buffer [50 mmol/L Tris (pH 8), 120 mmol/L NaCl, 0.5% NP40]; Phosphatase and protease inhibitors were added freshly to lysis and wash buffers: 20 mM Na Pyrophosphate pH 7.5, 50 mM NaF, 2 mM PMSF in ethanol, 10mM Na vanadate, Protease Inhibitor Cocktail (Calbiochem). Cells were harvested directly on the plates using a cell scraper. About 300 µl of RIPA lysis buffer/10 cm plates and 50 µl RIPA buffer/for one well of a 6-well plate were used. Lysates were incubated on ice for 30 min and centrifuged at 13,000 rpm for 30 min at 4°C. The supernatant was transferred to a new Eppendorf tube and protein concentration was measured by the Bradford assay (Biorad), following manufacturer's instructions.

6.9.2 SDS polyacrylamide gel electrophoresis (SDS-PAGE)

Gels for resolution of proteins were made from a 30%, 30:0.8 mix of acrylamide:bisacrylamide (Sigma). As polymerization catalysts, 10% ammonium persulphate (APS) and TEMED were used.

Separating gel mix

	5%	7,5%	8,75%	10%	12%	15%
H_2O (ml)	5.8	5	4.5	4.2	3.5	2.5
Lower Tris 4x (ml)	2.5	2.5	2.5	2.5	2.5	2.5
Acr.-Bis 30% (ml)	1.7	2.5	2.9	3.3	4	5
APS 10% (µl)	50	50	50	50	50	50
TEMED (µl)	10	10	10	10	10	10

Stacking gel mix

	MAXI	MINI
H_2O (ml)	5.8	2.92
Upper Tris 4x (ml)	2.5	1.25
Acr.-Bis 30% (ml)	1.7	0.83
APS 10% (µl)	50	25
TEMED (µl)	20	10

6.9.3 Immunoblotting

Desired amounts of proteins were loaded onto 0.75 - 1.5 mm thick polyacrylamide gels for electrophoresis (Biorad). Proteins were transferred in western transfer tanks (Biorad) to nitrocellulose (Schleicher and Schnell) in 1 x Western Transfer buffer (diluted in 20% methanol) at 30 V overnight, or 100 V for 2 hours for small gels and at 70 V for 3 hours for large gels. Ponceau coloring was used to reveal the amount of protein transferred to the filters. Filters were blocked 1 hour (or overnight) in 5% milk or 5% BSA in TBS 0.1% Tween (TBS-T). After blocking, filters were incubated with the primary antibody, diluted in TBS-T with 5% milk or BSA, for 1 hour at room temperature, or overnight at 4°C, followed by 3 washes of 10 min each in TBS-T. Filters were then incubated with the appropriate horseradish peroxidase (HRP)-conjugated secondary antibody diluted in TBS-T with 5% milk or BSA for 45 min. The primary antibody used were anti NUMB (moAb21) anti vinculin and anti actin produced in-house; anti p53 (FL-2393, Santa Cruz); anti FLAG (#2368, Cell Signaling); anti beta-catenin (Cat. 610153, BD); anti RBX1 (Cat. 5296-1, Epitomics); anti Eps15 (C-20, SC-534, Santa Cruz) and anti AP2 (A71107, Sigma). After the incubation with the secondary antibody, the filter was washed 3 times in TBS-T and the bound secondary antibody was revealed using the ECL (enhanced chemiluminescence) method (Amersham).

6.9.4 Immunoprecipitation

Lysates prepared in RIPA buffer (for moAb21 testing) or JS buffer (for co-immunopreipitation experiments) [50 mM Hepes (pH 7.5), 150 mM NaCl, 10% Glycerol, 1% Triton, 1.5 mM $MgCl_2$, 5mM EGTA] were incubated in the presence of specific antibodies for 2 hours at 4°C with rocking.

For co-immunopecipitation experiments an anti FLAG M2 affinity gel (Sigma Aldrich) was used: a purified murine IgG1 monoclonal antibody covalently attached to agarose.

Then, protein G Sepharose beads (Sigma) were added, and samples were left for an additional hour at 4°C, rocking. Immunoprecipitates were then washed 4 times in RIPA or JS buffer. After washing, beads were resuspended in 1:1 volume of 2x SDS-PAGE Sample Buffer, boiled for 5 min at 95°C, centrifuged for 1 minute and then loaded onto polyacrylamide gels.

6.9.5 Immunofluorescence

Cells were plated on glass coverslips pre-incubated with poly-D lysine (15 µg/ml) in PBS at 37°C for 15 min. Cells were fixed in 4% paraformaldehyde (in Pipes Buffer) for 10 min, washed with PBS and permeabilized in PBS 0.1% Triton X-100 for 10 min at room temperature. To prevent non-specific binding of the antibodies, cells were incubated with PBS in the presence of 3% BSA for 60 min. The coverslips were incubated with primary antibodies diluted (2 µg/ml) in PBS 3% BSA. After 1 hour of incubation at room temperature, coverslips were washed 3 times with PBS. Cells were then incubated for 45 min at room temperature with the appropriate secondary antibody Cy3 (Amersham), Alexa 488-conjugated (Molecular Probes). After three washes in PBS, coverslips were mounted in a 90% glycerol solution containing diazabicyclo-(2.2.2)octane antifade (Sigma) and examined under a wild-field immunofluorescence microscope (Leica).

DAPI was used to stain nuclei and was incubated for 3 minutes, RT.

Images were further processed with the Adobe Photoshop software (Adobe) or with Image J to merge the images of the single channels.

6.9.6 Immunohistochemistry

IHC was performed in collaboration with the Molecular Pathology Unit At the IFOM-IEO Campus, Milan. Briefly, MCF10A control cells (siCTRL) and MCF10A cells silenced for NUMB (siNUMB) were removed from the paraffin donor blocks and deposited on the recipient block using a custom-built precision instrument (Tissue Arrayer-Beecher Instruments, Sun Prairie, WI 53590, USA). Two-μm sections of the resulting recipient block were cut, mounted on glass slides, and used for IHC. Glass slides were analyzed for NUMB protein expression by IHC (IHC-NUMB). Slides sections were routinely processed, placed for 30 minutes in 0.25 mM EDTA at 95°C for antigen retrieval and incubated for 3 hours with the moAb21 anti-NUMB monoclonal antibody (1:1000, produced in-house); bound antibody was revealed using the EnVision Plus/HRP Detection system (DAKO) and diaminobenzidine as a chromogenic substrate. IHC sections were finally counterstained with hematoxylin and mounted.

Positive and negative controls were included in each experiment and only clear staining of the plasma membrane was considered positive for NUMB expression.

6.10 CONSTRUCTS AND PLASMIDS

The pLentilox 3.7 lentiviral vector expresses shRNA under the mouse U6 promoter and it was cloned in there a 21-nucleotide *shRNA* sequence for *NUMB (NUMB shRNA)*, which specifically silences endogenous *NUMB* gene.In the same construct, human FLAG-tagged full length (FL) NUMB (NUMB FL-FLAG) or a FLAG-tagged NUMB mutant lacking the PTB domain (NUMB ΔPTB-FLAG) were inserted by digestion with the restriction enzymes NheI and EcoRI, instead of EGFP sequence.

The pLVX-puro lentiviral vector was used to generate a construct to overexpress NUMB fused with GFP protein at the C-termini (NUMB-GFP) in mammalian cells. The human NUMB coding sequence, already present in the lab, was inserted by digestion with the restriction enzymes BamH1 and Sal1 and ligation into the pLVX-puro vector. With this system, expression of NUMB is driven by the human cytomegalovirus immediate early promoter, located just upstream of the multiple cloning site. pLVX contains a puromycin-resistance gene under the control of the murine phosphoglycerate kinase promoter for the selection of stable transductants.

6.11 BASIC CLONING TECHNIQUES

6.11.1 Agarose gel electrophoresis

DNA samples were loaded onto 0.8 - 2% agarose gels along with DNA markers. Gels were made in TAE buffer containing 0.3 μg/ml ethidium bromide and run at 80 V until the desired separation was achieved. DNA bands were visualized under a UV lamp.

6.11.2 Transformation of competent cells

Fresh competent cells (50 μl), Top10 (Invitrogen) for cloning and DNA preparation or electrocompetent DH5alpha cells (produced in-house), were thawed on ice for approximately 10 min prior to the addition of plasmid DNA. Cells were incubated with DNA on ice for 30 min and then subjected to a heat shock for 45 sec at 42°C. Cells were then returned to ice for 2 min. SOC medium (300 μl) was then added and the cells were left at 37°C for 1 hour before plating them onto LB-agar plates with the appropriate antibiotic. Two plates for each reaction were used, one plated with 2/3 of the transformed bacterial cells and the other one with the rest. Plates were incubated overnight at 37°C.

6.11.3 Minipreps

Clones picked from individual colonies were used to inoculate 5 ml LB (containing the appropriate antibiotic) and grown overnight at 37°C. Bacteria cells were transferred to Eppendorf tubes and pelleted for 5 min at 13,000 rpm. Minipreps were performed with the Wizard Plus SV Minipreps Kit (Promega) following the manufacturer's instructions. The plasmids were eluted in 50 µl nuclease free H_2O.

6.11.4 Diagnostic DNA restriction

Between 0.5 and 5 µg DNA were digested for 2 hours at 37°C with 10 – 20 units of restriction enzyme (New England Biolabs). For digestion, the volume was made up depending on the DNA volume to 20 – 50 µl with the appropriate buffer and ddH_2O.

6.11.5 Large-scale plasmid preparation

Cells containing transfected DNA were expanded into 300 ml cultures overnight. Plasmid DNA was isolated from these cells using the Qiagen Maxi-prep kit according to the manufacturer's instructions.

6.12 BIOLOGICAL ASSAYS

6.12.1 ELISA assay

To monitor changes in NUMB expression in a 384-wells format, we customized a capture ELISA assay kit (Human/Mouse/Rat Total NUMB, DuoSet IC) from R&D. As a capture antibody, we used an in-house monoclonal antibody for NUMB detection (moAb21).

REAGENTS USED

Wash Buffer - 0.05% Tween 20 in PBS, pH 7.2 - 7.4 (R&D Systems, Catalog # WA126).

Block Buffer - 1% BSA, 0.05% NaN_3, in PBS, pH 7.2 - 7.4.

IC Diluent #1 - 1% BSA in PBS, pH 7.2 - 7.4, 0.2 µm filtered.

IC Diluent #4 - 1 mM EDTA, 0.5% Triton X-100 in PBS, pH 7.2 - 7.4.

Lysis Buffer - 1 mM EDTA, 0.5% Triton X-100, 10 µg/mL Leupeptin, 10 µg/mL Pepstatin, 100 µM PMSF, 3 µg/mL Aprotinin in PBS, pH 7.2 - 7.4.

Substrate Solutions: A) 1:1 mixture of Color Reagent A (H2O2) and Color Reagent B (Tetramethylbenzidine) (R&D Systems, Catalog # DY999), which should be inactivated by a **Stop Solution** - 2 N H_2SO_4 (R&D Systems, Catalog # DY994).

We subsituted this substrate with **B) Supersignal ELISA Pico Luminol Chemiluminescence substrate** from Thermo Scientific, which had to be used by mixing equal parts of SuperSignal ELISA Pico Luminol/Enhancer and SuperSignal ELISA Pico Stable Peroxide Solution. After 1 minute, a luminometer was used to measure relative light units (~425 nm), between 1-5 minutes after adding the substrate.

For the remaining part of the protocol, we followed the manufacturer's instructions elencated below:

1. Dilute the Capture Antibody to a working concentration of 4.0 µg/ml in PBS, without carrier protein. Immediately coat a 384 well microplate with 25 µl per well of the diluted Capture Antibody. Seal the plate and incubate overnight at room temperature.

2. Aspirate each well and wash with Wash Buffer, repeating the process two times for a total of 3 washes. Wash by filling each well with Wash Buffer (25 µl). After the last wash, remove any remaining Wash Buffer by aspirating or by inverting the plate and blotting it against clean paper towels.

3. Block plates by adding 50 µl of Block Buffer to each well. Incubate at room temperature for 2 hours.

4. Repeat the aspiration/wash as in step 2. The plates are now ready for sample addition.

Assay Procedure

1. Add 25 µl of sample or standards in IC Diluent #4 per well. Use IC Diluent #4 as the zero standard. Cover with a plate sealer and incubate 2 hours at room temperature.

Note: A seven point standard curve using 2-fold serial dilutions and a high standard of 1600 pg/ml is recommended.

2. Repeat the aspiration/wash as in step 2 of Plate Preparation.

3. Dilute the Detection Antibody to a working concentration of 100 ng/ml in IC Diluent #1 before use. Add 25 µl of the diluted Detection Antibody to each well. Cover with a new plate sealer and incubate 2 hours at room temperature.

4. Repeat the aspiration/wash as in step 2 of Plate Preparation.

5. Immediately before use, dilute the Streptavidin-HRP to the working concentration specified on the vial label using IC Diluent #1. Add 25 µl of the diluted Streptavidin-HRP to each well. Incubate for 20 minutes at room temperature. Avoid placing the plate in direct light.

6. Repeat the aspiration/wash as in step 2 of the Plate Preparation.

7. Add 25 µl of Substrate Solution to each well. Incubate for 20 minutes at room temperature (TMB substrate) or for 1 minute (Supersignal PICO Chemiluminescent substrate). Avoid placing the plate in direct light.

8. Add 25 µl of Stop Solution to each well (only if TMB substrate was used). Gently tap the plate to ensure thorough mixing.

9. Determine the optical density of each well immediately, using a microplate reader set to 450 nm (TMB substrate) or to 425 nm (Supersignal PICO Chemiluminescent substrate).

6.12.2 Cell viability assay

Cell viability was assessed by the Cell Titer-Fluor Cell Viability assay, a non-lytic fluorescence assay, from Promega.

The CellTiter-Fluor Cell Viability Assay is a nonlytic, single-reagent addition fluorescence assay that measures the relative number of live cells in a culture population after experimental manipulation. The CellTiter-Fluor Cell Viability Assay measures a conserved and constitutive protease activity within live cells and therefore serves as a marker of cell viability, using a fluorogenic, cell-permeant, peptide substrate (glycylphenylalanyl-aminofluorocoumarin; GF-AFC). The substrate enters intact cells where it is cleaved by the live-cell protease activity to generate a fluorescent signal proportional to the number of living cells. This live-cell protease becomes inactive upon loss of cell membrane integrity and leakage into the surrounding culture medium. The CellTiter-Fluor Cell Viability Assay also can be used in a single-well, sequential, multiplex format with other downstream chemistries to normalize data by cell number. Data from the assay can serve as an internal control and allow identification of errors resulting from cell clumping or compound cytotoxicity.

The CellTiter-Fluor Cell Viability Assay is compatible with most luminescence assays or spectrally distinct fluorescence assay methods. The assay was performed following the manufacturer's instructions; briefly, a CellTiter-Fluor Reagent in an equal volume (25µl per well) was added to all wells, mixed briefly by orbital shaking and incubated for 30 minutes at 37°C. Finally, resulting fluorescence was measured using a fluorometer (380nmEx/505nmEm).

6.12.3. *In vivo* xenograft assays

Six to 8 week-old NOD/SCID IL2R gamma-chain null female mice were injected in the inguinal mammary fat pad with 150,000 MDA-MB-231 and 1,500,000 MDA-MB-361 cells resuspended in 40 µL of a 1:1 Matrigel-PBS solution. Mice were monitored by hand-palpation for tumor development. Tumor growth was measured by using a vernier caliper and applying the standard formula: tumor volume = $(a \times b^2)/2$, where a and b are the long and short side respectively. Mice were treated with MG-132 when tumors reached a dimension of 150 mm^3 for two weeks, every 3 days, for a total of 4 treatments. Tumors were explanted, weighed, and processed for formalin-fixing, paraffin embedding and lysis for WB analysis.

6.13 PHENOTYPIC HIGH-THROUGHPUT siRNA-BASED SCREENING

6.13.1 siRNA E3 ligases library

The library used for the screening was the Dharmacon siGENOME® SMARTpool® siRNA Library- Human Ubiquitin Conjugation subset 1-3 (G-005615 Lot 08119), which was provided in 9 x 96well plates. For each plate, 3 x 384 well pre-spotted "daughter" plates were prepared and directly used in the screen.

6.13.2 Statistical analysis for the identification of positive candidate hits from siRNA high-throughput screening

STEP ONE: Self- Normalization

Each plate was assayed for Cell Viability (CellTiterFluor reagent: CTF) and NUMB levels (ELISA).

- siCTRL, siNUMB and MG-132 were run in 16 replicates
- siRNAs were run in 4 replicates.

STEP TWO: Normalization

This step is a process intended to remove systematic errors from the data and to allow comparison and combination of data from different plate in the screen. We performed the normalization *per* plate.

Three different scores were calculated:

1) Robust Z-score

2) Fraction of Control

3) Fraction of sample median

1) ROBUST Z-SCORE

This method relies on the use of samples as *de facto* negative controls. Thus, siCTRL and MG132 are excluded from the analysis. This approach is based on the assumption that most samples display no biological effect in the assay.

For each plate, we calculated:

i) Median of samples

ii) MAD (Median Absolute deviation), for more details see below, step 3.

iii) Z-score: (X_i – Median) / MAD

2) FRACTION OF CONTROL

This is the classical approach: each sample is divided by the mean of the control (siCTRL=1)

3) FRACTION OF SAMPLE MEDIAN

The median of the samples on the plate can be substituted for the mean of siCTRL. Again, the assumption that most samples display no biological effect in the assay is made.

STEP THREE: Hits identification

Normalized data were processed for hit identification using a Median Absolute Deviation approach (MAD). MAD can be defined as follows:

$$MAD: = Median(|X_i – median(X)|),$$

Where X indicates all the normalized values in the sample wells of a plate and X_i indicates the sample at position *i* in the plate.

To score for potential hits, we applied a threshold of: Median(X) ± 3 x MAD.

7 BIBLIOGRAPHY

1. Uemura, T., Shepherd, S., Ackerman, L., Jan, L.Y. & Jan, Y.N. numb, a gene required in determination of cell fate during sensory organ formation in Drosophila embryos. Cell 58, 349-360 (1989).
2. Rhyu, M.S., Jan, L.Y. & Jan, Y.N. Asymmetric distribution of numb protein during division of the sensory organ precursor cell confers distinct fates to daughter cells. Cell 76, 477-491 (1994).
3. Spana, E. & Doe, C. Numb antagonizes Notch signaling to specify sibling neuron cell fates. Neuron 17, 21-26 (1996).
4. Spana, E., Kopczynski, C., Goodman, C. & Doe, C. Asymmetric localization of numb autonomously determines sibling neuron identity in the Drosophila CNS. Development (Cambridge, England) 121, 3489-3494 (1995).
5. Verdi, J., et al. Mammalian NUMB is an evolutionarily conserved signaling adapter protein that specifies cell fate. Current biology : CB 6, 1134-1145 (1996).
6. Zhong, W., Jiang, M., Weinmaster, G., Jan, L. & Jan, Y. Differential expression of mammalian Numb, Numblike and Notch1 suggests distinct roles during mouse cortical neurogenesis. Development (Cambridge, England) 124, 1887-1897 (1997).
7. Zhong, W., Feder, J., Jiang, M., Jan, L. & Jan, Y. Asymmetric localization of a mammalian numb homolog during mouse cortical neurogenesis. Neuron 17, 43-53 (1996).
8. Wakamatsu, Y., Maynard, T., Jones, S. & Weston, J. NUMB localizes in the basal cortex of mitotic avian neuroepithelial cells and modulates neuronal differentiation by binding to NOTCH-1. Neuron 23, 71-81 (1999).
9. Bork, P. & Margolis, B. A phosphotyrosine interaction domain. Cell 80, 693-694 (1995).
10. Salcini, A., et al. Binding specificity and in vivo targets of the EH domain, a novel protein-protein interaction module. Genes & development 11, 2239-2249 (1997).
11. Verdi, J., et al. Distinct human NUMB isoforms regulate differentiation vs. proliferation in the neuronal lineage. Proceedings of the National Academy of Sciences of the United States of America 96, 10472-10476 (1999).
12. Dho, S., French, M., Woods, S. & McGlade, C. Characterization of four mammalian numb protein isoforms. Identification of cytoplasmic and membrane-associated variants of the phosphotyrosine binding domain. The Journal of biological chemistry 274, 33097-33104 (1999).
13. Karaczyn, A., et al. Two novel human NUMB isoforms provide a potential link between development and cancer. Neural development 5, 31 (2010).
14. Pece, S., Confalonieri, S., R Romano, P. & Di Fiore, P. NUMB-ing down cancer by more than just a NOTCH. Biochimica et biophysica acta 1815, 26-43 (2011).
15. Guo, M., Jan, L. & Jan, Y. Control of daughter cell fates during asymmetric division: interaction of Numb and Notch. Neuron 17, 27-41 (1996).
16. Zhong, W., et al. Mouse numb is an essential gene involved in cortical neurogenesis. Proceedings of the National Academy of Sciences of the United States of America 97, 6844-6849 (2000).
17. Knoblich, J., Jan, L. & Jan, Y. Asymmetric segregation of Numb and Prospero during cell division. Nature 377, 624-627 (1995).
18. Nishimura, T. & Kaibuchi, K. Numb controls integrin endocytosis for directional cell migration with aPKC and PAR-3. Developmental cell 13, 15-28 (2007).
19. Wang, Z., Sandiford, S., Wu, C. & Li, S. Numb regulates cell-cell adhesion and polarity in response to tyrosine kinase signalling. The EMBO Journal 28, 2360-2373 (2009).
20. Smith, C., et al. aPKC-mediated phosphorylation regulates asymmetric membrane localization of the cell fate determinant Numb. The EMBO Journal 26, 468-480 (2007).
21. Androutsellis-Theotokis, A., et al. Notch signalling regulates stem cell numbers in vitro and in vivo. Nature 442, 823-826 (2006).
22. Jiang, J. & Hui, C.-C. Hedgehog signaling in development and cancer. Developmental cell 15, 801-812 (2008).

23. Di Fiore, P.P., Pelicci, P.G. & Sorkin, A. EH: a novel protein-protein interaction domain potentially involved in intracellular sorting. Trends Biochem Sci 22, 411-413 (1997).
24. Paoluzi, S., et al. Recognition specificity of individual EH domains of mammals and yeast. The EMBO Journal 17, 6541-6550 (1998).
25. Santolini, E., Salcini, A.E., Kay, B.K., Yamabhai, M. & Di Fiore, P.P. The EH network. Exp Cell Res 253, 186-209 (1999).
26. Coda, L., et al. Eps15R is a tyrosine kinase substrate with characteristics of a docking protein possibly involved in coated pits-mediated internalization. The Journal of biological chemistry 273, 3003-3012 (1998).
27. Confalonieri, S., Salcini, A., Puri, C., Tacchetti, C. & Di Fiore, P. Tyrosine phosphorylation of Eps15 is required for ligand-regulated, but not constitutive, endocytosis. The Journal of cell biology 150, 905-912 (2000).
28. Fazioli, F., Minichiello, L., Matoskova, B., Wong, W. & Di Fiore, P. eps15, a novel tyrosine kinase substrate, exhibits transforming activity. Molecular and cellular biology 13, 5814-5828 (1993).
29. Confalonieri, S. & Di Fiore, P. The Eps15 homology (EH) domain. FEBS letters 513, 24-29 (2002).
30. Santolini, E., et al. Numb is an endocytic protein. The Journal of cell biology 151, 1345-1352 (2000).
31. Berdnik, D., Torok, T., Gonzalez-Gaitan, M. & Knoblich, J. The endocytic protein alpha-Adaptin is required for numb-mediated asymmetric cell division in Drosophila. Developmental cell 3, 221-231 (2002).
32. Hutterer, A. & Knoblich, J. Numb and alpha-Adaptin regulate Sanpodo endocytosis to specify cell fate in Drosophila external sensory organs. EMBO reports 6, 836-842 (2005).
33. Nishimura, T., et al. CRMP-2 regulates polarized Numb-mediated endocytosis for axon growth. Nature cell biology 5, 819-826 (2003).
34. Roegiers, F., Jan, L. & Jan, Y. Regulation of membrane localization of Sanpodo by lethal giant larvae and neuralized in asymmetrically dividing cells of Drosophila sensory organs. Molecular biology of the cell 16, 3480-3487 (2005).
35. McGill, M., Dho, S., Weinmaster, G. & McGlade, C. Numb regulates post-endocytic trafficking and degradation of Notch1. The Journal of biological chemistry 284, 26427-26438 (2009).
36. Smith, C., Dho, S., Donaldson, J., Tepass, U. & McGlade, C. The cell fate determinant numb interacts with EHD/Rme-1 family proteins and has a role in endocytic recycling. Molecular biology of the cell 15, 3698-3708 (2004).
37. Rasin, M.-R., et al. Numb and Numbl are required for maintenance of cadherin-based adhesion and polarity of neural progenitors. Nature neuroscience 10, 819-827 (2007).
38. Pollard, T. & Borisy, G. Cellular motility driven by assembly and disassembly of actin filaments. Cell 112, 453-465 (2003).
39. Casanova, J. PARtitioning numb. EMBO reports 8, 233-235 (2007).
40. Thiery, J. & Sleeman, J. Complex networks orchestrate epithelial-mesenchymal transitions. Nat Rev Mol Cell Biol 7, 131-142 (2006).
41. Skeath, J. & Doe, C. Sanpodo and Notch act in opposition to Numb to distinguish sibling neuron fates in the Drosophila CNS. Development (Cambridge, England) 125, 1857-1865 (1998).
42. De Strooper, B., et al. A presenilin-1-dependent gamma-secretase-like protease mediates release of Notch intracellular domain. Nature 398, 518-522 (1999).
43. Jarriault, S., et al. Signalling downstream of activated mammalian Notch. Nature 377, 355-358 (1995).
44. Mumm, J., et al. A ligand-induced extracellular cleavage regulates gamma-secretase-like proteolytic activation of Notch1. Molecular cell 5, 197-206 (2000).
45. Struhl, G. & Greenwald, I. Presenilin is required for activity and nuclear access of Notch in Drosophila. Nature 398, 522-525 (1999).
46. Qiu, L., et al. Recognition and ubiquitination of Notch by Itch, a hect-type E3 ubiquitin ligase. The Journal of biological chemistry 275, 35734-35737 (2000).
47. McGill, M. & McGlade, C. Mammalian numb proteins promote Notch1 receptor ubiquitination and degradation of the Notch1 intracellular domain. The Journal of biological chemistry 278, 23196-23203 (2003).
48. Talora, C., et al. Notch signaling and diseases: an evolutionary journey from a simple beginning to complex outcomes. Biochimica et biophysica acta 1782, 489-497 (2008).

49. Nusslein-Volhard, C. & Wieschaus, E. Mutations affecting segment number and polarity in Drosophila. Nature 287, 795-801 (1980).
50. Porter, J., et al. The product of hedgehog autoproteolytic cleavage active in local and long-range signalling. Nature 374, 363-366 (1995).
51. Porter, J.A., et al. Hedgehog patterning activity: role of a lipophilic modification mediated by the carboxy-terminal autoprocessing domain. Cell 86, 21-34 (1996).
52. Echelard, Y., et al. Sonic hedgehog, a member of a family of putative signaling molecules, is implicated in the regulation of CNS polarity. Cell 75, 1417-1430 (1993).
53. Marigo, V., Davey, R., Zuo, Y., Cunningham, J. & Tabin, C. Biochemical evidence that patched is the Hedgehog receptor. Nature 384, 176-179 (1996).
54. Stone, D., et al. The tumour-suppressor gene patched encodes a candidate receptor for Sonic hedgehog. Nature 384, 129-134 (1996).
55. Bellusci, S., et al. Involvement of Sonic hedgehog (Shh) in mouse embryonic lung growth and morphogenesis. Development (Cambridge, England) 124, 53-63 (1997).
56. Goodrich, L., Johnson, R., Milenkovic, L., McMahon, J. & Scott, M. Conservation of the hedgehog/patched signaling pathway from flies to mice: induction of a mouse patched gene by Hedgehog. Genes & development 10, 301-312 (1996).
57. St-Jacques, B., et al. Sonic hedgehog signaling is essential for hair development. Current biology : CB 8, 1058-1068 (1998).
58. Robbins, D.J., Fei, D.L. & Riobo, N.A. The Hedgehog signal transduction network. Sci Signal 5, re6 (2010).
59. Varjosalo, M. & Taipale, J. Hedgehog: functions and mechanisms. Genes & development 22, 2454-2472 (2008).
60. Dai, P., et al. Sonic Hedgehog-induced activation of the Gli1 promoter is mediated by GLI3. The Journal of biological chemistry 274, 8143-8152 (1999).
61. Sasaki, H., Nishizaki, Y., Hui, C., Nakafuku, M. & Kondoh, H. Regulation of Gli2 and Gli3 activities by an amino-terminal repression domain: implication of Gli2 and Gli3 as primary mediators of Shh signaling. Development (Cambridge, England) 126, 3915-3924 (1999).
62. Di Marcotullio, L., et al. Numb is a suppressor of Hedgehog signalling and targets Gli1 for Itch-dependent ubiquitination. Nature cell biology 8, 1415-1423 (2006).
63. Lane, D.P. & Crawford, L.V. T antigen is bound to a host protein in SV40-transformed cells. Nature 278, 261-263 (1979).
64. Linzer, D.I. & Levine, A.J. Characterization of a 54K dalton cellular SV40 tumor antigen present in SV40-transformed cells and uninfected embryonal carcinoma cells. Cell 17, 43-52 (1979).
65. Funk, W.D., Pak, D.T., Karas, R.H., Wright, W.E. & Shay, J.W. A transcriptionally active DNA-binding site for human p53 protein complexes. Mol Cell Biol 12, 2866-2871 (1992).
66. Farmer, G., et al. Wild-type p53 activates transcription in vitro. Nature 358, 83-86 (1992).
67. Shaw, P., et al. Induction of apoptosis by wild-type p53 in a human colon tumor-derived cell line. Proc Natl Acad Sci U S A 89, 4495-4499 (1992).
68. Yonish-Rouach, E., et al. Wild-type p53 induces apoptosis of myeloid leukaemic cells that is inhibited by interleukin-6. Nature 352, 345-347 (1991).
69. el-Deiry, W.S., Kern, S.E., Pietenpol, J.A., Kinzler, K.W. & Vogelstein, B. Definition of a consensus binding site for p53. Nat Genet 1, 45-49 (1992).
70. Kastan, M.B., Onyekwere, O., Sidransky, D., Vogelstein, B. & Craig, R.W. Participation of p53 protein in the cellular response to DNA damage. Cancer Res 51, 6304-6311 (1991).
71. Maltzman, W. & Czyzyk, L. UV irradiation stimulates levels of p53 cellular tumor antigen in nontransformed mouse cells. Mol Cell Biol 4, 1689-1694 (1984).
72. Vogelstein, B., Lane, D. & Levine, A.J. Surfing the p53 network. Nature 408, 307-310 (2000).
73. Lane, D.P. Cancer. p53, guardian of the genome. Nature 358, 15-16 (1992).
74. Bartek, J., et al. Patterns of expression of the p53 tumour suppressor in human breast tissues and tumours in situ and in vitro. Int J Cancer 46, 839-844 (1990).
75. Bartek, J., Iggo, R., Gannon, J. & Lane, D.P. Genetic and immunochemical analysis of mutant p53 in human breast cancer cell lines. Oncogene 5, 893-899 (1990).
76. Iggo, R., Gatter, K., Bartek, J., Lane, D. & Harris, A.L. Increased expression of mutant forms of p53 oncogene in primary lung cancer. Lancet 335, 675-679 (1990).
77. Haupt, Y., Maya, R., Kazaz, A. & Oren, M. Mdm2 promotes the rapid degradation of p53. Nature 387, 296-299 (1997).
78. Kubbutat, M., Jones, S. & Vousden, K. Regulation of p53 stability by Mdm2. Nature 387, 299-303 (1997).

79. Wu, X., Bayle, J.H., Olson, D. & Levine, A.J. The p53-mdm-2 autoregulatory feedback loop. Genes Dev 7, 1126-1132 (1993).
80. Perry, M.E. The regulation of the p53-mediated stress response by MDM2 and MDM4. Cold Spring Harb Perspect Biol 2, a000968 (2010).
81. Colaluca, I.N., et al. NUMB controls p53 tumour suppressor activity. Nature 451, 76-80 (2008).
82. Brown, C., Lain, S., Verma, C., Fersht, A. & Lane, D. Awakening guardian angels: drugging the p53 pathway. Nat Rev Cancer 9, 862-873 (2009).
83. Thomas, G. & Luther, H. Transcriptional and translational control of cytoplasmic proteins after serum stimulation of quiescent Swiss 3T3 cells. Proceedings of the National Academy of Sciences of the United States of America 78, 5712-5716 (1981).
84. Yenofsky, R., Bergmann, I. & Brawerman, G. Messenger RNA species partially in a repressed state in mouse sarcoma ascites cells. Proceedings of the National Academy of Sciences of the United States of America 79, 5876-5880 (1982).
85. Bohm, H., et al. The growth-related protein P23 of the Ehrlich ascites tumor: translational control, cloning and primary structure. Biochem Int 19, 277-286 (1989).
86. Chitpatima, S., Makrides, S., Bandyopadhyay, R. & Brawerman, G. Nucleotide sequence of a major messenger RNA for a 21 kilodalton polypeptide that is under translational control in mouse tumor cells. Nucleic Acids Res 16, 2350 (1988).
87. Gross, B., Gaestel, M., B√∂hm, H. & Bielka, H. cDNA sequence coding for a translationally controlled human tumor protein. Nucleic Acids Res 17, 8367 (1989).
88. Chen, S., et al. A knockout mouse approach reveals that TCTP functions as an essential factor for cell proliferation and survival in a tissue- or cell type-specific manner. Molecular biology of the cell 18, 2525-2532 (2007).
89. Cans, C., et al. Translationally controlled tumor protein acts as a guanine nucleotide dissociation inhibitor on the translation elongation factor eEF1A. Proceedings of the National Academy of Sciences of the United States of America 100, 13892-13897 (2003).
90. Jung, J., et al. Translationally controlled tumor protein interacts with the third cytoplasmic domain of Na,K-ATPase alpha subunit and inhibits the pump activity in HeLa cells. The Journal of biological chemistry 279, 49868-49875 (2004).
91. Liu, H., Urbé, S. & Clague, M. Selective protein degradation in cell signalling. Seminars in cell & developmental biology 23, 509-514 (2012).
92. Yoon, T., Jung, J., Kim, M., Lee, K. & Choi, E. Identification of the self-interaction of rat TCTP/IgE-dependent histamine-releasing factor using yeast two-hybrid system. Archives of biochemistry and biophysics 384, 379-382 (2000).
93. Li, F., Zhang, D. & Fujise, K. Characterization of fortilin, a novel antiapoptotic protein. The Journal of biological chemistry 276, 47542-47549 (2001).
94. Tuynder, M., et al. Translationally controlled tumor protein is a target of tumor reversion. Proceedings of the National Academy of Sciences of the United States of America 101, 15364-15369 (2004).
95. Tuynder, M., et al. Biological models and genes of tumor reversion: cellular reprogramming through tpt1/TCTP and SIAH-1. Proceedings of the National Academy of Sciences of the United States of America 99, 14976-14981 (2002).
96. Arcuri, F., et al. Translationally controlled tumor protein (TCTP) in the human prostate and prostate cancer cells: expression, distribution, and calcium binding activity. The Prostate 60, 130-140 (2004).
97. Amson, R., et al. Reciprocal repression between P53 and TCTP. Nature medicine 18, 91-99 (2012).
98. Kyriazis, G., et al. Numb endocytic adapter proteins regulate the transport and processing of the amyloid precursor protein in an isoform-dependent manner: implications for Alzheimer disease pathogenesis. The Journal of biological chemistry 283, 25492-25502 (2008).
99. Merdes, G., et al. Interference of human and Drosophila APP and APP-like proteins with PNS development in Drosophila. The EMBO Journal 23, 4082-4095 (2004).
100. Roncarati, R., et al. The gamma-secretase-generated intracellular domain of beta-amyloid precursor protein binds Numb and inhibits Notch signaling. Proceedings of the National Academy of Sciences of the United States of America 99, 7102-7107 (2002).
101. Caussinus, E. & Gonzalez, C. Induction of tumor growth by altered stem-cell asymmetric division in Drosophila melanogaster. Nat Genet 37, 1125-1129 (2005).
102. Bric, A., et al. Functional identification of tumor-suppressor genes through an in vivo RNA interference screen in a mouse lymphoma model. Cancer cell 16, 324-335 (2009).

103. Pece, S., et al. Loss of negative regulation by Numb over Notch is relevant to human breast carcinogenesis. J Cell Biol 167, 215-221 (2004).
104. Rennstam, K., et al. Numb protein expression correlates with a basal-like phenotype and cancer stem cell markers in primary breast cancer. Breast Cancer Res Treat 122, 315-324 (2010).
105. Pece, S., et al. Biological and molecular heterogeneity of breast cancers correlates with their cancer stem cell content. Cell 140, 62-73 (2010).
106. Maiorano, E., et al. Prognostic implications of NUMB immunoreactivity in salivary gland carcinomas. Int J Immunopathol Pharmacol 20, 779-789 (2007).
107. Westhoff, B., et al. Alterations of the Notch pathway in lung cancer. Proc Natl Acad Sci U S A 106, 22293-22298 (2009).
108. Gupta, P., Chaffer, C. & Weinberg, R. Cancer stem cells: mirage or reality? Nature medicine 15, 1010-1012 (2009).
109. Reya, T., Morrison, S., Clarke, M. & Weissman, I. Stem cells, cancer, and cancer stem cells. Nature 414, 105-111 (2001).
110. Lanzetti, L. & Di Fiore, P. Endocytosis and cancer: an 'insider' network with dangerous liaisons. Traffic (Copenhagen, Denmark) 9, 2011-2021 (2008).
111. Polo, S., Pece, S. & Di Fiore, P. Endocytosis and cancer. Current opinion in cell biology 16, 156-161 (2004).
112. Vaccari, T. & Bilder, D. At the crossroads of polarity, proliferation and apoptosis: the use of Drosophila to unravel the multifaceted role of endocytosis in tumor suppression. Molecular oncology 3, 354-365 (2009).
113. Aranda, V., Nolan, M. & Muthuswamy, S. Par complex in cancer: a regulator of normal cell polarity joins the dark side. Oncogene 27, 6878-6887 (2008).
114. Goldstein, B. & Macara, I. The PAR proteins: fundamental players in animal cell polarization. Developmental cell 13, 609-622 (2007).
115. Sancho, E., Batlle, E. & Clevers, H. Signaling pathways in intestinal development and cancer. Annu Rev Cell Dev Biol 20, 695-723 (2004).
116. Singh, A. & Settleman, J. EMT, cancer stem cells and drug resistance: an emerging axis of evil in the war on cancer. Oncogene 29, 4741-4751 (2010).
117. Thiery, J., Acloque, H., Huang, R. & Nieto, M. Epithelial-mesenchymal transitions in development and disease. Cell 139, 871-890 (2009).
118. Hershko, A. & Ciechanover, A. The ubiquitin system. Annu Rev Biochem 67, 425-479 (1998).
119. Koepp, D.M., Harper, J.W. & Elledge, S.J. How the cyclin became a cyclin: regulated proteolysis in the cell cycle. Cell 97, 431-434 (1999).
120. Ghosh, S., May, M.J. & Kopp, E.B. NF-kappa B and Rel proteins: evolutionarily conserved mediators of immune responses. Annu Rev Immunol 16, 225-260 (1998).
121. Rock, K.L. & Goldberg, A.L. Degradation of cell proteins and the generation of MHC class I-presented peptides. Annu Rev Immunol 17, 739-779 (1999).
122. Chau, V., et al. A multiubiquitin chain is confined to specific lysine in a targeted short-lived protein. Science 243, 1576-1583 (1989).
123. Hochstrasser, M. Protein degradation or regulation: Ub the judge. Cell 84, 813-815 (1996).
124. Hicke, L. Gettin' down with ubiquitin: turning off cell-surface receptors, transporters and channels. Trends Cell Biol 9, 107-112 (1999).
125. Ikeda, F. & Dikic, I. Atypical ubiquitin chains: new molecular signals. 'Protein Modifications: Beyond the Usual Suspects' review series. EMBO reports 9, 536-542 (2008).
126. Deng, L., et al. Activation of the IkappaB kinase complex by TRAF6 requires a dimeric ubiquitin-conjugating enzyme complex and a unique polyubiquitin chain. Cell 103, 351-361 (2000).
127. Spence, J., et al. Cell cycle-regulated modification of the ribosome by a variant multiubiquitin chain. Cell 102, 67-76 (2000).
128. Spence, J., Sadis, S., Haas, A.L. & Finley, D. A ubiquitin mutant with specific defects in DNA repair and multiubiquitination. Mol Cell Biol 15, 1265-1273 (1995).
129. Bennett, E. & Harper, J. DNA damage: ubiquitin marks the spot. Nature structural & molecular biology 15, 20-22 (2008).
130. Haglund, K. & Dikic, I. Ubiquitylation and cell signaling. The EMBO Journal 24, 3353-3359 (2005).
131. Katzmann, D., Odorizzi, G. & Emr, S. Receptor downregulation and multivesicular-body sorting. Nat Rev Mol Cell Biol 3, 893-905 (2002).

132. Mukhopadhyay, D. & Riezman, H. Proteasome-independent functions of ubiquitin in endocytosis and signaling. Science 315, 201-205 (2007).
133. Nalepa, G., Rolfe, M. & Harper, J.W. Drug discovery in the ubiquitin-proteasome system. Nat Rev Drug Discov 5, 596-613 (2006).
134. Hershko, A., Heller, H., Elias, S. & Ciechanover, A. Components of ubiquitin-protein ligase system. Resolution, affinity purification, and role in protein breakdown. J Biol Chem 258, 8206-8214 (1983).
135. Pickart, C. Mechanisms underlying ubiquitination. Annual review of biochemistry 70, 503-533 (2001).
136. McGrath, J.P., Jentsch, S. & Varshavsky, A. UBA 1: an essential yeast gene encoding ubiquitin-activating enzyme. EMBO J 10, 227-236 (1991).
137. Zacksenhaus, E. & Sheinin, R. Molecular cloning, primary structure and expression of the human X linked A1S9 gene cDNA which complements the ts A1S9 mouse L cell defect in DNA replication. EMBO J 9, 2923-2929 (1990).
138. Haas, A.L. & Rose, I.A. The mechanism of ubiquitin activating enzyme. A kinetic and equilibrium analysis. J Biol Chem 257, 10329-10337 (1982).
139. Tokgoz, Z., Bohnsack, R. & Haas, A. Pleiotropic effects of ATP.Mg2+ binding in the catalytic cycle of ubiquitin-activating enzyme. The Journal of biological chemistry 281, 14729-14737 (2006).
140. Schulman, B. & Harper, J. Ubiquitin-like protein activation by E1 enzymes: the apex for downstream signalling pathways. Nat Rev Mol Cell Biol 10, 319-331 (2009).
141. Wilkinson, K.D., et al. A specific inhibitor of the ubiquitin activating enzyme: synthesis and characterization of adenosyl-phospho-ubiquitinol, a nonhydrolyzable ubiquitin adenylate analogue. Biochemistry 29, 7373-7380 (1990).
142. Burroughs, A.M., Jaffee, M., Iyer, L.M. & Aravind, L. Anatomy of the E2 ligase fold: implications for enzymology and evolution of ubiquitin/Ub-like protein conjugation. J Struct Biol 162, 205-218 (2008).
143. Michelle, C., Vourc'h, P., Mignon, L. & Andres, C.R. What was the set of ubiquitin and ubiquitin-like conjugating enzymes in the eukaryote common ancestor? J Mol Evol 68, 616-628 (2009).
144. Winn, P.J., Religa, T.L., Battey, J.N., Banerjee, A. & Wade, R.C. Determinants of functionality in the ubiquitin conjugating enzyme family. Structure 12, 1563-1574 (2004).
145. Nagy, V. & Dikic, I. Ubiquitin ligase complexes: from substrate selectivity to conjugational specificity. Biol Chem 391, 163-169 (2010).
146. Huibregtse, J.M., Scheffner, M., Beaudenon, S. & Howley, P.M. A family of proteins structurally and functionally related to the E6-AP ubiquitin-protein ligase. Proceedings of the National Academy of Sciences 92(1995).
147. Scheffner, M. & Staub, O. HECT E3s and human disease. BMC biochemistry 8 Suppl 1(2007).
148. Deshaies, R. & Joazeiro, C. RING domain E3 ubiquitin ligases. Annual review of biochemistry 78, 399-434 (2009).
149. Petroski, M.D. & Deshaies, R.J. Function and regulation of cullin-RING ubiquitin ligases. Nat Rev Mol Cell Biol 6, 9-20 (2005).
150. Dou, H., Buetow, L., Sibbet, G., Cameron, K. & Huang, D. BIRC7-E2 ubiquitin conjugate structure reveals the mechanism of ubiquitin transfer by a RING dimer. Nature structural & molecular biology 19, 876-883 (2012).
151. Liew, C., Sun, H., Hunter, T. & Day, C. RING domain dimerization is essential for RNF4 function. The Biochemical journal 431, 23-29 (2010).
152. Mace, P., et al. Structures of the cIAP2 RING domain reveal conformational changes associated with ubiquitin-conjugating enzyme (E2) recruitment. The Journal of biological chemistry 283, 31633-31640 (2008).
153. Ohi, M., Vander Kooi, C., Rosenberg, J., Chazin, W. & Gould, K. Structural insights into the U-box, a domain associated with multi-ubiquitination. Nature structural biology 10, 250-255 (2003).
154. VanderBorght, A., et al. Effect of an hdm-2 antagonist peptide inhibitor on cell cycle progression in p53-deficient H1299 human lung carcinoma cells. Oncogene 25, 6672-6677 (2006).
155. Xu, Z., et al. Interactions between the quality control ubiquitin ligase CHIP and ubiquitin conjugating enzymes. BMC structural biology 8, 26 (2008).
156. Zhang, L., et al. The IDOL-UBE2D complex mediates sterol-dependent degradation of the LDL receptor. Genes & development 25, 1262-1274 (2011).

157. Brzovic, P., Rajagopal, P., Hoyt, D., King, M. & Klevit, R. Structure of a BRCA1-BARD1 heterodimeric RING-RING complex. Nature structural biology 8, 833-837 (2001).
158. Cao, R., Tsukada, Y.-I. & Zhang, Y. Role of Bmi-1 and Ring1A in H2A ubiquitylation and Hox gene silencing. Molecular cell 20, 845-854 (2005).
159. Joukov, V., Chen, J., Fox, E., Green, J. & Livingston, D. Functional communication between endogenous BRCA1 and its partner, BARD1, during Xenopus laevis development. Proceedings of the National Academy of Sciences of the United States of America 98, 12078-12083 (2001).
160. Bartkiewicz, M., Houghton, A. & Baron, R. Leucine zipper-mediated homodimerization of the adaptor protein c-Cbl. A role in c-Cbl's tyrosine phosphorylation and its association with epidermal growth factor receptor. The Journal of biological chemistry 274, 30887-30895 (1999).
161. Fang, S., et al. The tumor autocrine motility factor receptor, gp78, is a ubiquitin protein ligase implicated in degradation from the endoplasmic reticulum. Proceedings of the National Academy of Sciences of the United States of America 98, 14422-14427 (2001).
162. Scheffner, M., Nuber, U. & Huibregtse, J.M. Protein ubiquitination involving an E1-E2-E3 enzyme ubiquitin thioester cascade. Nature 373, 81-83 (1995).
163. Duda, D., et al. Structural regulation of cullin-RING ubiquitin ligase complexes. Current opinion in structural biology 21, 257-264 (2011).
164. Wu, K., et al. The SCF(HOS/beta-TRCP)-ROC1 E3 ubiquitin ligase utilizes two distinct domains within CUL1 for substrate targeting and ubiquitin ligation. Mol Cell Biol 20, 1382-1393 (2000).
165. Jin, J., et al. Systematic analysis and nomenclature of mammalian F-box proteins. Genes Dev 18, 2573-2580 (2004).
166. Skaar, J., D'Angiolella, V., Pagan, J. & Pagano, M. SnapShot: F Box Proteins II. Cell 137(2009).
167. Bedford, L., Lowe, J., Dick, L.R., Mayer, R.J. & Brownell, J.E. Ubiquitin-like protein conjugation and the ubiquitin-proteasome system as drug targets. Nat Rev Drug Discov 10, 29-46 (2011).
168. Ling, Y.-H., et al. Mechanisms of proteasome inhibitor PS-341-induced G(2)-M-phase arrest and apoptosis in human non-small cell lung cancer cell lines. Clinical cancer research : an official journal of the American Association for Cancer Research 9, 1145-1154 (2003).
169. Snoek, B., de Wilt, L., Jansen, G. & Peters, G. Role of E3 ubiquitin ligases in lung cancer. World journal of clinical oncology 4, 58-69 (2013).
170. Hoeller, D. & Dikic, I. Targeting the ubiquitin system in cancer therapy. Nature 458, 438-444 (2009).
171. Hoeller, D., Hecker, C.-M. & Dikic, I. Ubiquitin and ubiquitin-like proteins in cancer pathogenesis. Nat Rev Cancer 6, 776-788 (2006).
172. Nakayama, K.I. & Nakayama, K. Ubiquitin ligases: cell-cycle control and cancer. Nat Rev Cancer 6, 369-381 (2006).
173. Dahlmann, B. Role of proteasomes in disease. BMC biochemistry 8 Suppl 1(2007).
174. Adams, J., et al. Proteasome inhibitors: a novel class of potent and effective antitumor agents. Cancer Res 59, 2615-2622 (1999).
175. Sunwoo, J., et al. Novel proteasome inhibitor PS-341 inhibits activation of nuclear factor-kappa B, cell survival, tumor growth, and angiogenesis in squamous cell carcinoma. Clinical cancer research : an official journal of the American Association for Cancer Research 7, 1419-1428 (2001).
176. Boccadoro, M., Morgan, G. & Cavenagh, J. Preclinical evaluation of the proteasome inhibitor bortezomib in cancer therapy. Cancer cell international 5, 18 (2005).
177. Cusack, J., et al. Enhanced chemosensitivity to CPT-11 with proteasome inhibitor PS-341: implications for systemic nuclear factor-kappaB inhibition. Cancer Res 61, 3535-3540 (2001).
178. Hideshima, T., et al. The proteasome inhibitor PS-341 inhibits growth, induces apoptosis, and overcomes drug resistance in human multiple myeloma cells. Cancer Res 61, 3071-3076 (2001).
179. Ma, M., et al. The proteasome inhibitor PS-341 markedly enhances sensitivity of multiple myeloma tumor cells to chemotherapeutic agents. Clinical cancer research : an official journal of the American Association for Cancer Research 9, 1136-1144 (2003).
180. Russo, S., et al. Enhancement of radiosensitivity by proteasome inhibition: implications for a role of NF-kappaB. International journal of radiation oncology, biology, physics 50, 183-193 (2001).

181. Tan, C. & Waldmann, T. Proteasome inhibitor PS-341, a potential therapeutic agent for adult T-cell leukemia. Cancer Res 62, 1083-1086 (2002).
182. Meister, S., et al. Extensive immunoglobulin production sensitizes myeloma cells for proteasome inhibition. Cancer Res 67, 1783-1792 (2007).
183. Adams, J. The development of proteasome inhibitors as anticancer drugs. Cancer cell 5, 417-421 (2004).
184. Amiri, K., Horton, L., LaFleur, B., Sosman, J. & Richmond, A. Augmenting chemosensitivity of malignant melanoma tumors via proteasome inhibition: implication for bortezomib (VELCADE, PS-341) as a therapeutic agent for malignant melanoma. Cancer Res 64, 4912-4918 (2004).
185. LeBlanc, R., et al. Proteasome inhibitor PS-341 inhibits human myeloma cell growth in vivo and prolongs survival in a murine model. Cancer Res 62, 4996-5000 (2002).
186. Nawrocki, S., et al. Effects of the proteasome inhibitor PS-341 on apoptosis and angiogenesis in orthotopic human pancreatic tumor xenografts. Molecular cancer therapeutics 1, 1243-1253 (2002).
187. Shah, S., et al. 26S proteasome inhibition induces apoptosis and limits growth of human pancreatic cancer. Journal of cellular biochemistry 82, 110-122 (2001).
188. Teicher, B., Ara, G., Herbst, R., Palombella, V. & Adams, J. The proteasome inhibitor PS-341 in cancer therapy. Clinical cancer research : an official journal of the American Association for Cancer Research 5, 2638-2645 (1999).
189. Williams, S., et al. Differential effects of the proteasome inhibitor bortezomib on apoptosis and angiogenesis in human prostate tumor xenografts. Molecular cancer therapeutics 2, 835-843 (2003).
190. Aghajanian, C., et al. A phase I trial of the novel proteasome inhibitor PS341 in advanced solid tumor malignancies. Clinical cancer research : an official journal of the American Association for Cancer Research 8, 2505-2511 (2002).
191. Papandreou, C., et al. Phase I trial of the proteasome inhibitor bortezomib in patients with advanced solid tumors with observations in androgen-independent prostate cancer. Journal of clinical oncology : official journal of the American Society of Clinical Oncology 22, 2108-2121 (2004).
192. Richardson, P., et al. A phase 2 study of bortezomib in relapsed, refractory myeloma. The New England journal of medicine 348, 2609-2617 (2003).
193. Tobinai, K. Proteasome inhibitor, bortezomib, for myeloma and lymphoma. International journal of clinical oncology 12, 318-326 (2007).
194. Rajkumar, S., Richardson, P., Hideshima, T. & Anderson, K. Proteasome inhibition as a novel therapeutic target in human cancer. Journal of clinical oncology : official journal of the American Society of Clinical Oncology 23, 630-639 (2005).
195. Dorsey, B., et al. Discovery of a potent, selective, and orally active proteasome inhibitor for the treatment of cancer. Journal of medicinal chemistry 51, 1068-1072 (2008).
196. Nalepa, G., Rolfe, M. & Harper, J. Drug discovery in the ubiquitin-proteasome system. Nature reviews. Drug discovery 5, 596-613 (2006).
197. Piva, R., et al. CEP-18770: A novel, orally active proteasome inhibitor with a tumor-selective pharmacologic profile competitive with bortezomib. Blood 111, 2765-2775 (2008).
198. Nickeleit, I., et al. Argyrin a reveals a critical role for the tumor suppressor protein p27(kip1) in mediating antitumor activities in response to proteasome inhibition. Cancer cell 14, 23-35 (2008).
199. Chauhan, D., et al. Combination of proteasome inhibitors bortezomib and NPI-0052 trigger in vivo synergistic cytotoxicity in multiple myeloma. Blood 111, 1654-1664 (2008).
200. Thompson, J. Carfilzomib: a second-generation proteasome inhibitor for the treatment of relapsed and refractory multiple myeloma. The Annals of pharmacotherapy 47, 56-62 (2013).
201. Min, M. & Lindon, C. Substrate targeting by the ubiquitin-proteasome system in mitosis. Semin Cell Dev Biol 23, 482-491 (2012).
202. Cardozo, T. & Pagano, M. The SCF ubiquitin ligase: insights into a molecular machine. Nat Rev Mol Cell Biol 5, 739-751 (2004).
203. Guédat, P. & Colland, F.d.r. Patented small molecule inhibitors in the ubiquitin proteasome system. BMC biochemistry 8 Suppl 1(2007).
204. Hjerpe, R. & Rodriguez, M.S. Alternative UPS drug targets upstream the 26S proteasome. Int J Biochem Cell Biol 40, 1126-1140 (2008).
205. Vassilev, L. MDM2 inhibitors for cancer therapy. Trends in molecular medicine 13, 23-31 (2007).

206. Issaeva, N., et al. Small molecule RITA binds to p53, blocks p53-HDM-2 interaction and activates p53 function in tumors. Nature medicine 10, 1321-1328 (2004).
207. Adhikary, S., et al. The ubiquitin ligase HectH9 regulates transcriptional activation by Myc and is essential for tumor cell proliferation. Cell 123, 409-421 (2005).
208. Chen, C., Zhou, Z., Ross, J., Zhou, W. & Dong, J.-T. The amplified WWP1 gene is a potential molecular target in breast cancer. International journal of cancer. Journal international du cancer 121, 80-87 (2007).
209. Chen, D., et al. ARF-BP1/Mule is a critical mediator of the ARF tumor suppressor. Cell 121, 1071-1083 (2005).
210. Fukuchi, M., et al. High-level expression of the Smad ubiquitin ligase Smurf2 correlates with poor prognosis in patients with esophageal squamous cell carcinoma. Cancer Res 62, 7162-7165 (2002).
211. Dick, L. & Fleming, P. Building on bortezomib: second-generation proteasome inhibitors as anti-cancer therapy. Drug discovery today 15, 243-249 (2010).
212. Debnath, J., Muthuswamy, S. & Brugge, J. Morphogenesis and oncogenesis of MCF-10A mammary epithelial acini grown in three-dimensional basement membrane cultures. Methods (San Diego, Calif.) 30, 256-268 (2003).
213. Dimitrova, Y., et al. Direct ubiquitination of beta-catenin by Siah-1 and regulation by the exchange factor TBL1. The Journal of biological chemistry 285, 13507-13516 (2010).
214. Siciliano, M., Barker, P. & Cailleau, R. Mutually exclusive genetic signatures of human breast tumor cell lines with a common chromosomal marker. Cancer Res 39, 919-922 (1979).
215. Ponyeam, W. & Hagen, T. Characterization of the Cullin7 E3 ubiquitin ligase--heterodimerization of cullin substrate receptors as a novel mechanism to regulate cullin E3 ligase activity. Cellular signalling 24, 290-295 (2012).
216. Uhlik, M.T., et al. Structural and evolutionary division of phosphotyrosine binding (PTB) domains. J Mol Biol 345, 1-20 (2005).
217. Fahlbusch, F., et al. Cullin 7 and Fbxw 8 expression in trophoblastic cells is regulated via oxygen tension: implications for intrauterine growth restriction? J Matern Fetal Neona 25, 2209-2215 (2012).
218. Tsunematsu, R., et al. Fbxw8 is essential for Cul1-Cul7 complex formation and for placental development. Molecular and cellular biology 26, 6157-6169 (2006).
219. Tsutsumi, T., Kuwabara, H., Arai, T., Xiao, Y. & Decaprio, J. Disruption of the Fbxw8 gene results in pre- and postnatal growth retardation in mice. Molecular and cellular biology 28, 743-751 (2008).
220. Xu, X., et al. The CUL7 E3 ubiquitin ligase targets insulin receptor substrate 1 for ubiquitin-dependent degradation. Molecular cell 30, 403-414 (2008).
221. Salon, C., et al. Altered pattern of Cul-1 protein expression and neddylation in human lung tumours: relationships with CAND1 and cyclin E protein levels. J Pathol 213, 303-310 (2007).
222. Park, S.W., et al. Mutational analysis of hypoxia-related genes HIF1alpha and CUL2 in common human cancers. APMIS 117, 880-885 (2009).
223. Laszlo, G.S. & Cooper, J.A. Restriction of Src activity by Cullin-5. Curr Biol 19, 157-162 (2009).
224. Johnson, A.E., Le, I.P., Buchwalter, A. & Burnatowska-Hledin, M.A. Estrogen-dependent growth and estrogen receptor (ER)-alpha concentration in T47D breast cancer cells are inhibited by VACM-1, a cul 5 gene. Mol Cell Biochem 301, 13-20 (2007).
225. Chen, L.C., et al. The human homologue for the Caenorhabditis elegans cul-4 gene is amplified and overexpressed in primary breast cancers. Cancer Res 58, 3677-3683 (1998).
226. Melchor, L., et al. Comprehensive characterization of the DNA amplification at 13q34 in human breast cancer reveals TFDP1 and CUL4A as likely candidate target genes. Breast Cancer Res 11, R86 (2009).
227. Schindl, M., Gnant, M., Schoppmann, S.F., Horvat, R. & Birner, P. Overexpression of the human homologue for Caenorhabditis elegans cul-4 gene is associated with poor outcome in node-negative breast cancer. Anticancer Res 27, 949-952 (2007).
228. Signoretti, S., et al. Oncogenic role of the ubiquitin ligase subunit Skp2 in human breast cancer. The Journal of clinical investigation 110, 633-641 (2002).
229. Lu, L., Schulz, H. & Wolf, D. The F-box protein SKP2 mediates androgen control of p27 stability in LNCaP human prostate cancer cells. BMC cell biology 3, 22 (2002).
230. Waltregny, D., et al. Androgen-driven prostate epithelial cell proliferation and differentiation in vivo involve the regulation of p27. Molecular endocrinology (Baltimore, Md.) 15, 765-782 (2001).

231. Carrano, A., Eytan, E., Hershko, A. & Pagano, M. SKP2 is required for ubiquitin-mediated degradation of the CDK inhibitor p27. Nature cell biology 1, 193-199 (1999).
232. Sutterluty, H., et al. p45SKP2 promotes p27Kip1 degradation and induces S phase in quiescent cells. Nature cell biology 1, 207-214 (1999).
233. Strohmaier, H., et al. Human F-box protein hCdc4 targets cyclin E for proteolysis and is mutated in a breast cancer cell line. Nature 413, 316-322 (2001).
234. Akhoondi, S., et al. FBXW7/hCDC4 is a general tumor suppressor in human cancer. Cancer Res 67, 9006-9012 (2007).
235. Calhoun, E., et al. BRAF and FBXW7 (CDC4, FBW7, AGO, SEL10) mutations in distinct subsets of pancreatic cancer: potential therapeutic targets. The American journal of pathology 163, 1255-1260 (2003).
236. Koh, M.S., Ittmann, M., Kadmon, D., Thompson, T.C. & Leach, F.S. CDC4 gene expression as potential biomarker for targeted therapy in prostate cancer. Cancer Biol Ther 5, 78-83 (2006).
237. Lee, J.W., et al. Mutational analysis of the hCDC4 gene in gastric carcinomas. Eur J Cancer 42, 2369-2373 (2006).
238. Liu, J., et al. Oncogenic BRAF regulates beta-Trcp expression and NF-kappaB activity in human melanoma cells. Oncogene 26, 1954-1958 (2007).
239. Muerkoster, S., et al. Increased expression of the E3-ubiquitin ligase receptor subunit betaTRCP1 relates to constitutive nuclear factor-kappaB activation and chemoresistance in pancreatic carcinoma cells. Cancer Res 65, 1316-1324 (2005).
240. Ougolkov, A., et al. Associations among beta-TrCP, an E3 ubiquitin ligase receptor, beta-catenin, and NF-kappaB in colorectal cancer. Journal of the National Cancer Institute 96, 1161-1170 (2004).
241. Spiegelman, V., et al. Induction of homologue of Slimb ubiquitin ligase receptor by mitogen signaling. The Journal of biological chemistry 277, 36624-36630 (2002).
242. Jia, L., Soengas, M. & Sun, Y. ROC1/RBX1 E3 ubiquitin ligase silencing suppresses tumor cell growth via sequential induction of G2-M arrest, apoptosis, and senescence. Cancer Res 69, 4974-4982 (2009).
243. Jia, L., et al. RBX1 (RING box protein 1) E3 ubiquitin ligase is required for genomic integrity by modulating DNA replication licensing proteins. The Journal of biological chemistry 286, 3379-3386 (2011).
244. Wei, D. & Sun, Y. Small RING Finger Proteins RBX1 and RBX2 of SCF E3 Ubiquitin Ligases: The Role in Cancer and as Cancer Targets. Genes & cancer 1, 700-707 (2010).
245. Lin, P., et al. Fbxw8 is involved in the proliferation of human choriocarcinoma JEG-3 cells. Molecular biology reports 38, 1741-1747 (2011).
246. Okabe, H., et al. A critical role for FBXW8 and MAPK in cyclin D1 degradation and cancer cell proliferation. PLoS One 1(2006).
247. Andrews, P., He, Y. & Xiong, Y. Cytoplasmic localized ubiquitin ligase cullin 7 binds to p53 and promotes cell growth by antagonizing p53 function. Oncogene 25, 4534-4548 (2006).
248. Fu, J., et al. Ubiquitin ligase cullin 7 induces epithelial-mesenchymal transition in human choriocarcinoma cells. The Journal of biological chemistry 285, 10870-10879 (2010).
249. Barbash, O., Lee, E.K. & Diehl, J.A. Phosphorylation-dependent regulation of SCF(Fbx4) dimerization and activity involves a novel component, 14-3-3varepsilon. Oncogene 30, 1995-2002 (2011).
250. Liu, J., Furukawa, M., Matsumoto, T. & Xiong, Y. NEDD8 modification of CUL1 dissociates p120(CAND1), an inhibitor of CUL1-SKP1 binding and SCF ligases. Mol Cell 10, 1511-1518 (2002).
251. Siergiejuk, E., et al. Cullin neddylation and substrate-adaptors counteract SCF inhibition by the CAND1-like protein Lag2 in Saccharomyces cerevisiae. EMBO J 28, 3845-3856 (2009).
252. Chen, D., Frezza, M., Schmitt, S., Kanwar, J. & Dou, Q. Bortezomib as the first proteasome inhibitor anticancer drug: current status and future perspectives. Current cancer drug targets 11, 239-253 (2011).
253. Brownell, J., et al. Substrate-assisted inhibition of ubiquitin-like protein-activating enzymes: the NEDD8 E1 inhibitor MLN4924 forms a NEDD8-AMP mimetic in situ. Molecular cell 37, 102-111 (2010).
254. Soucy, T., et al. An inhibitor of NEDD8-activating enzyme as a new approach to treat cancer. Nature 458, 732-736 (2009).
255. Soucy, T., Dick, L., Smith, P., Milhollen, M. & Brownell, J. The NEDD8 Conjugation Pathway and Its Relevance in Cancer Biology and Therapy. Genes & cancer 1, 708-716 (2010).

256. Soucy, T., Smith, P. & Rolfe, M. Targeting NEDD8-activated cullin-RING ligases for the treatment of cancer. Clinical cancer research : an official journal of the American Association for Cancer Research 15, 3912-3916 (2009).
257. Wei, D., et al. Radiosensitization of human pancreatic cancer cells by MLN4924, an investigational NEDD8-activating enzyme inhibitor. Cancer Res 72, 282-293 (2012).

ACKNOLEDGMENTS

First and foremost, I am greatful to my PhD supervisor, Prof. Pier Paolo Di Fiore, for giving me the opportunity to work in his exciting laboratory and for his guidance during the years of my PhD study.

A special thanks goes to Prof. Salvatore Pece for his constant support during these years and especially for teaching me to enjoy my job.

I want also to express all my gratitude to Dr. Ivan Colaluca for having taught me, since I was an undergraduated student, everything I know from a scientific point of view, and for his constant support in everyday life in the lab during the last five years; he gave me the passion he put in science and the concept that sacrifice is the first step toward success. I want also thank him for all his support, from a personal point of view, during the hard moments I encountered during these years and for his friendship.

I thank also Dr. Daniele Galvagno, which started this thesis project with me and Dr. Andrea Basile for his precious scientific advices and for his friendship.

I thank all the people from Pier Paolo Di Fiore's Lab for their friendship and scientific discussions, all the IFOM-IEO Campus Facilities, the SEMM Graduate Office and all my friends at IFOM-IEO Campus, which shared with me the hard and the good moments.

I thank Dr. Rosalind Gunby for critically reviewing this thesis.

Finally, I thank Prof. Robert Clarke, from Paterson Institute for Cancer Research, University of Manchester, and Prof. Giorgio Scita, from IFOM-IEO-Campus, for co-supervising this thesis.